CHALMERS
UNIVERSITY OF TECHNOLOGY

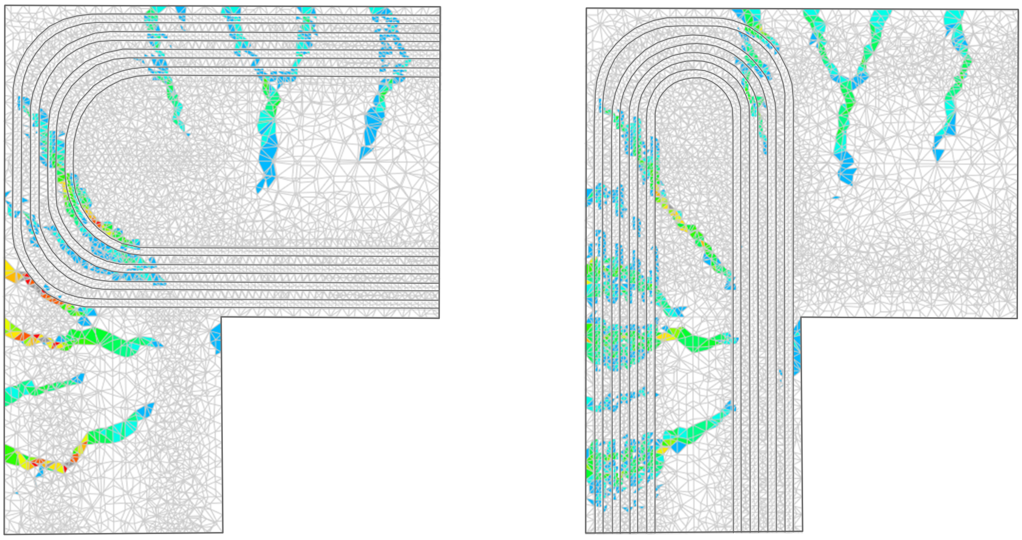

Loop connections in heavily reinforced concrete frame corners

Master's thesis in Master Program Structural Engineering and Building Technology

JENNY BERGLUND

MALIN IVARSSON HOLMSTRÖM

Department of Architecture and Civil Engineering
Chalmers University of Technology
Master's thesis ACEX30-19-29
Gothenburg, Sweden 2019

Master's thesis ACEX30-19-29

Loop connections in heavily reinforced concrete frame corners

JENNY BERGLUND
MALIN IVARSSON HOLMSTRÖM

Department of Architecture and Civil Engineering
Division of Structural Engineering
Chalmers University of Technology
Gothenburg, Sweden 2019

Loop connections in heavily reinforced concrete frame corners

JENNY BERGLUND
MALIN IVARSSON HOLMSTRÖM

Supervisor: Christoffer Svedholm, Structural Engineer at ELU
Examiner: Professor Karin Lundgren, Department of Architecture and Civil Engineering

Department of Architecture and Civil Engineering
Division of Structural Engineering
Chalmers University of Technology
SE-412 96 Gothenburg
Telephone +46 31 772 1000

Cover: Illustration of crack pattern in the analysed heavily reinforced frame corner

Typeset in LaTeX
Department of Architecture and Civil Engineering
Gothenburg, Sweden 2019

Loop connections in heavily reinforced concrete frame corners
JENNY BERGLUND
MALIN IVARSSON HOLMSTRÖM
Department of Architecture and Civil Engineering
Chalmers University of Technology

Abstract

Loop connections are formed by U-shaped reinforcement bars and are often preferred by contractors, over a more conventional detailing in frame corners, requested mainly from a working environment safety aspect. Varying design equations, to estimate the moment capacity using loop connections, have been developed from performed tests on slabs by a few researchers. However, there are no clear guidelines or restrictions of how to utilize this reinforcement configuration in large and heavily reinforced frame corners, which can be expected to differ from frame corners with smaller dimensions and less reinforcement amount due to higher radial stresses. For that reason, it is of interest to analyse the structural response of large frame structures with multiple layers of reinforcement, since detailing with loop connections also has potential to be suitable for bridges, tunnels and retaining walls.

A recent example was an underground structure utilized for car parking, planned to be built at Skeppsbron in Gothenburg. Further analyses and understanding of the usage of loop reinforcement in these type of structures, subjected to static closing moment, were requested. Since no experiments have been performed in the scale of interest, a finite element modelling method was developed in ABAQUS. The process started with small scale analyses that were verified against already performed tests; thereafter the size of the analysed specimens was increased to requested dimensions and ratios.

Available design equations were studied, to distinguish if and to which extent they may be applicable in design of larger structures and frame corners, leading to divergent results. The results of the finite element analyses showed that large frame corners detailed with loop connections fails in bending due to yielding of the reinforcement and crushing of the concrete in the inner corner. Accordingly, no indications of decrease in capacity in comparison to frame corners having conventional reinforcement detailing were found.

Keywords: loop connections, U-bars, reinforced concrete frame corners, ABAQUS

Looparmering i kraftigt armerade ramhörn
JENNY BERGLUND
MALIN IVARSSON HOLMSTRÖM
Institutionen för Arkitektur och Samhällsbyggnadsteknik
Chalmers Tekniska Högskola

Sammanfattning

Armeringsanslutningar med C-järn, looparmering, efterfrågas ofta av entrepenören främst ur ett arbetsmiljöperspektiv, som ersättning till konventionell armeringsutformning i ramhörn. Olika förslag återfinns i litteraturen på hur man bör beräkna momentkapaciteten vid användning av looparmering, framtagna av forskare utifrån experiment utförda på platt-konstruktioner. Emellertid finns dock inga tydliga riktlinjer eller begränsningar huruvida denna armeringsutformning är applicerbar vid design av stora och kraftigt armerade ramhörn, där beteendet förväntas skilja sig på grund av höga radiella spänningar inom looparna. Eftersom denna armeringsutformning även har potential att användas i broar, tunnlar och stödmurar finns intresse att analysera de brottmoderna som uppstår i dessa stora konstruktioner, där flera lager armering är nödvändigt, och jämföra mot beteendet vid konventionell armeringsutformning.

Ett aktuellt exempel på detta var i den parkeringskonstruktion, under marknivå, som planeras att byggas vid Skeppsbron i Göteborg. Ytterligare analyser av sådana större ramkonstruktioner, utsatta för ett statiskt stängande moment, efterfrågades. Då inga experiment har genomförts på ramhörn av denna storlek, skapades ett antal finita element analyser i ABAQUS. Först i liten skala, där modellen kunde verifieras mot redan utförda experiment, för att sedan skalas upp till de efterfrågade dimensionerna.

De olika metoderna för beräkning av momentkapaciteten med looparmering har analyserats och jämförts, för att kunna avgöra huruvida de är applicerbara på större konstruktioner och ramhörn, med varierande utfall. Resultaten från de numeriska analyserna visar att ramhörn utformade med looparmering går sönder i ett böjbrott, där armeringen flyter och betongen i det inre hörnet krossas. Därmed upptäcktes inga indikationer på försämring av kapaciteten vid användning av looparmering i jämförelse med konventionell armeringsutformning.

Nyckelord: looparmering, C-järn, armerade betonghörn, ABAQUS

Contents

Abstract I

Sammanfattning II

Preface VI

List of Figures VII

List of Tables XI

List of Symbols XIII

1 Introduction 1

1.1 Background . . . 1
1.2 Aim . . . 2
1.3 Method . . . 3
1.4 Limitations . . . 4
1.5 Outline . . . 5

2 Theory 7

2.1 Frame corners . . . 7
2.1.1 Closing moment . . . 9
2.1.2 Opening moment . . . 11
2.2 Loop connections . . . 12
2.2.1 Failure modes . . . 12
2.2.2 Influencing parameters . . . 14
2.2.3 Design recommendations . . . 16
2.2.4 Estimated capacity according to Dragosavic et al. . . . 18
2.2.5 Estimated capacity according to Hao . . . 20
2.2.6 Estimated capacity according to Joergensen & Hoang . . . 21

2.2.7 Comparison of methods used to estimate the capacity of loop moment 23

3 Numerical modelling of reinforced concrete **27**
3.1 Concrete under tension 28
3.2 Concrete under compression 30
3.3 Steel reinforcement 31
3.4 Material models 32
3.5 Bond interaction 35
3.5.1 Bond transfer phenomena 35
3.5.2 Modelling of bond interaction 36
3.5.2.1 Spring model 38
3.5.2.2 Friction model 39
3.5.2.3 Cohesive zone elements 40
3.5.2.4 Cohesive surface interaction 40

4 Verification of numerical modelling techniques **43**
4.1 Pull-out tests 43
4.1.1 Experimental setup 43
4.1.2 Material model 46
4.1.3 Numerical model with spring elements 47
4.1.4 Numerical model with cohesive surface interaction 48
4.1.5 Conclusions 52
4.2 Frame corner tests 53
4.2.1 Experimental setup 53
4.2.2 Material 54
4.2.3 Numerical model 55
4.2.4 Comparison between tests and analyses 58
4.2.5 Verification 61
4.2.6 Conclusions 63

5 Case study **65**
5.1 Structure 65
5.2 Material 67
5.3 Numerical model 67
5.4 Results 69
5.4.1 SB1 69
5.4.2 SB2 72

5.4.3 Moment capacities 74
5.4.4 Validation 75

6 Conclusions **77**
6.1 General 77
6.2 Suggestions for further research 79

References **81**

A Appendix A **I**

B Appendix B **I**

C Appendix C **I**

D Appendix D **I**

E Appendix E **I**

Preface

This thesis is the final part of the master program Structural engineering and Building technology which resulted from a cooperation project between *ELU Konsult AB* and the *Division of Structural Engineering at Chalmers University of Technology* over a period of six months. The work was mainly carried out at ELU's office in Gothenburg and started in the end of January 2019. Professor Karin Lundgren from the Division of Structural Engineering was the examiner, to whom we would like to express our gratitude for her continuous critical reviews and feedback on the project.

A special thanks is addressed to our supervisor Christoffer Svedholm, ELU, for his highly appreciated guidance and continuous support throughout the project. We would also like to thank Adjunct Professor Morgan Johansson, Chalmers and Adjunct Professor Costin Pacoste-Calmanovici, KTH for contributing with valuable knowledge and experience.

Finally, we would like to thank our opponents Joakim Larsson and Ahmad Alalwan their feedback on the thesis, so it can be perceived more clearly for an external reader.

Jenny Berglund
Malin Ivarsson Holmström

Gothenburg, June 2019

List of Figures

1.1 *Schematic figure of reinforcement detailing in frame corner* 1
1.2 *Methodology flow chart* 4

2.1 *Example of typical loading situations for frame corners* 7
2.2 *Schematic figure of moment rigid frames loaded with opening/closing moment* 8
2.3 *Expected crack pattern, at the boundary of the corner area, for a frame subjected to a closing moment, reproduced from Nilsson (1973)* 10
2.4 *Design recommendation of closing frame corner, reproduced from Eurocode (CEN, 2005)* 10
2.5 *Tensile (positive) and compressive (negative) stress distribution at a corner subjected to positive moment in the elastic stage, reproduced from Nilsson (1973)* 11
2.6 *Expected crack pattern for a frame subjected to an opening moment, reproduced from Nilsson (1973)* 11
2.7 *Design recommendation of opening frame corner, reproduced from Eurocode (CEN, 2005)* 12
2.8 *Schematic view of stresses arising when a reinforcement bar changes direction (Johansson, 2000b)* 13
2.9 *Crack pattern in a slab with loop connections, numbering illustrates the order the cracks appear, reproduced from Dragosavic et al. (1975)* . . . 14
2.10 *Definition of influencing parameters on loop connections* 15
2.11 *Radial stresses in loop connections, reproduced from Modelcode (CEB-FIB, 2010)* 17
2.12 *Stresses in the in-plane direction, reproduced from Modelcode (CEB-FIB, 2010)* 17
2.13 *Sandwich model to estimate moment capacity, reproduced from Joergensen & Hoang (2015)* 21

2.14 *Moment capacities compared to the estimated capacity, with varying heights* 24
2.15 *Moment capacities compared to the estimated capacity, with varying concrete side cover* 25

3.1 *Typical uni-axial stress-strain relations in structural materials* 27
3.2 *Tension softening behaviour proposed by Hordijk (1992) and Hillerborg (1985)* 28
3.3 *Discrete and distributed cracks, reproduced from Malm (2016)* 29
3.4 *Displacement divided into a stress-strain relation and a stress-crack opening relation, reproduced from Plos (1996)* 30
3.5 *Stress-strain relation for concrete in compression (CEN, 2005)* 31
3.6 *Simplified stress-strain for steel reinforcement* 32
3.7 *Representation of material behaviour using different models, reproduced from Alfarah et al. (2017)* 33
3.8 *Strength envelope of concrete under biaxial stress, reproduced from Malm (2006)* 33
3.9 *Schematic figure of contact stresses, reproduced from Plos (1996)* 36
3.10 *Analytic bond stress-slip relation, reproduced from Modelcode (CEB-FIB, 2010)* 37
3.11 *Models describing bond stress-slip and force-slip* 38
3.12 *Schematic figure of a spring element connected between concrete and reinforcement* 39
3.13 *Frictional model, reproduced from ABAQUS Analysis User's Guide (Dassault-Systèmes, 2014)* 39
3.14 *Cohesive zone elements (Dassault-Systèmes, 2014)* 40
3.15 *Approximations for the bond interaction* 41

4.1 *Dimensions of test specimen for pull-out tests (Jansson et al., 2012)* . . 44
4.2 *Average σ-w curves for the compared tests, numbering in brackets refers to specimen in experiment. Reproduced from Jansson et al. (2012)* . . . 46
4.3 *FE-model set up and mesh configuration for pull-out numerical model with spring elements* 47
4.4 *Relationship between bond stress and active slip together with a contour plot of the plastic strain generated in the finite element analysis, on the passive side. The maximum strain illustrated reaches 0.3. On the right the absence of cracks on the active side in comparison to the expected cracks are presented.* 48

4.5 *Relationship between normal stresses (σ) and shear stresses (τ) from simplified pull-out tests, resulting in splitting stresses in the concrete* . . 49
4.6 *FE-model set up and mesh configuration for pull-out numerical model with cohesive surface interaction* 49
4.7 *Relationship between bond stress and active slip. Comparison between the plastic strain generated in the finite element analysis with the crack pattern from the experiments, on the active side. The maximum strain illustrated reached 0.09* 50
4.8 *Relationship between bond stress and active slip. Comparison between the plastic strain generated in the finite element analysis with the crack pattern from the experiments, on the active side. The maximum strain illustrated reached 0.005* 51
4.9 *Experimental setup RV5/RV6 (Johansson, 2000b)* 53
4.10 *Schematic figure of the force components, F_V and F_H, from the applied force $F_{framecorner}$* at a distance l from the corner-beam interface. 54
4.11 *FE-model set up for RV5/RV6* 56
4.12 *Mesh specifications of numerical model* 57
4.13 *Force-displacement response of numerical model compared to experiment RV5/RV6* 58
4.14 *Comparison of crack pattern, on the free edge* 59
4.15 *Plastic strains in concrete displaying the crack pattern in the numerical analyses of RV5/RV6. Taken in section cuts at position of horizontal and vertical loops* 59
4.16 *Yielding of steel in numerical analysis* 60

5.1 *Schematic figure of SB1 and SB2 with two and four layers of reinforcement respectively compared to RV5/RV6 with its smaller dimensions and one layer reinforcement* 66
5.2 *FE-model set up for corner part* 68
5.3 *Mesh specifications of numerical model SB1/SB2* 68
5.4 *Force-displacement response for SB1* 70
5.5 *Plastic strains in concrete displaying the crack pattern in the last step of the analyses of SB1. Taken in section cuts at position of vertical and horizontal loops* 71
5.6 *Von Mises stresses in reinforcement at last step for SB1* 71
5.7 *Force-displacement response for SB2* 72
5.8 *Compressive stresses in concrete exceeding 35 MPa* 73

5.9 *Plastic strains in concrete displaying the crack pattern in the last step of the numerical model of SB2. Taken in section cuts at position of vertical and horizontal loops* 73
5.10 *Von Mises stresses in reinforcement at last step for SB2* 74
5.11 *Mesh convergence study for SB1/SB2* 75

List of Tables

2.1 *Summary of input used when comparing the estimated moment capacities* 23
2.2 *Moment capacities [kNm], comparison of results from different suggested equations with varying heights and c_e=0.100.* 23
2.3 *Moment capacities [kNm], comparison of results from different suggested equations with varying side concrete cover, and h=0.200.* 25

3.1 *Plastic damage parameters used as input values in CDP model* 34

4.1 *Summary of concrete material input used in the FE-analyses of the pull-out tests* 47
4.2 *Cohesive stiffness input used in the FE-analyses* 50
4.3 *Summary of concrete input used in the FE-analyses of the frame corner tests* 55
4.4 *Summary of reinforcement input used in the FE-analyses of the frame corner tests* 55
4.5 *Approximate mesh size used in the presented results* 57
4.6 *Summary of moment capacities [kNm]* 61

5.1 *Reinforcement amount and detailing in frame corner SB1 and SB2* . . 67
5.2 *Summary of concrete input used in the FE-analysis of SB1/SB2* 67
5.3 *Summary of reinforcement input used in the FE-analysis of SB1/SB2* . 67
5.4 *Approximate mesh size used in the presented result of SB1/SB2* 69
5.5 *Summary of moment capacities [kNm]* 74

List of Symbols

Greek Characters

α	reduction factor
δ_i	separation in i-direction
ϵ	eccentricity parameter
γ	partial factor
μ	viscosity parameter
μ_f	friction coefficient
ω	reinforcement ratio (area steel over effective area of concrete)
ϕ	bar diameter
ψ	dilation angle
ρ	density
ρ_c	denisity concrete
ρ_s	denisity steel
σ	normal stresses
σ_{al}	steel stress at radial concrete compression failure
$\sigma_{c.rad}$	radial concrete stress
σ_c	concrete stress
σ_r	radial stress
σ_s	steel stress
τ	shear stresses
τ_{crit}	critical friction shear stress
τ_f	friction shear stress
τ_l	bond stress in longitudinal direction
τ_{max}	bond strength
θ	angle of compressive strut
υ_c	Poisson's ratio concrete
υ_s	Poisson's ratio steel

ε_v^{pl}	viscous plastic strain
ε^{pl}	plastic strain
ε_{c1}	strain at peak stress, dependent on concrete class
ε_c	concrete strain
ε_s	steel strain
ε_y	steel strain at yield

Lower Case Letters

a	distance between top and bottom reinforcement
b	cross sectional width
c	top concrete cover
c_e	side concrete cover
d	distance from top cover to bottom reinforcement
d	stiffness degradation
d_v	viscous stiffness degradation
f_{b0}	biaxial concrete compressive strength
f_{c0}	uniaxial concrete compressive strength
f_{cd}	design concrete compressive strength
f_{cm}	mean concrete compressive strength
f_{ctk}	characteristic concrete tensile strength
f_{ctm}	mean concrete tensile strength
f_{ct}	concrete tensile strength
f_{cu}	cube concrete compressive strength
f_c	concrete compressive strength
f_u	steel ultimate strength
f_{yd}	design steel yield strength
f_y	steel yield strength
h	cross sectional height
l	lever arm
l_{lap}	lap length
n	number of loops
n_{spring}	total amount of springs used in numerical model
p	contact pressure
r	loop radius
t	loop spacing between pairs
t_i	traction in i-direction

t_{pair}	loop spacing within the pairs
x	thickness of compression field
z	lever arm between compression and tension centers

Upper Case Letters

A_{ad}	area of transverse reinforcement
A_{at}	area of cross section in tension for one loop
A_a	area of cross section for one loop
A_c	cross sectional concrete area
A_c^*	effective cross sectional concrete area
A_s	cross sectional steel area
C	compression force
D_0^{el}	elastic stiffness matrix
E_c	Young's modulus concrete
E_s	Young's modulus steel
$F_{framecorner}$	force applied in frame corner tests
F_H	force in the horizontal direction
F_l	force in bond slip in longitudinal direction
$F_{pullout}$	force applied in pull-out tests
F_V	force in the vertical direction
G_f	fracture energy
K_c	parameter dependent on stress invariants
K_{ii}	Stiffness between conctact elements in ii-direction
$M_{l.Drago}$	loop moment capacity according to Dragosavic et al.
$M_{l.Hao}$	loop moment capacity according to Hao
$M_{l.Joerg}$	loop moment capacity according to Joergensen & Hoang
M_l	loop moment capacity
M_{Rd}	moment capacity according to Eurocode
N	normal force
N_u	pure tensile capacity
N_y	yield load of one leg of the U-bar
S_l	bond slip in longitudinal direction
S_{max}	maximum slip
T	tension force

1

Introduction

1.1 Background

Contractors have an obligation to ensure a safe work environment for its workers. Therefore, the concept of loop connections as reinforcement detailing in frame corners is often preferred, over a more conventional detailing, illustrated in Figure 1.1. Loop connections are created by U-shaped reinforcement bars and can be applied in different parts of the structure. Using this type of detailing when the first part of the corner is cast prevents sharp protruding pieces sticking out at the construction site, resulting in a safer working site until the next part of the frame is mounted. In addition, this configuration is also preferred for precast members since the loop of the reinforcement is closed and thereby creates a member that can be built elsewhere and transported easily. When arriving on site only the corner part must be in-situ cast instead of the full structure, showing the advantage of loop connections from an economic point of view as they make the production faster and safer.

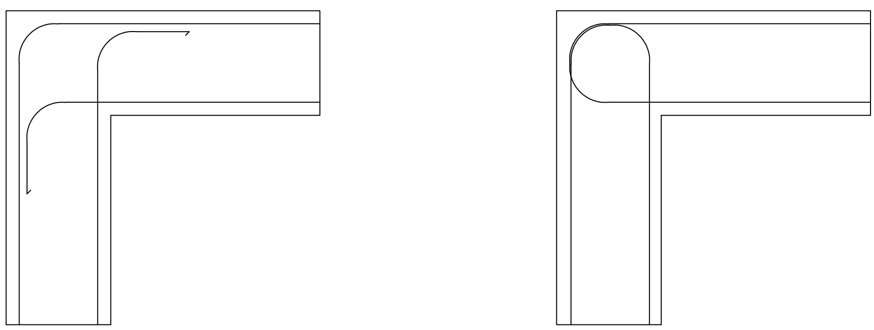

(a) *Conventional detailing* **(b)** *Loop connection*

Figure 1.1: *Schematic figure of reinforcement detailing in frame corner*

Dependent on the type of construction and loading situation a concrete frame corner can be exposed to two type of moments, negative (closing of the corner) and positive (opening of the corner). These two types of loading situations will give rise to different failure modes and therefore demand different reinforcement detailing. To achieve enough bearing capacity in concrete frames, the detailing of the corner and the reinforcement connecting the independent members plays an important role. To obtain a safe structural behaviour, the joints must ensure a ductile behaviour and be at least as strong as the structural members that connects them.

Until today, the concept of loop connections has been studied rather widely in the aspect of transfer forces between solid slabs where continuity is demanded, but also to some extent when used in frame corners. Some design recommendations for cases exposed to pure tension have been brought into Modelcode (CEB-FIB, 2010) but are still not included in the current Eurocode standards (CEN, 2005).

Although this method has been used in building construction based on the recommendations in ModelCode (2010), there are no clear guidelines or restrictions of how to utilize this reinforcement configuration with respect to large and heavily reinforced frame corners. The dimension used in those cases may be far larger than the ones studied in tests and consequently a different behaviour may be obtained. For that reason, the structural response of heavily reinforced structures is of interest since detailing with loop connections also has potential to be suitable for bridges, tunnels and retaining walls.

1.2 Aim

The aim of the thesis was to investigate to which extent it was possible to implement loop connections in large concrete frame corners, heavily reinforced with multiple layers of reinforcement. Structures that have long dimensions out of the plane of the corner were of main interest, such as tunnels, bridges and retaining walls.

To ensure the aim, the following objectives were stated:

- Understand and describe the failure modes appearing in concrete frame corners when using loop connections.
- Compare theoretical moment capacities for loop connections with capacities from

experiments and FE-analyses.

- Study the effect of increased reinforcement ratio when detailing with loop connections

1.3 Method

A comprehensive literature study was carried out to gain knowledge and understanding of frame corners, which treated the structural behaviour in general and conventional reinforcement detailing. In addition, available research published on the subject of loop connections, bond-slip models and non-linear finite element modelling of concrete structures were studied.

The structural response of frame corners was analysed using the finite element software ABAQUS 2017 v.2.7.3. Different levels of complexity were studied to find an appropriate model to describe the failure mechanisms of loop connections. Important choices regarding material parameters and how they were treated in the finite element software were studied continuously. To obtain reliable results, an appropriate interaction model describing the interaction between reinforcement and concrete had to be established together with representative material models. This was done through analysing a pull-out test according to existing experimental data, where the following two models to describe the interaction were considered:

- Spring elements
- Cohesive surface interaction

Further on, finite element analyses of frame corners with loop connections were carried out. First, with reinforcement in one layer where the model was verified against experimental results published by Johansson (2000b).

Finally, analyses on a case study with large dimensions and reinforcement in two layers were established. The structure was a frame corner analysed at ELU Konsult AB for an underground structure planned to be built at Skeppsbron, Gothenburg, where the loop connections have been designed according to the available recommendations in Model Code 2010. Further, the same structure was increased in reinforcement ratio to see how the structural behaviour would differ. A schematic figure over the workflow of the thesis is presented in Figure 1.2.

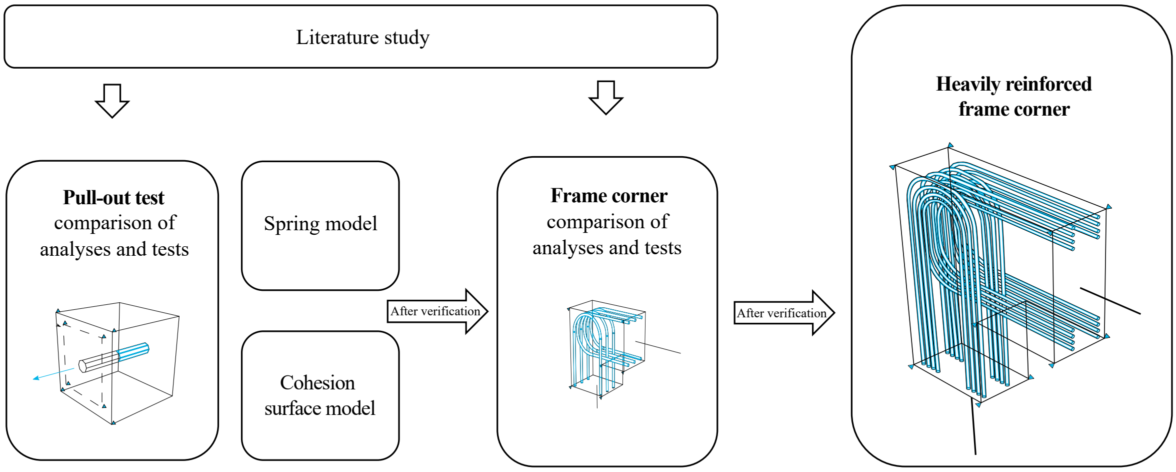

Figure 1.2: *Methodology flow chart*

1.4 Limitations

The scope of this thesis is focused on structures with long dimensions out of the plane such as tunnels and bridges, consequently treating middle sections with relatively low thickness where plane strain condition is fulfilled. Also, while many structures may be subjected to both opening and closing moments during its lifetime, this thesis treats frame corners loaded with closing moments.

The extent of this analysis focused on short time loading for static conditions, limited to consider ultimate state. In addition, 90° corners without haunches or deviating geometric properties were studied and possible construction joints from different casting periods were neglected.

Lastly, to save computational power the FE-model was simplified to mainly study the corner in detail and not the whole frame structure, as the corner part of the structure was of main interest and required to be analysed thoroughly. Other failure modes that could occur on the structure, outside of the boundary of the corner, were consequently not considered in detail.

1.5 Outline

This thesis consists of four main parts. The theory described in **Chapter 2** is presented to introduce the reader to the concept of frame corners and how the difference between positive and negative moments are treated in design. In addition, this chapter includes failure modes, stress distribution and influencing parameters when using loop connections, as well as available design recommendations. **Chapter 3** focuses on the material behaviour of reinforced concrete and gives the reader information for assessing the workflow and presented results. This chapter also contains the theory behind bond behaviour and available modelling techniques in finite element software.

In **Chapter 4** the verification of the numerous numerical models is presented. Initially, in Section 4.1, a study treating different bond modelling techniques are presented. These techniques were used in a pull-out test and compared with test data from "*Bond of reinforcement in self-compacting steel-fibre-reinforced concrete*" (Jansson et al., 2012).

Secondly, in Section 4.2 the analyses of the frame corner with one layer of reinforcement are presented. The results from these analyses are verified against laboratory tests to ensure that the finite element analyses represent the response properly. The chosen data to compare with is extracted from "*Structural behaviour in concrete frame corners of civil defence shelters*" (Johansson, 2000b) as it contains comprehensive test data regarding frame corners exposed to closing moments.

Chapter 5 contains the numerical analyses on a case study; a large frame corner with reinforcement in two layers, and all associated results. It also contains the numerical analyses and results of the same structure with increased reinforcement ratio. Finally, summarising conclusions and suggestions for future research are given in **Chapter 6**.

2
Theory

The purpose of this chapter is to introduce the reader to the concept of frame corners and how the reinforcement configuration is treated today according to rules and requirements. In addition, the aim is to give the reader enough theoretical background required to follow and understand possible failure modes that arises when using loop connections and to be able to correctly interpret the results of the analyses.

2.1 Frame corners

Frame corners are structural units consisting of two members joined together forming a corner. However, these corners do not always have 90° angle as presented in Figure 2.1, though this is the most common and the only type treated in the scope of this thesis.

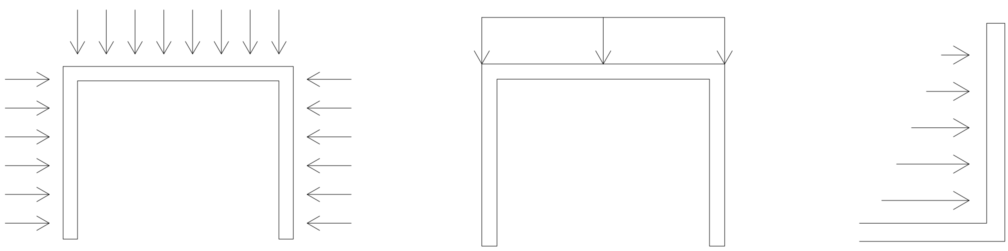

(a) *External loads* **(b)** *Self weight* **(c)** *Earth pressure*

Figure 2.1: *Example of typical loading situations for frame corners*

The structural behaviour of single members like columns and beams has over the years been widely studied especially separately but also when combined in joints. However, the best configuration of the reinforcement in these types of corners are not always given but summarised by Nilsson (1973) as:

- The joint should be able to withstand at least the same ultimate moment as the adjacent members, resulting in a failure risk of equal magnitude anywhere in the structure.
- If the first condition is not fulfilled the reinforcement in the joint should be designed with enough ductility to enable redistribution.
- When a corner is subjected to bending crack propagation initiates. Consequentially the crack widths should be limited to an acceptable value.
- The reinforcement should be easy to mount and manufacture.

Even if the strength of the corner is of high importance, especially for heavily loaded structures such as bridges and tunnels, it must also show a ductile behaviour preventing a brittle failure leading to total collapse. The ductility of the corner is governed by the ability for redistribution and highly dependent on the reinforcement configuration of the connected members (Johansson, 2000b). In short, it is important that the reinforcement yields before the concrete is crushed or burst in a brittle matter.

Concrete frame corners with moment rigid connections can be divided in two types: closing and opening corner, presented in Figure 2.2. These two actions will obviously give rise to very different failure modes and must be treated separately in design, described in the following two sections.

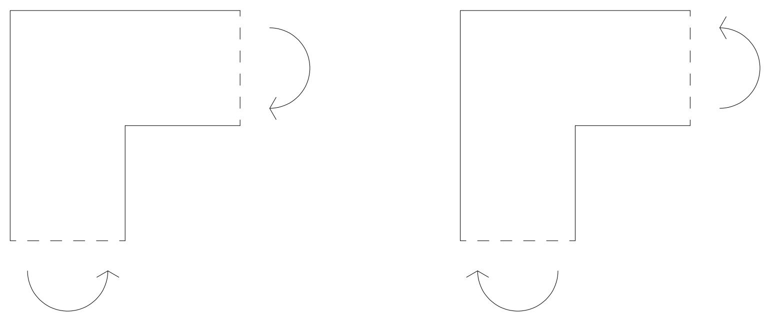

(a) *Closing corner* **(b)** *Opening corner*

Figure 2.2: *Schematic figure of moment rigid frames loaded with opening/closing moment*

2.1.1 Closing moment

A frame corner subjected to a negative moment will be exposed to closing of the corner, as illustrated in Figure 2.2a, causing confinement of the concrete in the inner part of the corner. Therefore, a corner subjected to a negative moment is said to be governed by the concrete compressive strength. Also, this type of loading situation is easier to design for in comparison to opening of the corner since the internal forces after cracking can be balanced by a proper reinforcement detailing more easily (Johansson, 2000b).

Even though the corner should technically have a higher strength compared to the rest of the structure, it has been shown in experiments that in some cases the concrete fails before the yielding of the tensile reinforcement, resulting in lower capacity than expected. The failure modes appearing in these cases are according to Johansson (2000b):

- Spalling of the concrete at the outside of the corner, resulting in anchorage failure.
- Premature crushing of the concrete at the inside of the corner.
- Crushing of the diagonal compressive strut within the corner.

However, since the scope of this thesis treats structures under plane-strain condition, it is mainly the latter two that are of interest. For high reinforcement ratios, premature crushing of concrete at the inside of the corner has shown to be highly possible, being dependant on the concrete compressive strength, reinforcement ratio and steel strength. Though, at the same time high multi-axial compressive stresses prevents this failure to appear. This is not always the case in the diagonal compressive strut, and for large reinforcement ratios crushing of the concrete might appear in this region (Johansson, 2000b).

Bending cracks are expected to initiate where high tensile stresses are concentrated, starting from the outside at the edge of the corner area, propagating inwards. This crack pattern is illustrated in Figure 2.3. Minor, less severe bending cracks may also appear along the length of the adjoining members.

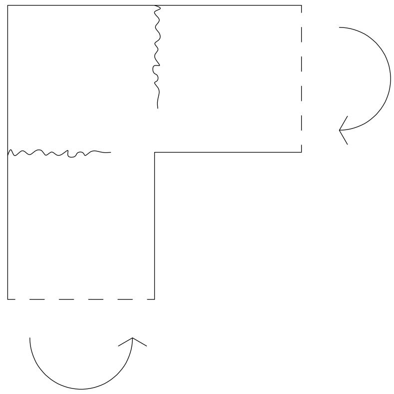

Figure 2.3: *Expected crack pattern, at the boundary of the corner area, for a frame subjected to a closing moment, reproduced from Nilsson (1973)*

The strut and tie model presented in Eurocode (CEN, 2005) describes the force patterns of a frame corner subjected to a negative moment (tension at outer border), for cases when the adjacent members have approximately the same dimensions ($h_1 \approx h_2$), see Figure 2.4a. The conventional detailing of this type of corner follows as presented in Figure 2.4b, clearly showing the need for tension reinforcement at the outer border of the corner.

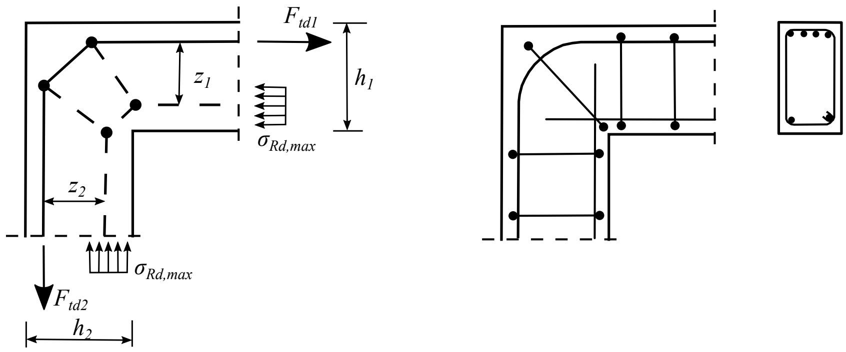

(a) *Strut and tie model* **(b)** *Detailing*

Figure 2.4: *Design recommendation of closing frame corner, reproduced from Eurocode (CEN, 2005)*

2.1.2 Opening moment

A positive moment, resulting in opening of the corner, may appear in different kind of structures and loading situations. One example is a retaining wall subjected to earth pressure, presented in Figure 2.1c. In stage I (before cracking), theory of elasticity can be used to calculate the stress state in corners and joints; even though this is not valid in stage II and III it gives a good indication of where expected cracks will appear. As shown in Figure 2.5, the stresses (σ_x) initiated from bending have their peak at the inside of the corner explaining the risk of crack initiation from this intersection.

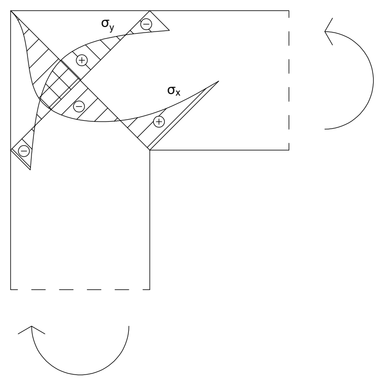

Figure 2.5: *Tensile (positive) and compressive (negative) stress distribution at a corner subjected to positive moment in the elastic stage, reproduced from Nilsson (1973)*

Further on, this loading situation leads to formation of tension cracks from the inner corner, propagating inwards presented in Figure 2.6a. In addition, the tensile stresses going across the diagonal of the corner (σ_y), seen in Figure 2.5, might in some cases cause a tensile crack. This gives rise to a crack pattern similar to Figure 2.6b (Nilsson, 1973).

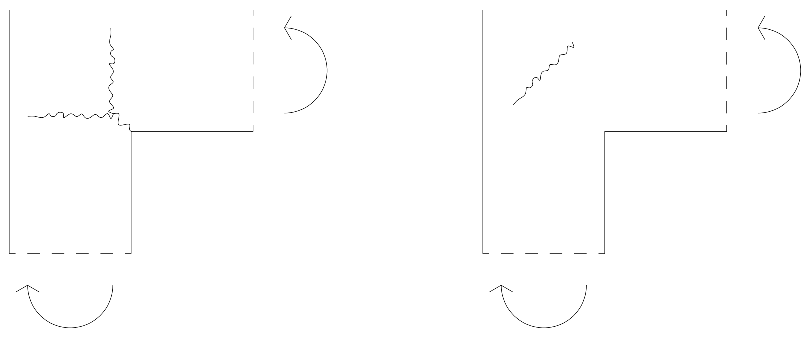

(a) *Crack from inner corner* **(b)** *Diagonal crack*

Figure 2.6: *Expected crack pattern for a frame subjected to an opening moment, reproduced from Nilsson (1973)*

The strut and tie model recommended by Eurocode (CEN, 2005) describes the force patterns of a frame corner subjected to a positive moment. One example, where the adjacent members have the same dimensions ($h_1 \approx h_2$), is presented in Figure 2.7a. The two types of conventional detailing for an opening corner is accordingly presented in figure 2.7b, clearly showing the need of tension reinforcement at the inner border of the corner.

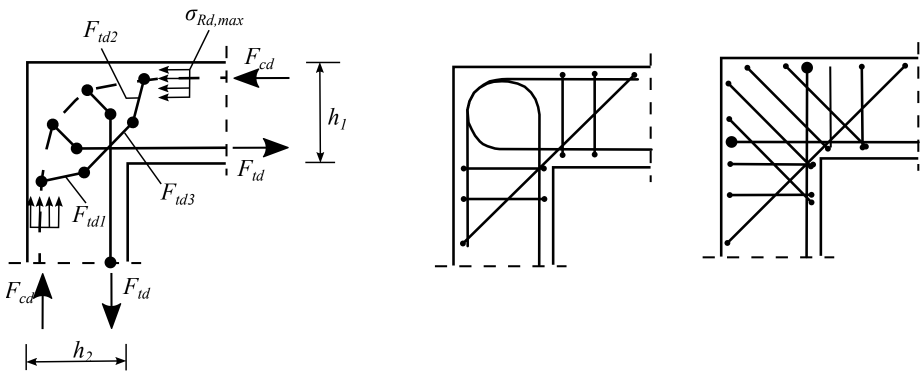

(a) *Strut and tie model* **(b)** *Detailing*

Figure 2.7: *Design recommendation of opening frame corner, reproduced from Eurocode (CEN, 2005)*

2.2 Loop connections

Loop connections describe the configuration of reinforcement bars formed as loops, both exiting and entering the same concrete member, see Figure 1.1b. Loops connected to different members are placed alternately within the joined structure with a certain distance from each other. This type of reinforcement configuration is most commonly used today in slabs, where also most of the research has been carried out.

2.2.1 Failure modes

A structure with loop connection reinforcement has been shown to mainly exhibit three failure modes. These are: crushing of concrete due to radial stresses, rupture of the reinforcement bars, or splitting of the joint concrete in the plane of overlapping loops, crack (1) and (2) in Figure 2.9. The aim is that none of these failure modes happen before the reinforcement yields, to ensure a ductile failure of the structure (Dragosavic et al., 1975).

When a reinforcement bar changes direction it will give rise to a radial compressive pressure according to Figure 2.8a. These stresses force the concrete to a lateral expansion that tries to split the concrete, shown in Figure 2.8b. This might occur using conventional detailing; however loop connections increase the risk due to the 180 °change of direction of the bars. Furthermore, due to the lack of counteractive forces at the border of the frame corner, this part is particularly exposed and spalling of the corner is likely to happen, resulting in anchorage failure (Johansson, 2000b). However, an advantage of the curved part of the loop is the increased anchorage capacity, generated from an additional friction resistance caused by the radial pressure. This makes a complete pull-out of the reinforcement failure nearly impossible compared to when the bars are geometrically straight (Grassl, 1999).

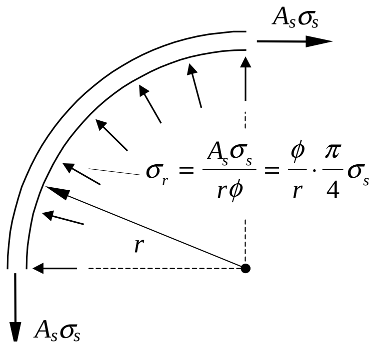

(a) *Radial stresses*

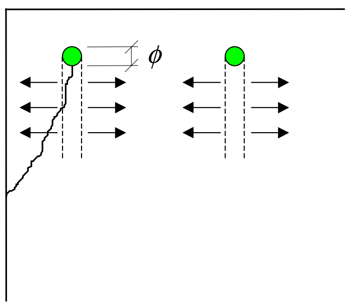

(b) *Lateral stresses*

Figure 2.8: *Schematic view of stresses arising when a reinforcement bar changes direction (Johansson, 2000b)*

Studies on loop connections subjected to bending was performed early by Dragosavic et al. (1975), with loops located in joints between slabs. The observed crack pattern is shown in Figure 2.9, viewed from above, caused by stresses in between the overlapping reinforcement bars. The cracks appear where the tensile stresses have the highest magnitude, as a result from the formed compressive stresses.

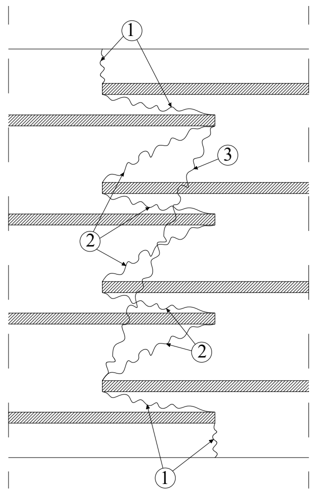

Figure 2.9: *Crack pattern in a slab with loop connections, numbering illustrates the order the cracks appear, reproduced from Dragosavic et al. (1975)*

Here the observed crack pattern from the experiment is marked with numbers (1)-(3). Each loop exerts lateral outward-directed forces which are resisted by the adjacent loops. This applies for all loops apart from the outermost two where the force must be resisted by the concrete solely, which subsequently gives the first crack initiation at position (1). In some experiments, crack (2) is the next one to appear and in some, crack (3) may be formed, extending over several loops. If transverse reinforcement is used it results in less cracking of type (1) and (2) and more extensive cracking perpendicular to the plane of the loops (Dragosavic et al., 1975).

2.2.2 Influencing parameters

Several parameters influence the load capacity when loop reinforcement is used, defined in Figure 2.10:

- Loop radius
- Bar diameter
- Bond between reinforcement and concrete
- Concrete cover
- Transverse reinforcement
- Width of the beam
- Material quality of the concrete and reinforcement
- Lap length of the loop
- Spacing of the loops

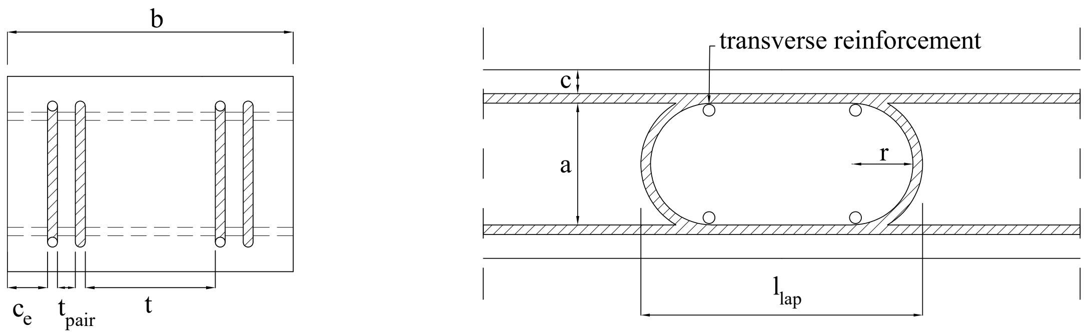

(a) *Transverse section* **(b)** *Longitudinal section*

Figure 2.10: *Definition of influencing parameters on loop connections*

The loop radius (r) has a direct relation to the pressure on the concrete in the splice zone, resulting in both concrete crushing within the loop and tensile failure in the lateral direction. The risk for both types of failures to appear decrease with increased loop radius.

Furthermore, an increased bar diameter (ϕ) can transmit larger forces resulting in higher radial pressure. In the same way, a smaller bar diameter will decrease the risk of the two failure modes mentioned earlier. In addition, a smaller bar diameter results in a higher perimeter to cross section ratio and thereby a higher bond resistance relative the area.

The distance from the outer loop to the edge, the side concrete cover (c_e), has also been proven to have a great influence on the load capacity. An increased cover delays the development of the first cracks in a favourable way, presented in tests carried out by Dragosavic et al. (1975). Still, in case of spalling of the concrete in the outer loop, the reinforcement loses its anchorage and can no longer transfer the load. In this case, the remaining structure must carry the load, making the load capacity directly related to the total width (in case of constant reinforcement ratio). The influence of transverse reinforcement may prevent cracking between loops and in some cases resist spalling of the outer loop, dependent on how it is anchored. However, these must be manually placed between the loops and results in a more difficult mounting procedure. Furthermore, it should be noted that only bars inside the loops qualify as transverse reinforcement in the aspect of preventing cracking between the loops.

Moreover, increased concrete material properties will increase both the compressive and tensile strength. This leads to increased load capacity and delayed crushing or cracking. Increased steel tensile strength will delay the yield of the reinforcement but also lead to a more brittle behaviour. Both these material factors must be considered since a ductile failure mode is desired.

The lap length (l_{lap}) of the loop will determine the area of the in-situ cast concrete and thereby its availability to withstand radial stresses. An increased lap length might prevent side spalling, resulting in higher stiffness and load capacity, but has also shown a more brittle post peak behaviour (Grassl, 1999).

Regarding the influence of loop spacing, two different spacing can be distinguished. One between loop pairs (t) and one within the pairs (t_{pair}). Having a distance (t) being to small results in decrease of the bond strength. However, as the distance between two reinforcement pairs (t_{pair}) increase, the angle (θ) of the compressive strut in between decrease and the tensile component that must be resisted becomes larger. Same goes for the spacing within a pair. The most unfavourable case is when the bars are equally placed, i.e. evenly distanced through the cross section. The influence of this was briefly studied by Johansson (2000b) but showed not to have any influence worth mentioning on the bearing capacity. In practice the loops are commonly placed with abutment.

2.2.3 Design recommendations

As mentioned in the introduction, design recommendations for loop connections are not yet presented in Eurocode (CEN, 2005), but some guidelines are to be found in Model Code (CEB-FIB, 2010) and more detailed in Bulletin 43 (CEB-FIB , 2008). Important to mention, though, is that the recommendations presented in the two latter are valid for usage between solid slabs where continuity is demanded. The recommendations are based on guidelines developed by Dragosavic et al. (1975) after extensive experimental investigations.

The configuration of the loop connection together with the radial stresses ($\sigma_{c.rad}$) that follows, are illustrated in Figure 2.11.

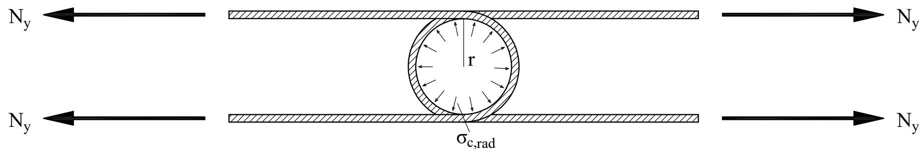

Figure 2.11: *Radial stresses in loop connections, reproduced from Modelcode (CEB-FIB, 2010)*

The inclined transverse compressive strut, originating from the radial stresses, is schematically shown in a strut and tie model in Figure 2.12. This compressive strut transfers the tensile force from one element to another between the overlapping loops. Further, the inclination gives a transverse tensile force that needs to be balanced. Due to high bearing stresses inside the loop, local splitting stresses between the loop and the strut may appear.

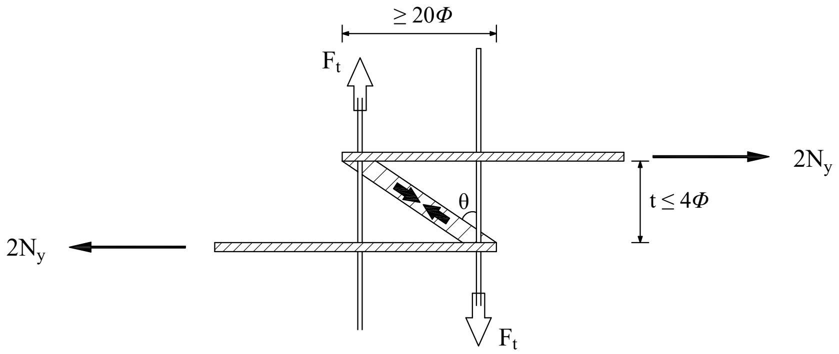

Figure 2.12: *Stresses in the in-plane direction, reproduced from Modelcode (CEB-FIB, 2010)*

Consequently, the transverse reinforcement must be placed between the two ends inside the loop to balance the tensile force (F_t). The transverse force can be calculated as presented in Equation 2.1 according to Bulletin 43 (CEB-FIB , 2008).

$$F_t = 2N_y cot\theta \tag{2.1}$$

In addition, it is mentioned that the overlapping length (l_{lap}) of the loops should not be less than the height of the U-bar but larger than 20ϕ. Finally, the spacing (t) between overlapping loops must be less than 4ϕ (CEB-FIB , 2008).

Design recommendations for loop connections in slabs have been developed and presented in Model Code 2010 (CEB-FIB, 2010), where the radius of the loop should satisfy the demand presented in Equation 2.2.

$$r \geq max\left(\frac{\pi \cdot \phi}{4}\frac{f_{yd}}{\sigma_{c.rad}}, 8\phi\right) \tag{2.2}$$

Further, to be able to limit the bearing stresses the condition in Equation 2.3 needs to be fulfilled.

$$\sigma_{c.rad} \leq min\left(f_{cd} \cdot \sqrt{b_i/\phi}, 3f_{cd}\right) \tag{2.3}$$

where: $b_i = max\left(2 \cdot (c_e + \frac{\phi}{2}), t\right)$

2.2.4 Estimated capacity according to Dragosavic et al.

Dragosavic et al. (1975) established a reasonably good estimation to calculate the loop moment capacity (M_l), after comprehensive experimental investigations. This was performed on slabs with loop connection undergoing a bending moment. The moment capacity comprising of n pairs of loops is expressed in Equation 2.4.

$$M_l = n \cdot A_a \cdot z \cdot \sigma_{al} \tag{2.4}$$

Maximum steel strength, (σ_{al}) presented in Equation 2.5, describes the strength of the loop attained before failure. The equation was derived through trial and error taking lap length (l_{lap}), area of transverse reinforcement (A_{ad}), area of cross section for one loop (A_a) and the tensile strength of the concrete (f_{ctk}) into consideration.

$$\sigma_{al} = 230 \cdot f_{ctk} \cdot (0.7 + 0.03\frac{l_{lap}}{\phi}) \cdot (1 + 0.25\frac{A_{ad}}{A_a}) \cdot \alpha \tag{2.5}$$

where: $\alpha = (0.5 + 0.05\frac{c_e}{\phi}) \leq 1.0$

Apart from this a few other conditions has to be fulfilled, the lap length $l_{lap} \geq (10\phi, 2r, 3t_{pair})$, the radius $r \geq 2.5\phi$ and lastly the concrete cover $c_e \geq 5\phi$. No upper limits were given though with the restriction that it is only applicable to connections largely similar to the performed tests. To ensure the reinforcement is yielding when the maximum capacity is reached, a design recommendation is stated as $\sigma_{al} \geq f_y$ (Dragosavic et al., 1975).

When comparing the moment capacity in Equation 2.5 to the estimated capacity of the cross section with force equilibrium, some important factors can be distinguished. Equation 2.5 takes crushing of the concrete within the loop in consideration, together with the effect of side spalling. However, the expression does not have any factor representing the strength of the reinforcement. In some cases, this results in higher steel stresses (σ_{al}) than the yield strength, before the concrete on the inside of the loop crushes, which would not occur in reality.

The risk of side spalling is taken into account with an alpha factor from where the critical cover can be estimated. As soon as (c_e) undergoes 10ϕ, as presented in Equation 2.6 the moment capacity will be reduced with a factor, since alpha takes a value below 1.

$$c_e \leq \frac{0.5 \cdot \phi}{0.05} = 10\phi \tag{2.6}$$

In Dragosavic's performed experiments, which were used to verify the equation, the maximum strength reached were 84.0 kNm when having a cross sectional height of approximately 200 mm. This is mentioned for the reader to highlight the small loads and dimensions, when later on in this thesis presenting the results of the large and heavily reinforced structures.

2.2.5 Estimated capacity according to Hao

Hao (2004) presented a systematic study on the strength of flexural and tensile joints with loop connections. He did numerous experimental investigations of test specimens with in-situ joints as well as monolithic specimens with loop connections. This resulted in an empirical expression to compute the joint strength by considering the stress in the reinforcement loop at the critical section, taking into account among other parameters the compressive strength of concrete in the joint. This expression was based on 193 tests performed by different researchers and is presented in Equation 2.7.

$$\sigma_{al} = 236.22 \cdot f_{cu}^{0.14} \cdot e^{\frac{0.01 l_{lap}}{\phi}} e^{\frac{0.11 A_{ad}}{A_{at}}} e^{\frac{0.01 c_e}{\phi}} \phi^{-0.01} \tag{2.7}$$

In the same manner as in Section 2.2.4 Hao gave the design recommendation $\sigma_{al} \geq f_y$, ensuring that the reinforcement is yielding when the flexural capacity of the joint is reached. Furthermore, this resulted in an expression for estimating the loop moment capacity (M_l) according to Equation 2.8, under the assumption that the upper segment of the reinforcement loop are located in the compressive zone.

$$M_l = A_a \cdot \sigma_{al} \cdot \left(d - \frac{0.075 A_a \sigma_{al}}{f_{cu} b} \right) \tag{2.8}$$

if: $A_a \sigma_{al} \geq 0.3 f_{cu} b d$

If instead both loop segments are yielding in tension, Equation 2.9 are valid.

$$M_l = A_a \cdot \sigma_{al} \cdot \left(h - \frac{3 A_a \sigma_{al}}{f_{cu} b} \right) \tag{2.9}$$

if: $A_a \sigma_{al} < 0.3 f_{cu} b d$

The tests used to verify Equation 2.7 were a combination of the experiments presented in the paper by Hao (2004), in combination with results from Dragosavic (1975). In the experiments performed by himself a maximum strength of 32.5 kNm were reached with a cross sectional height of 0.150 m, which makes the moment of 84.0 kNm in Dragosavic's experiments the highest value used in Hao's study.

In addition, a number of conditions had to be met for Equation 2.7 to be applied. The loops should be of semicircular shape and have a diameter (ϕ) between 5 mm to 24 mm. In relation to this the concrete cover (c_e) should be in the range of (1.25-25)ϕ and the lap length (l_{lap}) between (10.5-39.5)ϕ . It is valid for concrete cube strength (f_{cu}) up to 66.6 MPa.

2.2.6 Estimated capacity according to Joergensen & Hoang

Joergensen and Hoang (2015) developed a model to estimate the strength of loop connections in slabs loaded in combined tension and bending. It was an extension from a model previously developed by the same authors for the case of only tension (Joergensen & Hoang, 2013). It neglects the tensile strength of concrete and consist of a sandwich model according to Figure 2.13. The first layer, of thickness x, transfers a uniaxial compression stress while the second layer include both rebars and carries a tensile force.

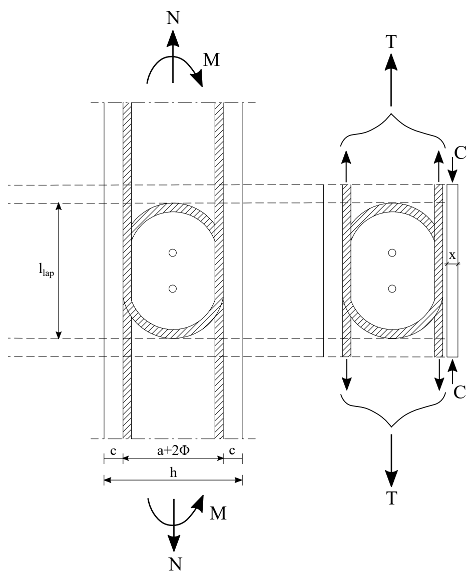

Figure 2.13: *Sandwich model to estimate moment capacity, reproduced from Joergensen & Hoang (2015)*

$$\frac{M(N)}{f_c b c^2} = min \begin{cases} \frac{1}{2}\frac{N_u}{f_c bc}\left(1 - \frac{N}{N_u}\left(\frac{t}{c} - \frac{N_u\left(1-\frac{N}{N_u}\right)}{f_c bc}\right)\right) & (a) \\ \frac{1}{2}\left(\frac{h}{c} - 1\right) & (b) \end{cases} \tag{2.10}$$

where: $\quad t = t_{pair}$

Hence, by taking in both the scenario of failure in the joint concrete as well as yielding of the reinforcement bars the following solution may be used to predict the pure tensile capacity (N_u):

$$N_u = min \begin{cases} max \begin{cases} N_{c\Phi_T=0} & ,concrete\ failure \\ N_c & ,concrete\ failure \end{cases} \\ N_y = n \cdot A_s \cdot f_y & ,yielding\ of\ rebars \end{cases} \tag{2.11}$$

In a case where transverse reinforcement is non-existing or neglected, ($N_{c\Phi_T=0}$) can be estimated according to Equation 2.12. If so, it should be noted that connections without transverse reinforcement have not been tested in the presented research, but this theoretical estimation has been shown to be applicable according to the authors (Joergensen & Hoang, 2015).

$$\frac{N_{c\Phi_T=0}}{vf_cA_c} = nl \begin{cases} \sqrt{\left(\frac{t}{l_{lap}}\right)^2 + 1 - \left(\frac{2n-1}{n}\frac{A_c^*}{A_c}\left(\frac{m}{l} - 1 + \frac{m}{l}\right)\right)^2} - \frac{t}{l_{lap}}\frac{m}{l} & ;if\ \alpha \geq \theta\ \&\ \alpha \geq \phi \\ \frac{\frac{2n-1}{n}\left(3-4\frac{t}{l_{lap}}\right)\left(1-\frac{m}{l}\right)\frac{A_c^*}{A_c}\left(\left(\frac{t}{l_{lap}}\right)^2+1\right)\left(5-3\frac{m}{l}\right)}{4+3\frac{t}{l_{lap}}} & ;if\ \alpha < \phi\ \&\ \frac{t}{l_{lap}} < \frac{3}{4} \\ \sqrt{\left(1 + \frac{t}{l_{lap}}\right)^2} - \frac{t}{l_{lap}}\frac{m}{l} & ;if\ \alpha < \theta\ \&\ \frac{t}{l_{lap}} \leq \frac{3}{4} \end{cases} \tag{2.12}$$

where: l, m and α are factors according to Joergensen & Hoang (2015)

The presented test results were verified for the case of pure tension, pure bending and with combined tension and bending. The tested slabs had a moment capacity of 71.7 kNm in pure bending at largest, with a height between 0.230-0.250 m and $4\phi10$ reinforcement .

Keeping the picture of a sandwich model in mind, it is clear that the thickness of the compression field (x) cannot be larger than the concrete cover, limited by Equation 2.10b. The model can thereby not predict a bending capacity which is larger than the moment obtained for $x = c$. For such case it would provide a conservative estimation.

2.2.7 Comparison of methods used to estimate the capacity of loop moment

Through a parametric study, the expressions presented under Section 2.2.4-2.2.6 were analysed. This to estimate if and how the moment capacity of larger structures, different than the slabs they were developed from, could be calculated when using loop reinforcement. To establish this, for a situation similar to a frame corner, the lap length (l_{lap}) was set equal to two times the loop radius ($2r$), which also represents the lever arm (z) between the top and bottom reinforcement within the loop. The lever arm was assumed to have a distance of $0.8h$. The normal tension force, which only could be accounted for in Joergensen's equation, was set to zero to mimic a pure bending case. Other fixed parameters during the analyses are presented in Table 2.1.

Table 2.1: *Summary of input used when comparing the estimated moment capacities*

$\boldsymbol{\phi}$ [mm]	$\boldsymbol{n}$ [-]	$\boldsymbol{b}$ [m]	$\boldsymbol{f_{cm}/f_{ctm}}$ [MPa]	$\boldsymbol{f_y}$ [MPa]
10	3	0.600	30/2.5	550

By varying the height within a range of 0.07-0.40 m the trend of the different moment capacities from presented equations could be estimated for larger cross sections. These were also compared to the conventional moment capacity (M_{Rd}) according to Eurocode, with the stress block factors $\lambda = 0.8$ and $\eta = 1.0$, and partial factors $\gamma = 1$, presented in Table 2.2 and Figure 2.14.

Table 2.2: *Moment capacities [kNm], comparison of results from different suggested equations with varying heights and c_e=0.100.*

$\boldsymbol{h}$ [m]	$\boldsymbol{M_{Rd}}$	$\boldsymbol{M_{l.Drago}}$ Eq. (2.4)	$\boldsymbol{M_{l.Hao}}$ Eq.(2.8)	$\boldsymbol{M_{l.Joerg}}$ Eq.(2.10)
0.07	7.8	6.6	6.2	4.6
0.10	11.2	10.2	9.3	11.1
0.15	17.4	17.2	14.7	17.5
0.20	23.6	25.6	20.6	24.0
0.30	37.0	46.6	33.6	37.0
0.40	50.8	72.0	48.7	50.0
0.50	63.0	103.0	66.2	62.9
0.60	76.0	139.0	86.1	75.9

It was found that Dragosavic's capacity corresponds rather well with the estimated capacity calculated with cross sectional force equilibrium, up to a height of h=0.20. However, for larger sectional heights it overestimates the moment capacity due to the fact it does not take the yielding of reinforcement into account. For the highest capacity of 139.0 kNm, the corresponding steel stress was 954 MPa, which is much higher than the yield strength. Though indicating that ductile failure through yielding definitely will happen before any other brittle failure.

The moment capacities according to Hao were slightly below the capacity according to Eurocode and only resulted in yielding of the reinforcement before the maximum capacity was reached when the height was 0.4 m or higher. Joergensen's equation estimated the capacity very similar to Eurocode but indicated a drop for the smallest heights.

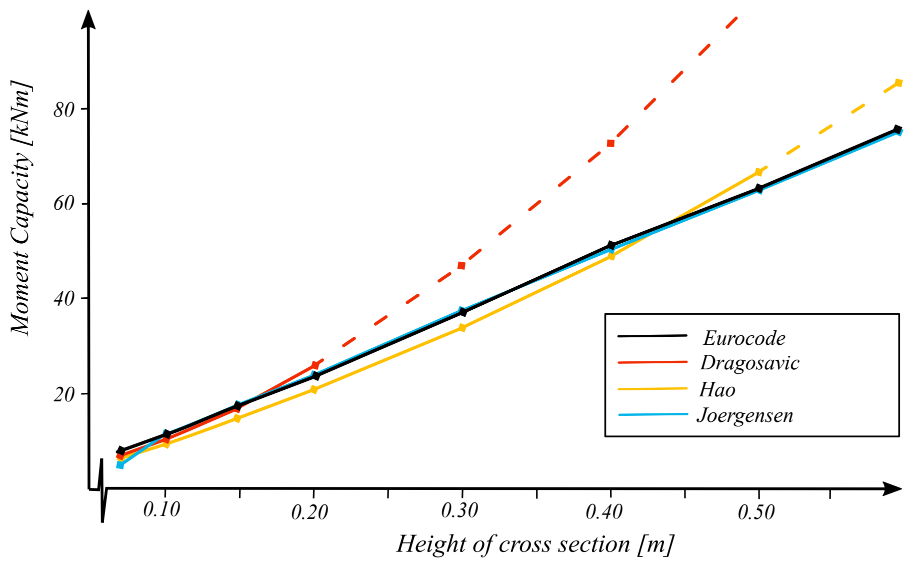

Figure 2.14: *Moment capacities compared to the estimated capacity, with varying heights*

Another aspect of interest was to distinguish if the equations accounted for the impact of the side concrete cover and the risk of spalling, presented in Table 2.3. The height of the cross section was fixed to 0.200 m and the side cover was varied between 0.025 m and 0.200 m.

Table 2.3: *Moment capacities [kNm], comparison of results from different suggested equations with varying side concrete cover, and h=0.200.*

c_e [m]	M_{Rd}	$M_{l.Drago}$ Eq. (2.4)	$M_{l.Hao}$ Eq.(2.8)	$M_{l.Joerg}$ Eq.(2.10)
0.025	23.6	16.0	19.1	24.0
0.050	23.6	19.2	19.6	24.0
0.075	23.6	22.4	20.1	24.0
0.100	23.6	25.6	20.6	24.0
0.125	23.6	25.6	21.1	24.0
0.150	23.6	25.6	21.6	24.0
0.175	23.6	25.6	22.1	24.0
0.200	23.6	25.6	22.7	24.0

When varying the thickness of the side cover it clearly shows in Figure 2.15 how the capacity is reduced linear after a certain limit in Dragosavic's equation and slightly exponentially decreasing with Hao's equation. While Eurocode and Joergensen does not take the side concrete cover into consideration, making the capacity constant. This is an important factor to keep in mind when having small covers on structures with finite thickness, as side spalling has shown to reduce the capacity in experiments performed by Grassl (1999), Johansson (2000b) among others.

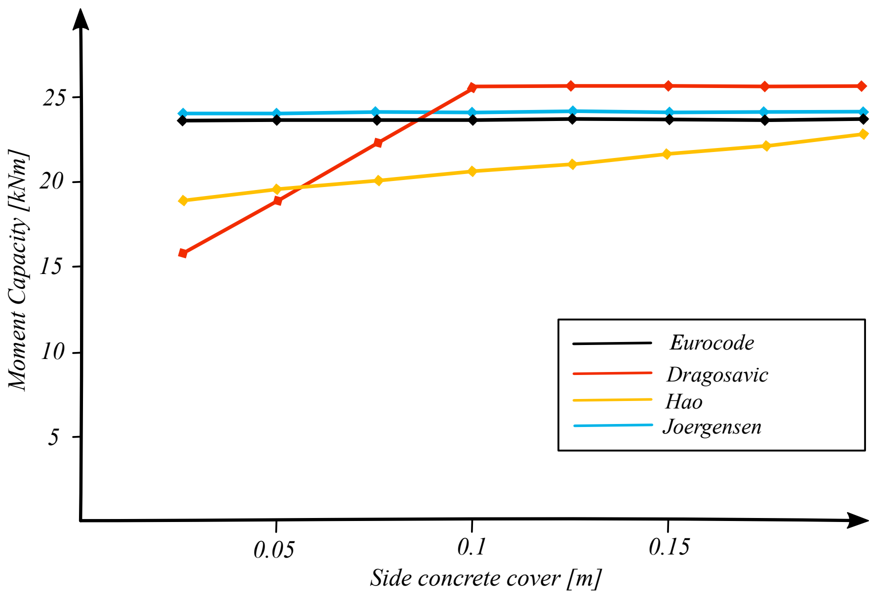

Figure 2.15: *Moment capacities compared to the estimated capacity, with varying concrete side cover*

3

Numerical modelling of reinforced concrete

This section intends to give an understanding of the material behaviour of reinforced concrete, the relevant chosen numerical modelling technique and a sufficient theoretical background to follow the results of the analyses. As mentioned earlier, the software ABAQUS was used in the finite element (FE) analyses to study the behaviour and structural response of the model.

The structural behaviour of reinforced concrete structures is highly complex. To describe the material response for concrete, which behaves different in tension and compression as shown in Figure 3.1a, the material models are often based on different theories describing each specific phase. The two main failure mechanisms are tensile cracking and compressive crushing of the concrete material. Linear elasticity in concrete is normally used when describing the initial uncracked phase while after cracking or close to compression failure the behaviour is described as non-linear.

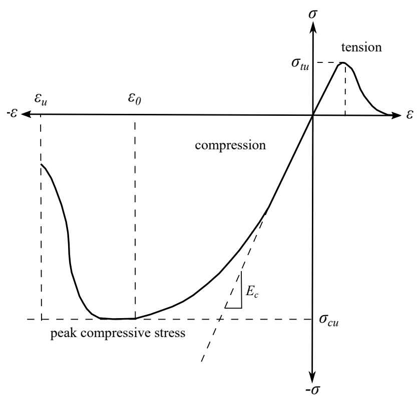

(a) *Concrete*

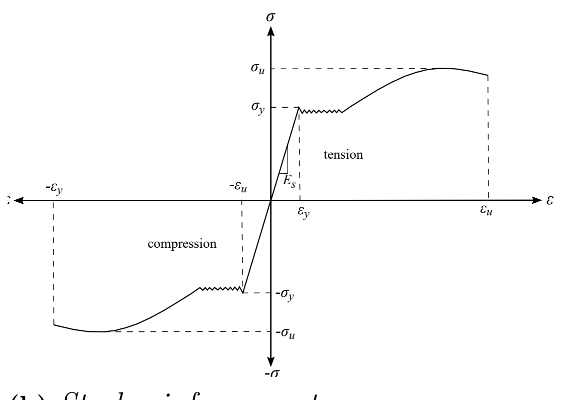

(b) *Steel reinforcement*

Figure 3.1: *Typical uni-axial stress-strain relations in structural materials*

The ductile response of reinforcement steel is properly described as linear elastic until yielding of the reinforcement. Thereafter it deforms plastically with some effect of strain hardening until failure, illustrated in Figure 3.1b.

3.1 Concrete under tension

The tensile behaviour of concrete before cracking is assumed to be linear elastic and thereby defined by the elastic modulus and peak tensile stress. The most accurate model to describe the post-peak tension behaviour is an exponential function derived by Hordijk (1992). This curve can also be approximated by a bilinear model proposed by Hillerborg (1985). Both theories are compared in Figure 3.2, and dependent on material parameters such as mean tensile strength (f_{ctm}) and fracture energy (G_f).

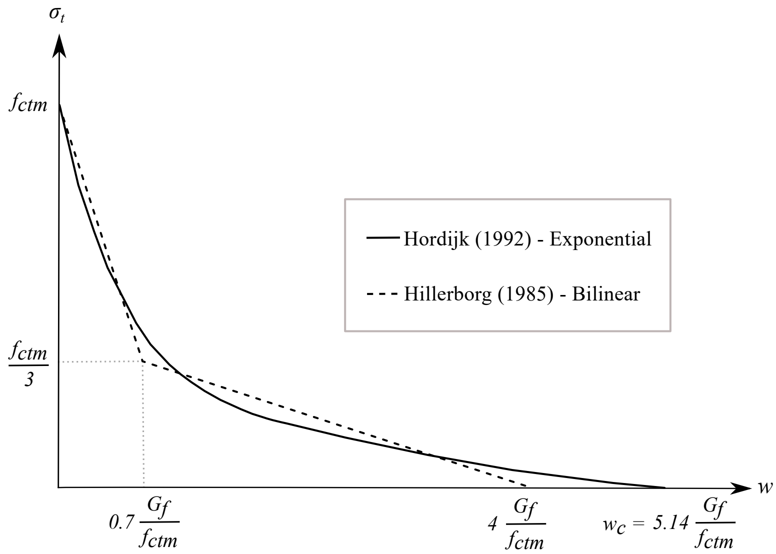

Figure 3.2: *Tension softening behaviour proposed by Hordijk (1992) and Hillerborg (1985)*

In general, the crack propagation of concrete in finite element analyses can be described by two main approaches. They can either be considered as discrete cracks with a physical separation of the two crack surfaces, or considered in a continuum approach where they are distributed (smeared) over the elements, as illustrated in Figure 3.3.

(a) *Discrete crack* **(b)** *Distributed (smeared) crack*

Figure 3.3: *Discrete and distributed cracks, reproduced from Malm (2016)*

When analysing the nonlinear material properties of concrete in large structures the smeared crack approach is the most common technique used today (Malm, 2016). The cracks appear in the integration points of the element and their effect is distributed over the whole element. Consequently, the post-peak softening behaviour of concrete is directly related to the element size and becomes mesh dependant.

In the distributed (smeared) crack model, two different approaches exist to describe the propagation of cracks; fixed (orthogonal) crack model and rotating crack model. The first, where the normal direction to the first crack is aligned with the direction of maximum tensile principal stress at the time of crack initiation. Whereon it memorises this crack direction, and subsequent cracks can only continue to form in directions orthogonal to the first crack. In the rotating crack model, a single crack can form at any point aligned with the direction of maximum tensile principal stress. Thus, it does not memorise the crack direction and the single crack direction rotates with the direction of the principal stress axis.

When the material reaches its tensile strength (f_{ct}), the material around the fracture zone unloads while micro-cracks are developed in front of a crack. This process can be described by a stress-displacement relation divided into one stress-strain part and one stress-crack opening part as presented in Figure 3.4. To generate a total stress-displacement relation the tension softening part must be dependent on the element size. This is solved by dividing the area under the curve with the crack band width - in this case chosen as the length of one element when the smeared crack approach is used (Dassault-Systèmes, 2014).

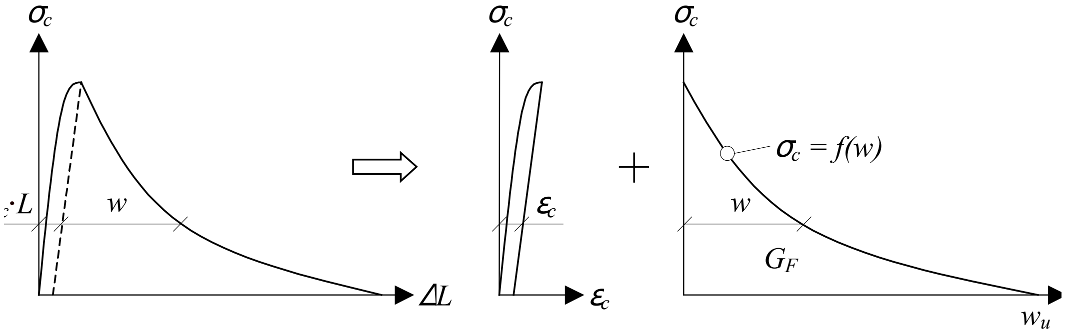

Figure 3.4: *Displacement divided into a stress-strain relation and a stress-crack opening relation, reproduced from Plos (1996)*

The area under the softening curve represents the energy released during crack opening. It is defined as the energy required to propagate a tensile crack of unit area. The higher the fracture energy (G_f), the more brittle the failure will be. The fracture energy is often determined by tests, but in absence of experimental data it can be estimated from Equation 3.1 according to Model Code (CEB-FIB, 2010).

$$G_f = 73 f_{cm}^{0.18} \tag{3.1}$$

where: f_{cm} = mean concrete compressive strength in [MPa]

In ABAQUS, the behaviour of concrete in tension is defined by the user provided uniaxial stress-displacement relation. In case of unloading after the tensile peak stress has been reached, the software will convert this curve to a plastic strain curve automatically based on the assumption of a damaged elasticity modulus. The cracking model assumes fixed cracks with the maximum of three cracks at a material point, in a three-dimensional model (Dassault-Systèmes, 2014).

3.2 Concrete under compression

The compressive strength is defined as the highest value for a specimen in uniaxial compression before failure (f_c). The response is elastic until approximately 40 percent whereon small micro cracks are formed, the stiffness decreases and becomes non-linear. After the maximum strength has been reached the curve decreases until the specimen is crushed. This post-peak part is called the softening phase (CEN, 2005).

The relation between the concrete stress (σ_c) and relative strain (ε_c), according to Eurocode (CEN, 2005), is described by Equation 3.2 and schematically shown in Figure 3.5 for short-term uniaxial loading.

$$\frac{\sigma_c}{f_c} = \frac{k\eta - \eta^2}{1 + (k-2)\eta} \tag{3.2}$$

where: $\eta = \varepsilon_c / \varepsilon_{c1}$

$k = 1.05 E_{cm} \left|\varepsilon_{c1}\right| / f_{cm}$

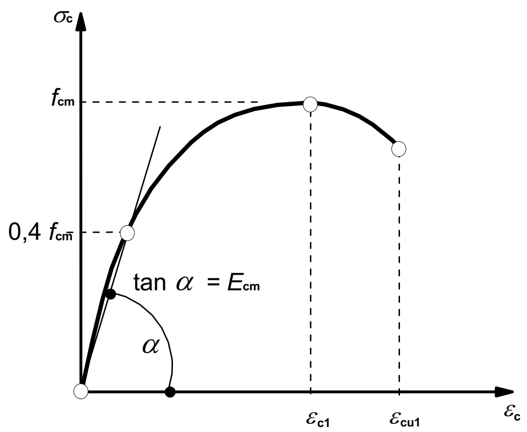

Figure 3.5: *Stress-strain relation for concrete in compression (CEN, 2005)*

3.3 Steel reinforcement

The stress–strain relation curves for steel obtained from experiments, introduced in Figure 3.1, are seldom directly applied in analyses of reinforced concrete structures. Instead, a theoretical model idealized from the experimental curves are commonly used. It is simplified with an elastic-plastic material model, Equation 3.3.

$$\sigma_s = \begin{cases} E_s \varepsilon_s, & \varepsilon_s \leq \varepsilon_y \\ f_y & \varepsilon_s > \varepsilon_y \end{cases} \tag{3.3}$$

This simplification does not take the strain hardening into account but gives a result on the safe side, as the steel is assumed to constantly yield after the yield strength of the material is reached. The same properties are applied for compression as for tension as shown in Figure 3.6a.

The strain hardening can be accounted for in a simplified way with a yield plateau, followed by a linear hardening until maximum strength is reach. This is illustrated in 3.6b.

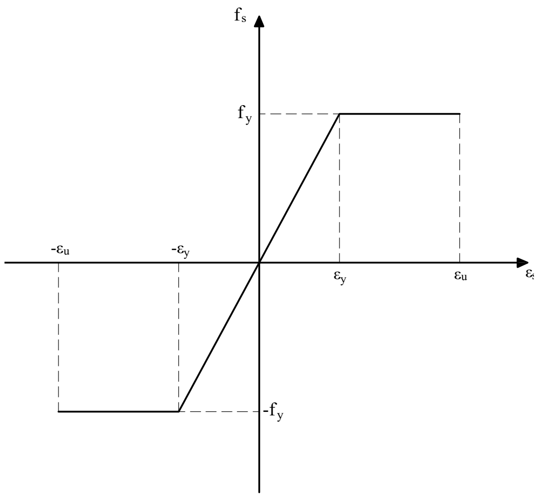

(a) *Without strain hardening*

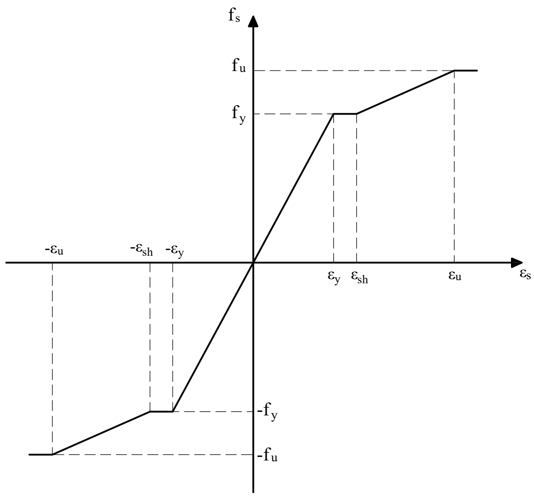

(b) *With strain hardening*

Figure 3.6: *Simplified stress-strain for steel reinforcement*

3.4 Material models

The ductile properties of steel reinforcement are well described by a plasticity model while the brittle properties of plain concrete are better described by a damage model or a combination by both of them. These three models and their different behaviours are described as illustrated in Figure 3.7 (Alfarah et al., 2017).

The plasticity model has constant stiffness when unloaded but a remaining plastic strain. While the damage model shows degraded stiffness, but without any plastic deformation. Consequently, the plastic damage model has a combined behaviour. If however damage is not specified, as in the case of static loading where no unloading takes place, the latter model behaves as a plasticity model (Dassault-Systèmes, 2014).

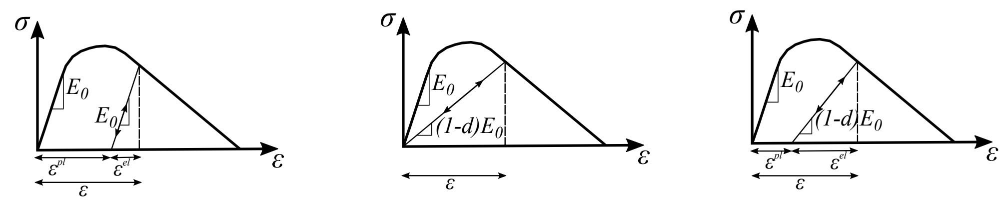

(a) *Plasticity Model* (b) *Damage Model* (c) *Plastic Damage Model*

Figure 3.7: *Representation of material behaviour using different models, reproduced from Alfarah et al. (2017)*

Concrete in uniaxial compression (and tension) is typically very brittle by nature, but in case of compression in multiple directions the response becomes more plastic and ductile. When concrete is subjected to biaxial compression the strength of the material changes. In the case where the compression in both directions are equal, $\sigma_1 = \sigma_2$, the strength increases with 16 percent presented in Figure 3.8. The uniaxial stress curve is therefore modified in the numerical analyses with a factor 1.16 in case of biaxial compression, represented by the quota f_{b0}/f_{c0} (Kupfer et al., 1969).

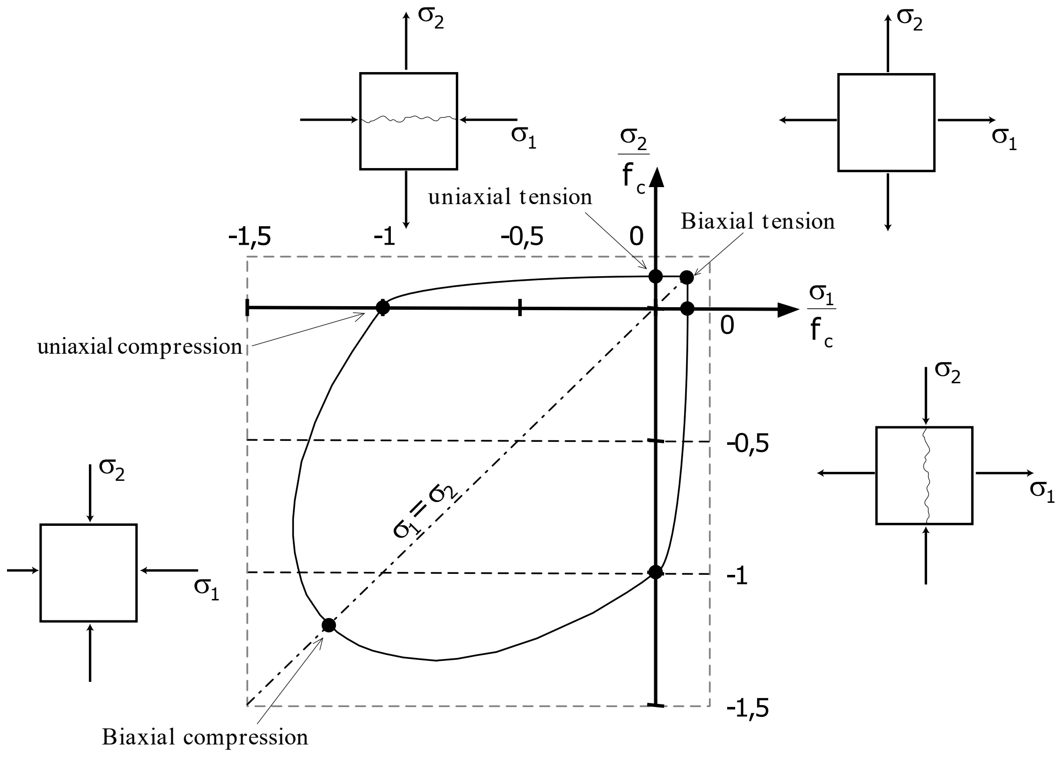

Figure 3.8: *Strength envelope of concrete under biaxial stress, reproduced from Malm (2006)*

At triaxial stress-states, the compressive strength can increase significantly, and the failure mode becomes even more ductile. The increase in compressive strength can be about 375% if the concrete is subjected to equal compressive stresses in three directions ($\sigma_1 = \sigma_2 = \sigma_3$) according to Eurocode (CEN, 2005).

In the Concrete Damage Plasticity (CDP) model in ABAQUS this behaviour is considered together with a number of other parameters. The model requires the modulus of elasticity (E_c), Poissons ratio (v_c), a description of the tensile and compressive stress-strain behaviour, as presented in Section 3.1 and 3.2, together with five plastic damage parameters. These parameters have been chosen as standard values according to ABAQUS recommendations and are presented in Table 3.1 (Dassault-Systèmes, 2014).

Table 3.1: *Plastic damage parameters used as input values in CDP model*

ψ	ϵ	f_{b0}/f_{c0}	K_c	μ
35°	0.1	1.16	2/3	0-0.00005

where: ψ = dilation angle
ϵ = eccentricity parameter
f_{b0}/f_{c0} = ratio of the equibiaxial compressive yield stress
K_c = parameter dependent on stress invariants
μ = viscosity parameter

During the softening regime, severe convergence difficulties might occur in an implicit analysis. The rate of convergence can be improved with the viscoplastic regularization as the viscoplastic system relaxes and permits stresses outside the yield surface, to that of the inviscid case as $\Delta t/\mu \to \infty$, for a characteristic time increment. The strain rate tensor ($\dot{\varepsilon}_v^{pl}$) is defined according to Equation 3.4, where the viscosity parameter (μ) represents the relaxation time of the viscoplastic system. The viscous stiffness degradation (d_v) can in a similar matter be defined as Equation 3.5 for the system.

$$\dot{\varepsilon}_v^{pl} = \frac{1}{\mu}(\varepsilon^{pl} - \varepsilon_v^{pl}) \tag{3.4}$$

$$\dot{d}_v = \frac{1}{\mu}(d - d_v) \tag{3.5}$$

Combined, this gives rise to a stress-strain relation of the viscoplastic model given as Equation 3.6.

$$\sigma = (1 - d_v)\boldsymbol{D}_0^{el} : (\boldsymbol{\varepsilon} - \boldsymbol{\varepsilon}_v^{pl}) \tag{3.6}$$

Using a small value for the viscosity parameter, in comparison to the time increment, typically improves the convergence rate of the model without compromising the numerical results (Dassault-Systèmes, 2014). This has shown to be the case if the parameter is in a range of 0 to 0.00005, as presented in Table 3.1 (Demir et al., 2018). Anyhow, a sensitivity analysis for this parameter, to obtain the proper results, is still recommended.

3.5 Bond interaction

The transfer of forces between concrete and reinforcement influence the performance of a structure in many ways; this interaction is commonly described as bond. In ultimate state, bond influences the rotational capacity of plastic hinge regions and anchorage strength.

3.5.1 Bond transfer phenomena

The bond action between concrete and reinforcement is a complex transfer phenomenon of mainly longitudinal forces. The initiated stresses are transferred mostly through the reinforcement ribs and the contact point with the concrete. Since these stresses arise with radiate outward angle they can be divided into components, shown in Figure 3.9. One in the normal direction to the mean surface, called splitting stress and one in the longitudinal direction, called bond stresses. In this direction shear stresses acts together with friction.

If the tensile ring stresses, formed in the surrounding concrete to balance the inclined force, becomes larger than the tensile capacity of concrete, splitting cracks will occur (Jansson et al., 2012).

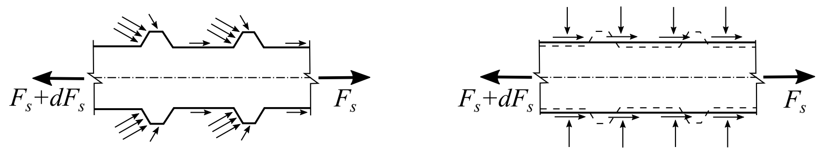

(a) *Contact stresses on reinforcement bar*

(b) *Components of contact stresses on mean surface*

Figure 3.9: *Schematic figure of contact stresses, reproduced from Plos (1996)*

The relation between traction and relative displacement for the interface can be expressed through an elastic stiffness matrix, presented in Equation 3.7. It describes both the longitudinal, normal and transverse direction.

$$\begin{bmatrix} t_l \\ t_n \\ t_t \end{bmatrix} = \begin{bmatrix} D_{11} & D_{12} & D_{13} \\ D_{21} & D_{22} & D_{23} \\ D_{31} & D_{32} & D_{33} \end{bmatrix} \begin{bmatrix} u_l \\ u_n \\ u_t \end{bmatrix} \tag{3.7}$$

3.5.2 Modelling of bond interaction

A common way to model the bond interaction, when analysing the structural behaviour of full-scale structures by looking into deflections and ultimate failure, is by assuming the reinforcement has complete interaction with the concrete and by that no separate degrees of freedom. In computer analyses, the reinforcement is modelled as embedded in the concrete. This method relates to a perfect bond condition and strengthens the concrete elements in the longitudinal direction of the bar without any slip occurring. In addition, Hao (2004) states in his report on loop connections in precast component joints, that implementations of bond stress-slip in the finite element analysis most often has negligible effect and by that promotes the reinforcement to be modelled as embedded also in more detailed analyses.

However, this method does not capture the nature of the interaction accordingly and does not display a proper cracking pattern as the effect of tension stiffening is not accounted for correctly. When a crack occurs, the high stresses in the reinforcement are directly transferred to the concrete element close by, resulting in all elements cracking. Instead, when accounting for bond-slip in the interaction, this tension stiffening effect is directly reflected in the structural response and accounts for the resulting higher stiffness in the cracked region (Plos, 1996).

Another way to describe the bond interaction is through a stress-slip relation. This depends on several different parameters, i.e. type of reinforcement, concrete strength, orientation of reinforcement, among other things. Therefore, the relation between bond stress and slip, presented by Modelcode (CEB-FIB, 2010), can only be seen as an average description for a wide range of cases, seen in Figure 3.10. For design bond stress-slip curves further investigations are required.

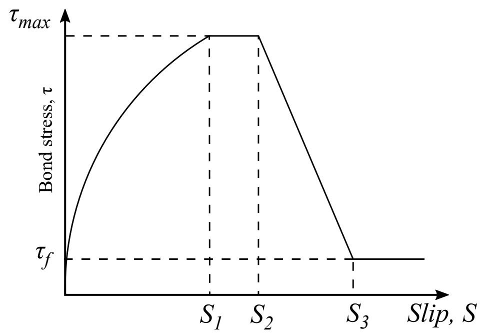

Figure 3.10: *Analytic bond stress-slip relation, reproduced from Modelcode (CEB-FIB, 2010)*

According to Grassl (1999), it has proven to be crucial with regard to side spalling, to implement a detailed interaction model when studying loop reinforcement. This, since a good bond delays the slip, which is required to activate the radial pressure, subsequently delaying the side spalling. Johansson (2000b) also suggests using a bond model that more accurately reflects the stress state around the reinforcement bars over a "perfect bond", since the anchorage of the reinforcement loops are vital to describe the true stress state in and around the loops.

How to model the interaction between reinforcement and concrete in numerical analyses has been a challenge for years and numerous studies has been conducted by researchers such as Lundgren (1999), Jansson et al. (2012), Henriques, Simonões da Silva & Valente (2013), Al-Osta et al. (2018) to mention some. Within the use of finite element analyses many different methods has been developed to represent the interaction. The most commonly used methods in ABAQUS are:

- Spring elements
- Friction model
- Cohesive zone elements
- Cohesive surface interaction

3.5.2.1 Spring model

One way is to assume a bond-slip relation when the interaction is modelled. This, by using simple spring elements connected between adjacent nodes on the concrete and the reinforcement, preferable in the exact same location. This is based on a non-linear stiffness (E_{Spring}) given as a force-slip relationship in ABAQUS, similar to the bond stress-slip curve (Dassault-Systèmes, 2014).

The corresponding force depends on the number of springs (n_{spring}) used in the model and the total surface area of the bonded part of the reinforcement ($A_{surf.bonded}$). This can be converted to input in ABAQUS by Equation 3.8.

$$F_l = \frac{\tau_l A_{surf.bonded}}{n_{spring}} \tag{3.8}$$

The bond stress (τ_l) varies with the slip (S_l). Consequently, the properties of the springs can be applied directly from the response obtained from experiment or the bond stress-slip according to Modelcode (CEB-FIB, 2010), presented under Section 3.5. This results in an identical application of the non-linear response, illustrated in Figure 3.11.

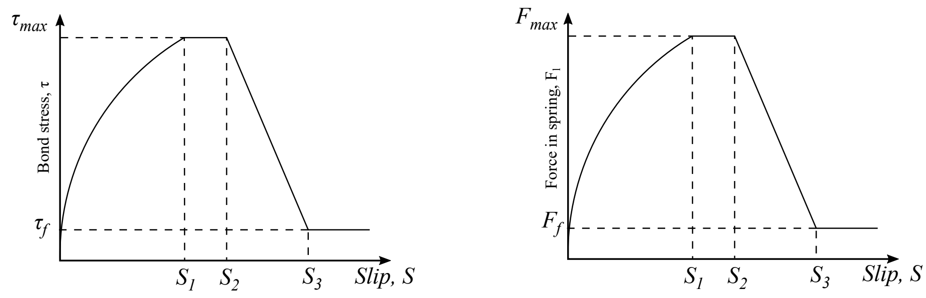

(a) *Bond stress-slip relation according to the Modelcode*

(b) *Force-slip in spring element implemented in ABAQUS*

Figure 3.11: *Models describing bond stress-slip and force-slip*

Since this is a nodal-based connection the reinforcement bar can be modelled as truss or beam element, resulting in a computationally easy model. The connection between the node on the reinforcement and the adjacent node in the concrete is illustrated in Figure 3.12. The node on the edge of the concrete should preferably be positioned as close as possible to the node on the reinforcement.

This simplified modelling technique of the interaction between two materials also has the advantage of being compatible with explicit solvers, giving the possibility to study the post-peak behaviour in detail and have a predictable calculation time.

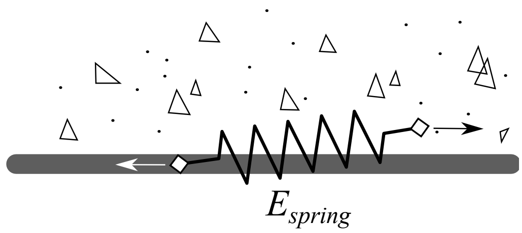

Figure 3.12: *Schematic figure of a spring element connected between concrete and reinforcement*

3.5.2.2 Friction model

The friction model, presented in Figure 3.13, can be connected as a face-to-face contact, compared to the node connection used for springs. It is defined in ABAQUS through an equivalent shear stress $\tau_f = \mu_f * p$, where μ_f is the friction coefficient and p the contact pressure, until the critical friction shear stress (τ_{crit}) is reached whereon the stress becomes constant (Dassault-Systèmes, 2014). Alone, this method cannot simulate the non-linear bond behaviour nor the cracking behaviour of concrete, as this model only represents the longitudinal direction.

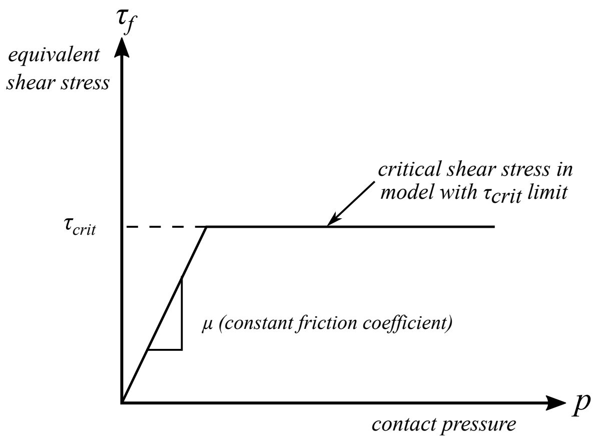

Figure 3.13: *Frictional model, reproduced from ABAQUS Analysis User's Guide (Dassault-Systèmes, 2014)*

3.5.2.3 Cohesive zone elements

Cohesive elements are useful when modelling adhesive bonded interfaces and can be equated to a glue-like material. In this technique the interface layer is modelled as separate element in a zone between the concrete and the reinforcement with its own material properties representing the bond, see Figure 3.14. Commonly they are linear elastic until a certain stress level where damage is initiated, thereafter damage evolution starts. The elements allow for several constitutive behaviours, such as traction-separation, continuum-based constitutive models for adhesive layers with finite thickness and uniaxial stress-based constitutive models. They are recommended for more detailed adhesive connection modelling, though often require a very small stable time increment resulting in large computational demand (Dassault-Systèmes, 2014).

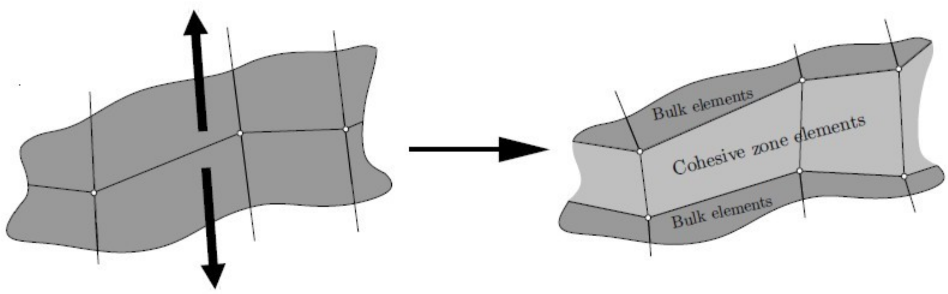

Figure 3.14: *Cohesive zone elements (Dassault-Systèmes, 2014)*

3.5.2.4 Cohesive surface interaction

The surface-based cohesive behaviour in ABAQUS offers capabilities similar to the cohesive elements mentioned in the previously section and is defined as a surface interaction property. It is intended for situations where the thickness of the interface is negligibly small, in contrast to if a finite thickness with stiffness and strength properties is needed where cohesive elements are more suitable. However, this technique is typically easier to define and commonly used when surfaces comes in contact during an analysis. It can also capture crack propagation in initially bonded surfaces through linear elastic fracture mechanics principles.

When two surfaces are assigned cohesive properties, the first will be treated as a slave surface and the second as a corresponding master surface. In a debonding situation, where it is desired to have the surfaces initially in contact, a strain-free correction of the slave nodes will take place in case of any over closure or small gaps in between.

According to Model Code (CEB-FIB, 2010) as mentioned previously, the stress-slip relation between the concrete and the reinforcement can theoretically be described in three different steps, presented in Figure 3.15a. When using surface-based cohesive interaction in ABAQUS it assumes a linear elastic traction-separation followed by a bond damage evolution, according to Figure 3.15b. The damage initiates when the corresponding stress exceeds the maximum bond strength (τ_{max}) (Dassault-Systèmes, 2014).

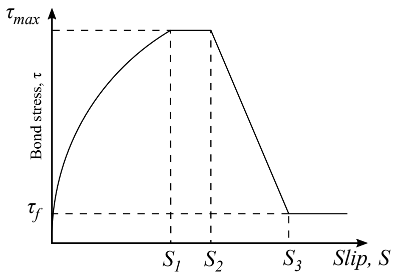

(a) *Bond-slip relation according to the Modelcode*

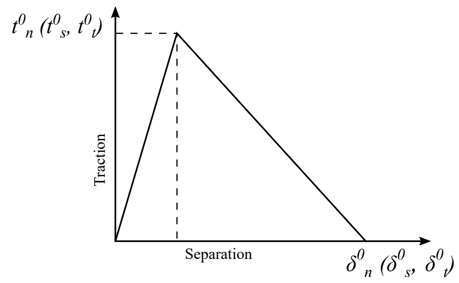

(b) *Traction-separation implemented in ABAQUS*

Figure 3.15: *Approximations for the bond interaction*

The initial elastic behaviour related to shear and normal separations across the interface is described by an elastic constitutive matrix. The constitutive relation is applied as uncoupled as suggested by many researchers using this method, and therefore differs from the stiffness matrix presented in Section 3.5. Thus, only the diagonal terms are non-zero, expressed in Equation 3.9.

$$t = \begin{pmatrix} t_n \\ t_s \\ t_t \end{pmatrix} = \begin{pmatrix} K_{nn} & 0 & 0 \\ 0 & K_{ss} & 0 \\ 0 & 0 & K_{tt} \end{pmatrix} \begin{pmatrix} \delta_n \\ \delta_s \\ \delta_t \end{pmatrix} = K\delta \tag{3.9}$$

K_{nn}, K_{ss}, K_{tt} describes the stiffness between the contact elements in the normal and tangential directions and have to be defined. Suggested by (Henriques et al., 2013) among others, the coefficients related to the shear deformations are taken as the quota between the maximum bond stress (τ_{max}) and the maximum slip (S_{max}), expressed in Equation 3.10. While the stiffness in the normal direction is made a hundred times stiffer to simulate a fully rigid connection, expressed in Equation 3.11.

$$K_{ss} = K_{tt} = \frac{\tau_{max}}{S_{max}} \tag{3.10}$$

$$K_{nn} = 100K_{tt} = 100K_{ss} \tag{3.11}$$

In the transverse direction it is assumed that the cohesive model is active, and the friction model is passive in the elastic state. Any slip is resisted by the cohesive strength of the bond, resulting in shear forces. The peak value of the elastic behaviour is described as: the maximum bond stresses the surfaces can withstand before breaking the contact and initiating the damage behaviour.

Furthermore, as damage starts evolving, the cohesive stiffness degrades and the friction model activates, resulting in shear stresses being a combination of the cohesive contribution and the friction model. When maximum damage has developed, the only contribution to the shear stresses is from the friction model. Subsequently the evolution of damage can be described in different ways, most commonly linear as in Figure 3.15b but also exponential decreasing or given a non-linear tabular damage evolution.

4

Verification of numerical modelling techniques

When studying concrete structures and their behaviour, a combination between experiments and numerical analyses is an efficient and powerful tool. To be able to ensure that a structure is modelled properly it is of high importance to have real experiments to verify against. In this thesis this verification was done in two steps, by modelling a pull-out test and a frame corner with one layer of loop connections, which could be validated against already performed tests. The first mentioned, to confirm that the interaction between the reinforcement and concrete worked properly and the latter to study the effect of loop connections, before further usage in the area of large and heavily reinforced concrete frame corners where no experiments have been carried out so far.

4.1 Pull-out tests

Pull-out tests were simulated and analysed in ABAQUS to define and ensure an appropriate interaction model between reinforcement and concrete. Input data from Jansson et al. (2012) was used as reference when defining dimensions and to verify the behaviour of the numerical model. These tests measured forces and deformations until failure both for plain concrete and for steel fibre reinforced concrete (SFRC) to get the corresponding traction stresses.

4.1.1 Experimental setup

In the experiments a concrete cube, with dimensions defined according to Figure 4.1, was used with a B500BT ϕ16 mm rebar cast centrally and bonded along a depth of 60 mm. Movements of the concrete in the direction of the load were prevented by a steel support layered with Teflon to minimize friction. This was attached as a frame around the four edges on the active side with a width of 16 mm, visible in Figure 4.1.

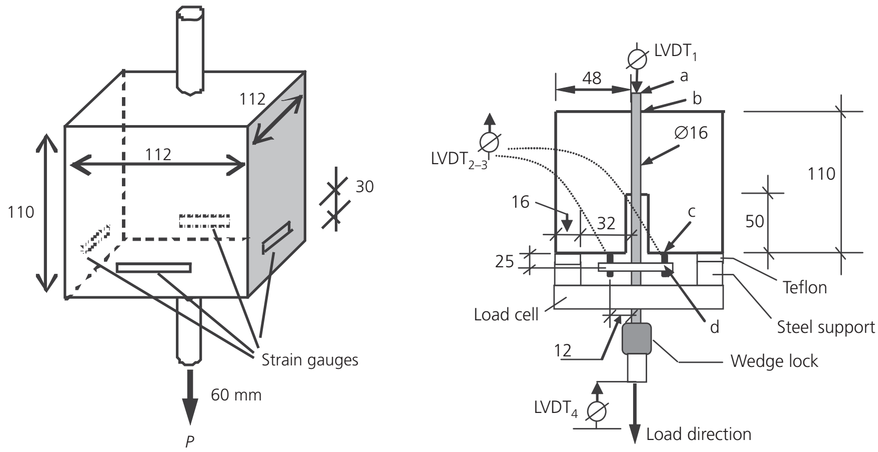

Figure 4.1: *Dimensions of test specimen for pull-out tests (Jansson et al., 2012)*

To be able to monitor the displacements, four linear variable displacement transducers (LVDT) were attached to the specimen. According to Jansson et al. (2012), the most appropriate position to extract measurements were at the location of the two LVDTs below the specimen ($LVDT_{2-3}$). This position was therefore chosen for extracting values in both the FE analysis and the experiment, and further referred to as the active side. For each experimental series, five pull-out specimens were tested giving the mean values used for comparison.

The concrete used in the test specimens was self-compacting concrete (SCC) which has been found to increase the bond-strength and consequently increase the pull-out force compared to normal cast concrete (Zhu et al., 2004). The bond stress-slip curve from the tests may therefore be a little bit higher and require to be modified accordingly in further analyses.

The experiments were performed using specimens cast with both regular concrete and SFRC. Initially, the aim was not to analyse the latter since knowledge about how to implement bond properties in plain concrete was the main reason for this study. However, to be able to distinguish if the analysis reflected the proper failure mode both cases ended up being evaluated.

For plain concrete, the experiments resulted in a maximum average bond stress of 20.9 MPa with splitting cracks in the failure state. While, for SFRC the maximum bond stress reached 22.5 MPa and a pull-out failure occurred.

To be able to find the most reliable way to model the interaction between reinforcement and concrete, two different numerical analyses were evaluated and compared to experimental data. In one analysis, the concrete cube was modelled using 3D solid elements and the reinforcement as 1D beam elements with springs attached in nodes along the bonded length. In the other analysis both concrete and reinforcement were modelled using 3D solid elements with cohesive surface contact properties given to the adjacent surfaces along this length.

4.1.2 Material model

A Concrete Damage Plasticity (CDP) model was used for both models, as described in Section 3.4. Hence, the concrete in compression was modelled with a non-linear relationship after $0.4f_{cm}$, according to Section 3.2, and constant post-peak behaviour. The concrete tensile relationship was modelled bi-linear, as described in Section 3.1.

The SFRC has a more ductile post-peak tensile behaviour which is represented by a different stress-crack width response. This was implemented in the material input in ABAQUS according to Figure 4.2.

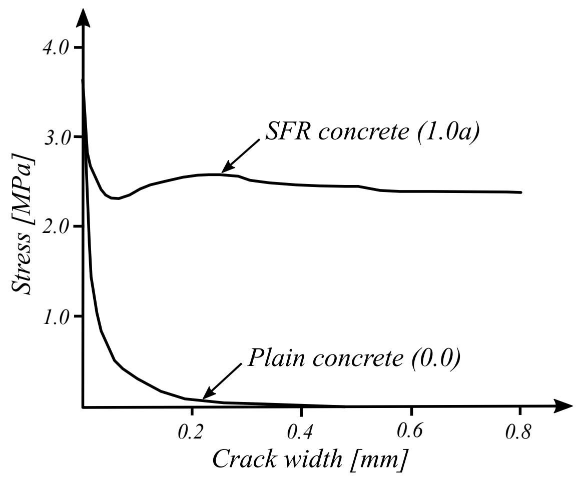

Figure 4.2: *Average σ-w curves for the compared tests, numbering in brackets refers to specimen in experiment. Reproduced from Jansson et al. (2012)*

The steel was modelled with a yield strength of 535 MPa and an elastic modulus of 200 GPa, according to the experimental description tested by the manufacturer. The input data used in the software to mimic the concrete properties in the experiments are presented in Table 4.1. The material properties were determined in the experiments performed by Jansson et al. (2012).

Table 4.1: *Summary of concrete material input used in the FE-analyses of the pull-out tests*

	f_c [MPa]	f_{ct} [MPa]	E_c [GPa]	ρ_c [kg/m^3]
Plain concrete	65	3.1	33	2330
SFR concrete	65	3.6	32	2390

4.1.3 Numerical model with spring elements

The first analyses were modelled, as previously described, with 1D beam elements representing the reinforcement embedded in the concrete. The interaction along the bonded length was modelled by connecting one end of each non-linear spring element to a node on the reinforcement and the other end to an adjacent node on the concrete. The numerical model is schematically shown in Figure 4.3, where the boundary conditions attached on the active side of the cube are marked and the applied displacement of the reinforcement bar is presented.

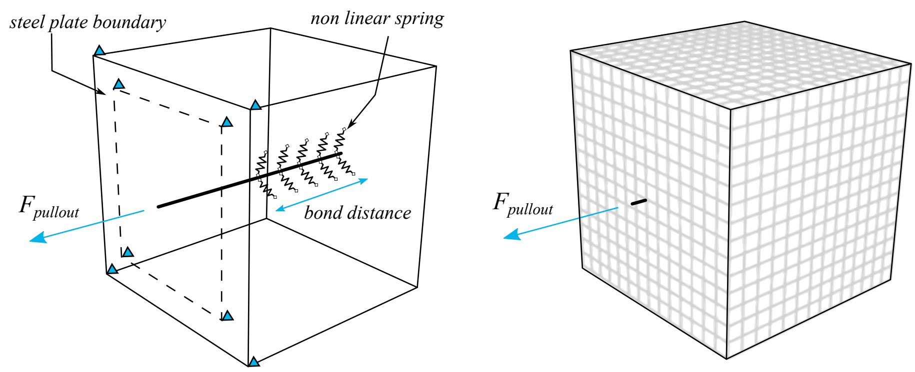

Figure 4.3: *FE-model set up and mesh configuration for pull-out numerical model with spring elements*

The non-linear behaviour of the spring was taken as the bond vs. slip results from the experiments. However, this had to be converted to a force vs. slip input according to the input criteria in the finite element software. The corresponding force in one spring was calculated by multiplying the stress with the real surface area of the bonded part, divided by the number of springs used, see Equation 3.8.

The results from the finite element analysis matched the bond-slip response from the experiments very accurately, shown in Figure 4.4. However, by using spring elements solely in the longitudinal direction no forces in the normal direction were generated, and thereby no splitting cracks occurred. Due to the complex stress distribution, expected in the future modelling of the frame corner, this method was regarded as not being suitable in further analyses in this thesis.

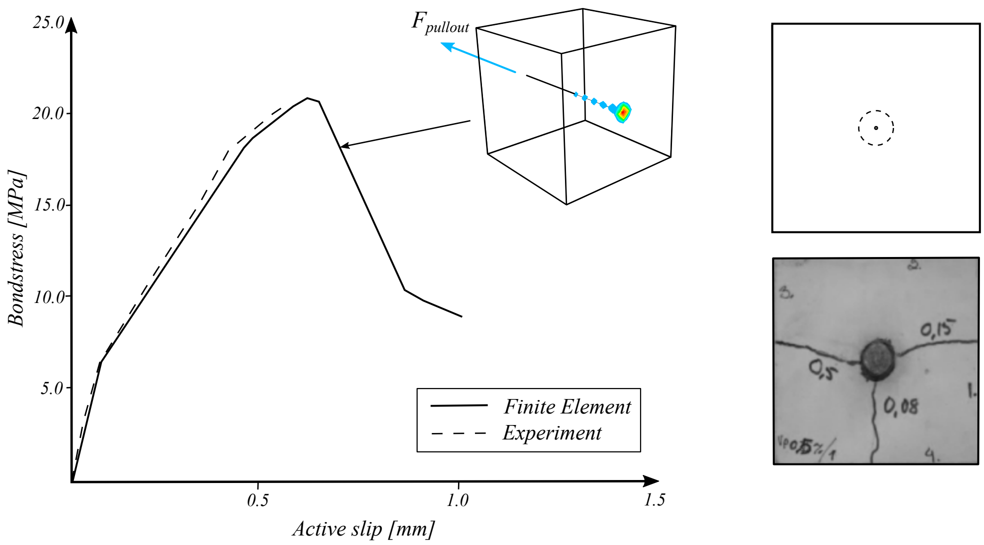

Figure 4.4: *Relationship between bond stress and active slip together with a contour plot of the plastic strain generated in the finite element analysis, on the passive side. The maximum strain illustrated reaches 0.3. On the right the absence of cracks on the active side in comparison to the expected cracks are presented.*

4.1.4 Numerical model with cohesive surface interaction

In the second analysis, the concrete cube was modelled using 3D solid elements, in the same manner as described in previous section. In addition, the reinforcement bar was also modelled using 3D solid elements and a hole was cut in the concrete cube where the bar was placed. The bond was treated as a surface-to-surface interaction in the FE-software with cohesive properties, applied over the aligned surfaces.

To understand the behaviour of the model properly a simple elastic model of nine elements was generated. It was fixed around the short edge on all four sides. When pulling out the reinforcement bar, represented by one cubic element, normal stresses were induced by the shear stresses on all four sides that were in contact. The relation between the stresses can be seen in Figure 4.5. This have been extracted from the one of the four grey elements, with a normal surface perpendicular to the cohesive bond, where the splitting stresses were the highest. The stress distribution over the edge surfaces have been illustrated in the same figure.

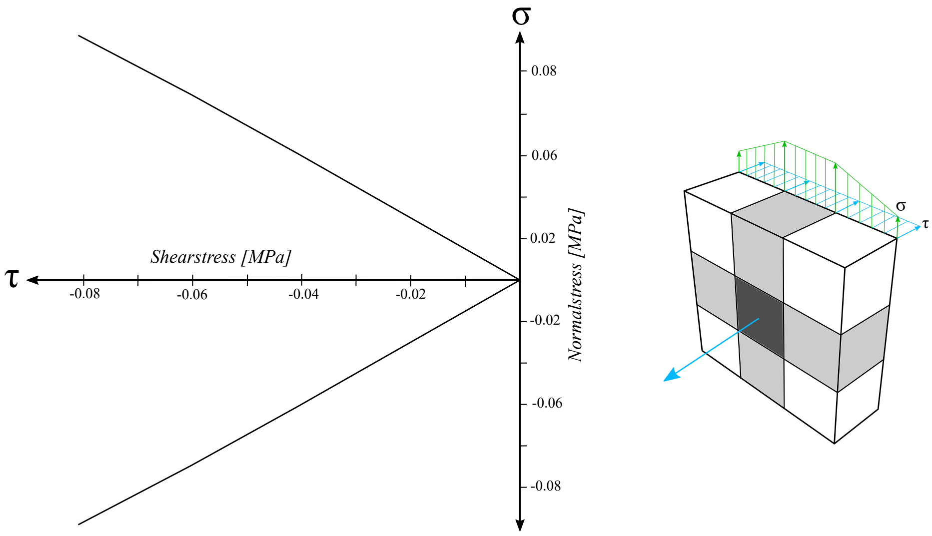

Figure 4.5: *Relationship between normal stresses (σ) and shear stresses (τ) from simplified pull-out tests, resulting in splitting stresses in the concrete*

Furthermore, to simulate the actual experiment configuration, the cross-section of the reinforcement bar was simplified with an octagonal shape with the diameter of 16 mm. It was bonded to the concrete cube over the distance of 60 mm, shown in Figure 4.1. The FE-model is presented in Figure 4.6 where the boundary conditions attached on the active side of the cube are marked together with the applied displacement of the reinforcement bar.

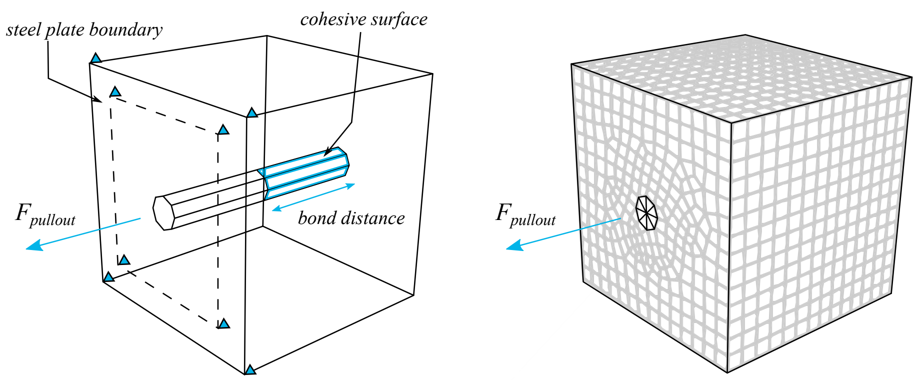

Figure 4.6: *FE-model set up and mesh configuration for pull-out numerical model with cohesive surface interaction*

As previously described in Section 3.5.2.4, the cohesion surface interaction model used in ABAQUS is recommended in analyses where the interface layer has a negligible thickness (Dassault-Systèmes, 2014). It describes the interaction between concrete and reinforcement with linear traction-separation condition previously presented in Figure 3.15. The initial values of the parameters representing the elastic behaviour of the traction-separation curve were obtained from Equation 3.10 and 3.11 (Henriques et al., 2013). These only acts as guidelines and the parameters were increased with approximately 25% to obtain results corresponding to the experiments. The values presented in Table 4.2 were used as input, representing the cohesive surface interaction.

Table 4.2: *Cohesive stiffness input used in the FE-analyses*

K_{nn} [MPa/m]	K_{ss} [MPa/m]	K_{tt} [MPa/m]	τ_{max} [MPa]
5 300 000	53 000	53 000	22.5

The results in Figure 4.7, shows that the method with cohesion properties gave similar results as obtained in the experiments. In the experiments splitting cracks occurred, which caused failure at a maximum stress of 20.9 MPa. A similar behaviour was shown in the finite element analysis in all four directions.

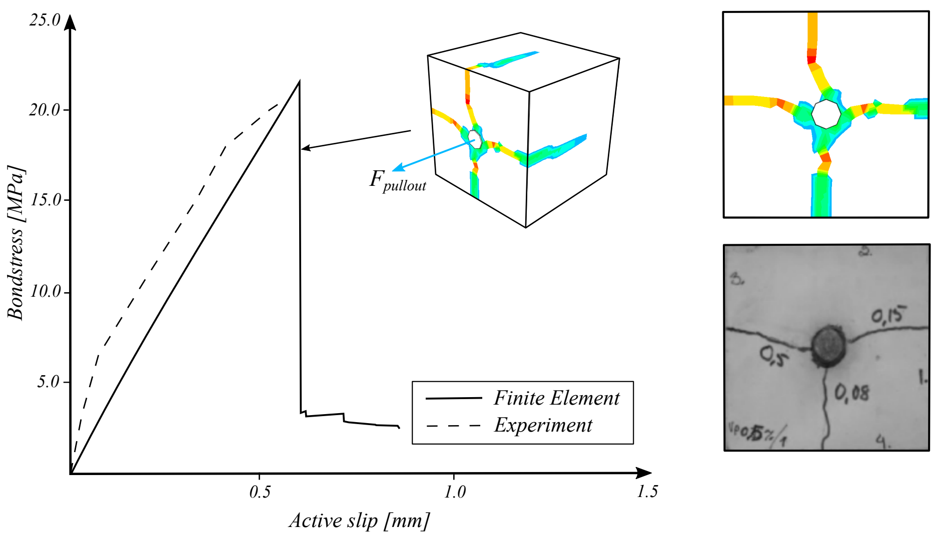

Figure 4.7: *Relationship between bond stress and active slip. Comparison between the plastic strain generated in the finite element analysis with the crack pattern from the experiments, on the active side. The maximum strain illustrated reached 0.09*

The post-peak behaviour in Figure 4.7, drops in a brittle manner since the concrete is bursting in tension, and there is no reinforcement otherwise in the cube.

The main purpose of this study was to confirm that the interaction properties assigned to the FE model reflected reality. As clearly seen in Figure 4.7 the failure mode is splitting cracks. Thought, this was the expected failure mode for this plain concrete specimen, according to experiments presented by Jansson (2012), this alone was not considered enough to confirm the reliability of the bond model.

So, to verify the accuracy of the bond model another FE analysis was executed. This time the behaviour of the concrete was increased to mimic the attributes of the SFRC specimen according to Table 4.1 and the stress-crack width relation presented in Figure 4.2. The aim was to achieve a pull-out failure confirming the strength of the bond being modelled accurately. In Figure 4.8 the change in behaviour in comparison to Figure 4.7 is clearly visible.

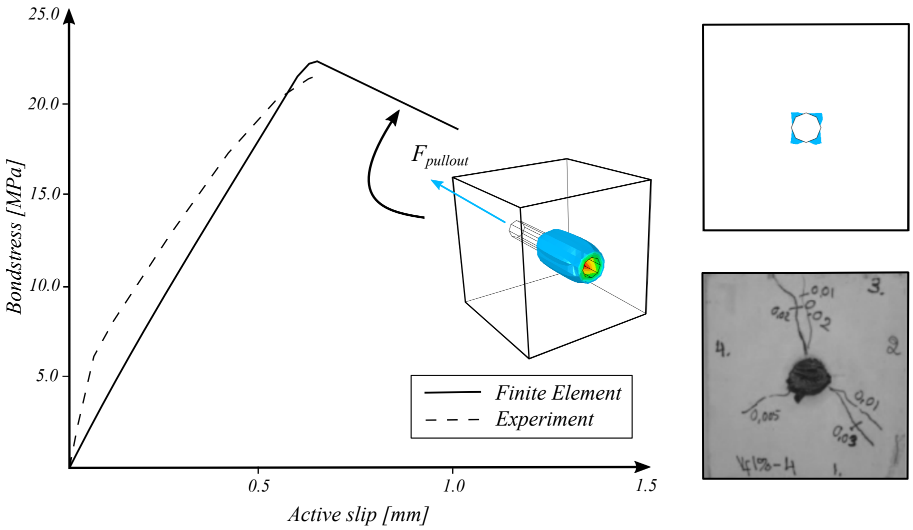

Figure 4.8: *Relationship between bond stress and active slip. Comparison between the plastic strain generated in the finite element analysis with the crack pattern from the experiments, on the active side. The maximum strain illustrated reached 0.005*

The failure mode was in this case instead a pull-out failure giving a bond strength of approximately 22.5 MPa similar to the experiments. The initial behaviour was described in the same way, elastic up to failure, but the post-peak behaviour turned out more ductile. This was the expected behaviour which therefore validated the modelled bond behaviour. The friction coefficient plays an important role after the bond has been damaged. However, further effort was not put into modelling nor evaluating the post-peak behaviour, mainly because it was not of importance in this study but also because there was limited information from the experiments to compare with.

4.1.5 Conclusions

The cohesive surface interaction model captured the real behaviour of the pull-out failure from the experiments in a desired way, both regarding the crack pattern, the bond stress vs. active slip relation and the strength of the bond.

The small differences in the crack pattern between the experiment specimens and the numerical models could be explained by imperfections in real concrete material. These imperfections causes an uneven crack initiation in concrete, compared to the perfectly symmetric material in a numerical model.

Both interaction models were tested parallel with implicit and explicit solution techniques when performing the analyses. The spring model gave similar results using both solutions. However, the cohesion surface properties could not be used directly in the explicit solver and demanded some adjustments in the contact properties before working properly. Since the computational time for both the implicit and explicit analyses were rather similar, both methods were brought into the next phase of modelling.

As previously mentioned, the post-peak behaviour was not studied in detail. This may have been interesting to look further into, for several reasons. However, it was not considered relevant for the proceeding of this thesis and therefore not further studied. The results were convincing enough to proceed the modelling process with this bond technique between the concrete and the reinforcement, and it appeared reasonable to be valid also in a larger scale and for varying geometries.

4.2 Frame corner tests

In the second type of analyses, a frame corner was analysed to verify proper behaviour of the finite element model. It was validated against laboratory tests performed by Johansson (2000b). In the mentioned report, closing frame corners with loop connection reinforcement were tested until failure, and a resulting force-displacement relationship was presented. However, these experiments were performed on structures smaller and less reinforced than the structures aimed to be treated in this thesis. They were therefore only used as a verification before scaling it up to the specific conditions relevant for this thesis.

4.2.1 Experimental setup

The experiments of interest consisted of a test series with four full-scale specimens, loaded with a closing moment. The specimens were designed with different reinforcement configurations, two tests with low mechanical reinforcement ratio of 0.2% and two with high ratio of 0.88%. The concrete dimensions and experimental setup common for all specimens are presented in Figure 4.9.

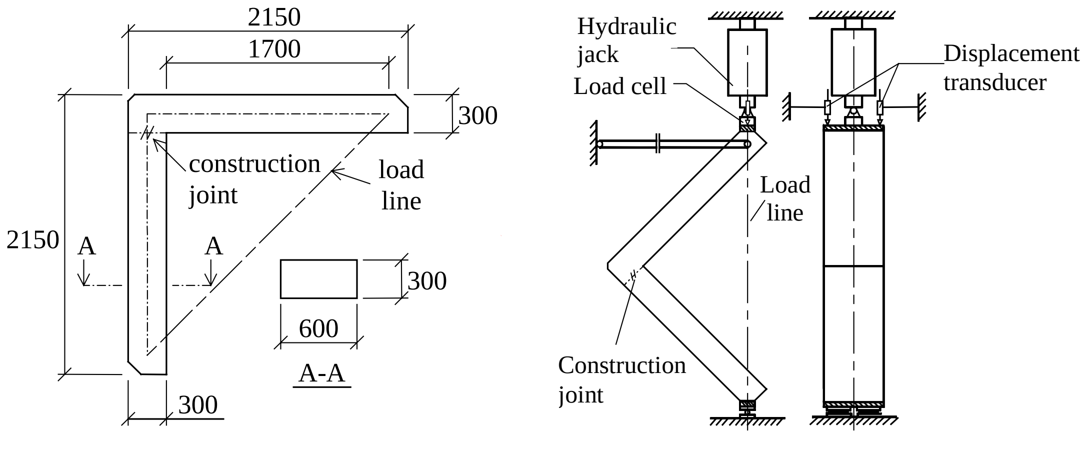

Figure 4.9: *Experimental setup RV5/RV6 (Johansson, 2000b)*

The test specimens chosen to be modelled and used as reference were referred to as *RV5* and *RV6* by Johansson (2000b). These specimens had the same reinforcement detailing in the corner of the frame, consisting of 2x7 reinforcement loops with a diameter of 16 mm. The vertical and horizontal loops were evenly placed through the cross section, with a concrete cover of 40 mm. This corresponded to the higher reinforcement ratio of 0.88%, and were expected to be the case most relevant to the upcoming analyses on heavily reinforced frame corners.

The maximum load for specimen *RV5* measured 147 kN and similarly specimen *RV6* reached 150 kN. Both underwent spalling of the side concrete cover, probably resulting in an anchorage failure. The applied load ($F_{framecorner}$) can be divided into two components according to Figure 4.10.

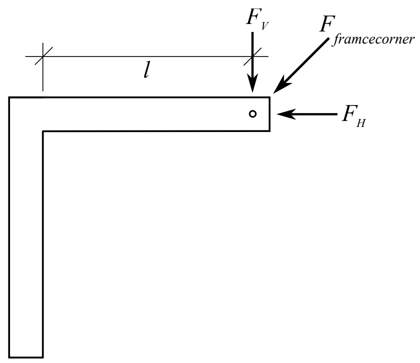

Figure 4.10: *Schematic figure of the force components, F_V and F_H, from the applied force $F_{framecorner}$* at a distance l from the corner-beam interface.

The corresponding moment in the critical section at failure was found by multiplying the vertical force component (F_V) with the perpendicular lever arm (l), according to Equation 4.1. Furthermore, the compressive force from the horizontal component (F_H) increased the moment capacity, which were considered when comparing the estimated moment capacity in the section.

$$M = F_V \cdot l \tag{4.1}$$

4.2.2 Material

The material model used in these analyses was similar to the one used in the pull-out test, described in Section 4.1.2, regarding both compressive and tensile strength implementation and the use of a CDP model. The concrete and reinforcement material properties for this specific case were obtained from the experiments by Johansson (2000a) and are presented as they were implemented in the numerical analysis in Table 4.3 and Table 4.4. The material densities were chosen as standard values since no specific values were defined in the experiments, and automatically implemented by the FE-software when applying gravity in the analyses. Finally, the fracture energy G_f

was calculated according to Eurocode (CEN, 2005), previously explained in Section 3.1.

Table 4.3: *Summary of concrete input used in the FE-analyses of the frame corner tests*

	$\boldsymbol{f_c}$ [MPa]	$\boldsymbol{f_{ct}}$ [MPa]	$\boldsymbol{G_f}$ [N/m]	$\boldsymbol{E_c}$ [GPa]	$\boldsymbol{\upsilon_c}$ [-]	$\boldsymbol{\rho_c}$ [kg/m^3]
Concrete	30.6	2.9	120	26	0.2	2500

The reinforcement was of model K500 with a characteristic yield strength of 567 MPa, measured by the manufacturer. The steel was modelled including strain hardening at 2.5% and with a strain at ultimate stress of 12.0% (Johansson, 2000a).

Table 4.4: *Summary of reinforcement input used in the FE-analyses of the frame corner tests*

	$\boldsymbol{f_y}$ [MPa]	$\boldsymbol{f_u}$ [MPa]	$\boldsymbol{E_s}$ [GPa]	$\boldsymbol{\upsilon_s}$ [-]	$\boldsymbol{\rho_s}$ [kg/m^3]
Reinforcement	567	652	189	0.3	7850

4.2.3 Numerical model

The corner part of the frame was modelled with 3D solid elements both for reinforcement and concrete, similar to the pull-out tests previously described. As the structural response of the corner was of highest interest it was modelled with higher detailing while the rest of the structure were simulated with linear elastic beam elements. The main reason for this simplification was to get a significant reduction of computational time for the analyses. A schematic figure of the finite element model is presented in Figure 4.11.

Additionally, by taking advantage of symmetry only half of the structure was modelled in depth, and by that the number of elements could be reduced drastically. The configuration of reinforcement is presented in Figure 4.11, with 2x3 reinforcement loops instead of 2x7 as in the experiments. The results were multiplied with a scaling factor accordingly, to get the full capacity of the corner section.

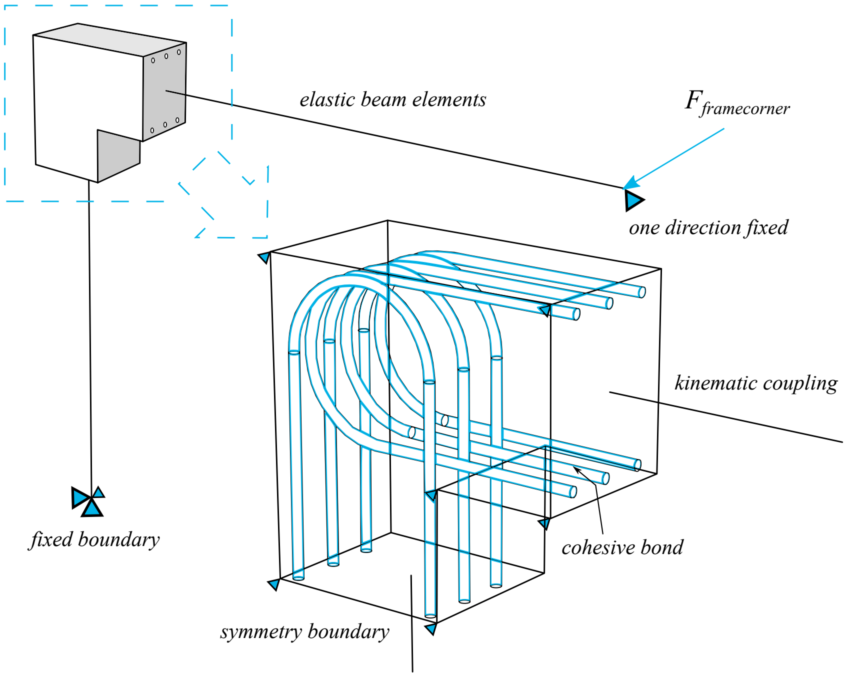

Figure 4.11: *FE-model set up for RV5/RV6*

The bond between reinforcement and concrete was modelled as described in Section 3.5.2.4 using cohesive surface interaction and attached over the whole surface area of the reinforcement bars, marked with blue in Figure 4.11. Based on the verification done in the pull-out tests, the same input values for the bond stiffness as in Table 4.2 were used in these analyses.

In Figure 4.12a, the mesh is presented. Because of the complicated curved shape of the reinforcement bars, tetrahedral elements had to be used. In addition, linear elements were considered to be sufficient in this model to describe bending due to the high number of elements. Further, the circular cross section of the reinforcement bars was simplified with a quadratic shape, seen in Figure 4.12b, which gave a reduction of the cross-section area and circumference. To account for this the reinforcement were made larger, to get the proper circumference after the assigned mesh, and the material properties were increased with a factor according to the difference in area (25%).

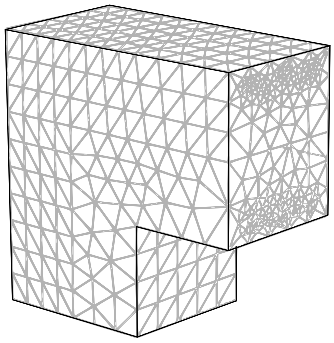

(a) *Mesh configuration on corner part*

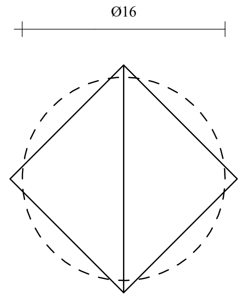

(b) *Simplified quadratic sectional steel area*

Figure 4.12: *Mesh specifications of numerical model*

The size of the elements varies a lot in the structure, presented in detail in Table 4.5. This was mainly because of the size difference between the cross section of the reinforcement bars and the size of the concrete frame, i.e. since the meshes had to be fitted together, the concrete surrounding the reinforcement bars were much smaller than close to the edges. A convergence study was performed, and presented in Section 4.2.5 related to how small the elements needed to be to ensure that the results of the finite element analysis were not affected when changing the size of the mesh. In that aspect the mesh presented in Table 4.5 was found satisfying.

Table 4.5: *Approximate mesh size used in the presented results*

	Mesh size [mm]	**No of elements**
Concrete corner	40	≈ 50 000
Concrete beam/column	100	≈ 15
Reinforcement	15	≈ 6 000

The analysis was set up with a displacement-controlled deformation, in the same direction as $F_{framecorner}$ marked in Figure 4.10, at the outer edge of the beam to mimic the experiments. The force was applied in the same direction as in the experiments, with a 45°angle to the column edge.

4.2.4 Comparison between tests and analyses

The force-displacement relation from the finite element analyses together with the results from the experiments are presented in Figure 4.13. As mentioned before, two equal specimens (*RV5* and *RV6*) were tested and their corresponding graphs represents their extracted values. Due to convergence problems the analyses could not go further, and no post peak response could be studied. The experiments however showed a ductile response even when the side concrete cover spalled (Johansson, 2000b).

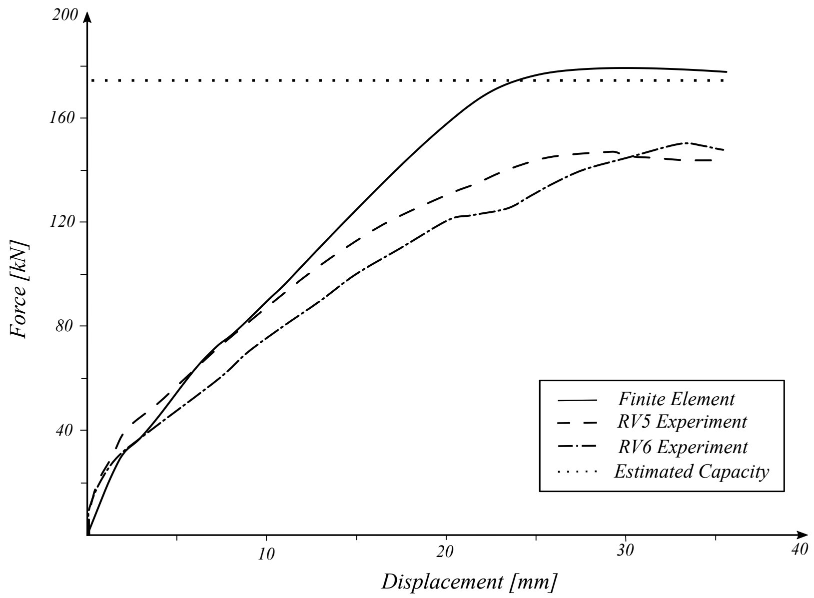

Figure 4.13: *Force-displacement response of numerical model compared to experiment RV5/RV6*

The results from the finite element analyses initially shows a similar structural behaviour as the experiments but has slightly higher capacity. Compared to the estimated cross-sectional moment capacity it corresponds rather well.

On the side edges of the frame corner, bending cracks were formed, but without any signs of side spalling as observed in the experiments. It appeared reasonable that this was why the results from the analyses became higher than the experimental results, as the failure mode from the experiments could not be captured. A comparison of crack pattern from the FE analyses and the experiments are shown in Figure 4.14. Cracks were formed only in one row of elements; this indicates that the crack band width is chosen properly. The crack width reached a maximum of approximately 1.5 mm.

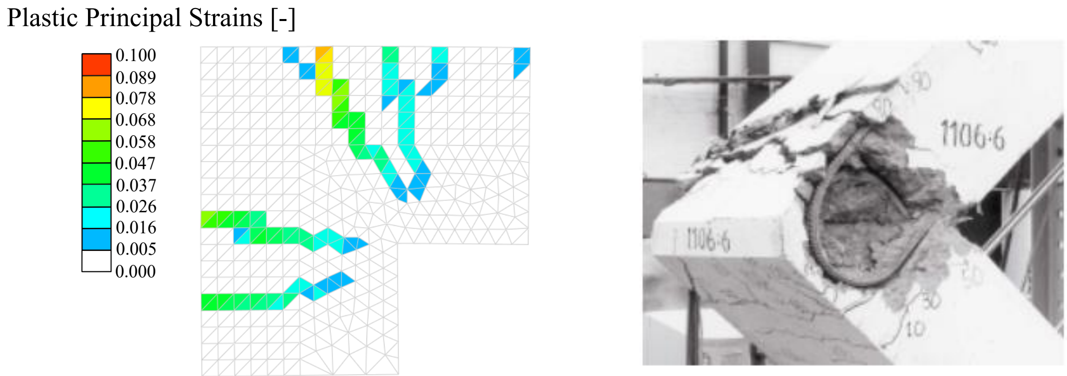

(a) *Numerical analysis* (b) *Experimental result*

Figure 4.14: *Comparison of crack pattern, on the free edge*

The mesh is more regular in the edges compared to the section cut seen in Figure 4.15, since the control parameters of the triangular mesh are set in the boundary without any irregularities from the reinforcement. Due to the dimensions of the beam and column being equally sized, a rather symmetric crack pattern developed from bending was developed. In Figure 4.15, cracks following the round shape of the reinforcement in the corner are also visible, close to the edge. The crack width in the figures corresponds to about 1 mm. This is however a rough approximation due to the large variation in size of the elements as seen in the same figure.

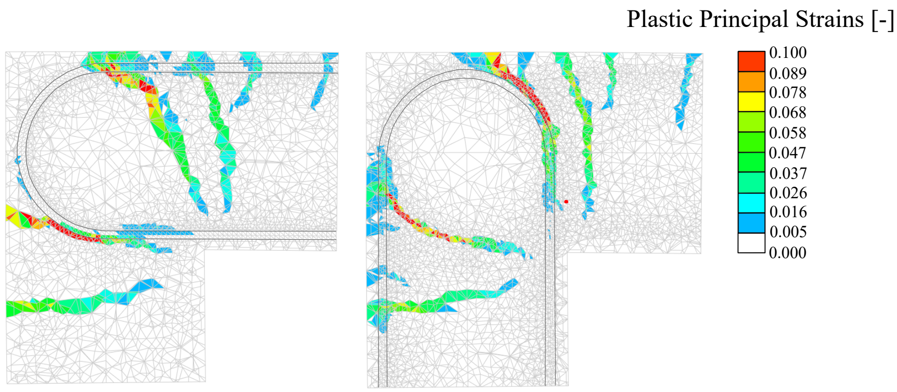

Figure 4.15: *Plastic strains in concrete displaying the crack pattern in the numerical analyses of RV5/RV6. Taken in section cuts at position of horizontal and vertical loops*

In the analyses yielding of the reinforcement bars was initiated before the maximum load was reached. Thereafter, a plastic hinge was formed. This, both in the vertical reinforcement and the horizontal, due to equal dimensions, at the location where the corner part meets the column and beam. This is illustrated in Figure 4.16, with a maximum stress of 567 MPa; indicating that no strain hardening of the reinforcement took place. Similar behaviour was noted during the experiments from monitoring the strains in the reinforcement.

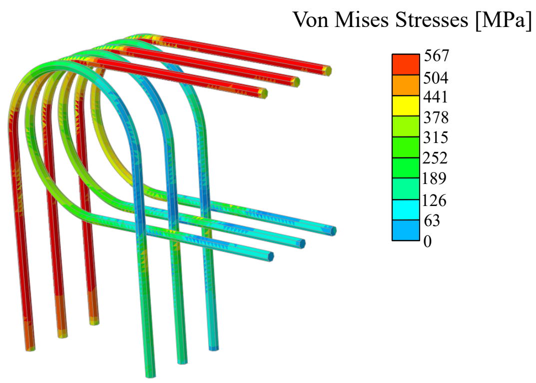

Figure 4.16: *Yielding of steel in numerical analysis*

The corresponding moment at maximum applied force from the experiments and FE-analyses are presented and compared in Table 4.6, to the estimated moment capacity, with partial factors $\gamma = 1$, as presented in detail in Appendix A. As the moment capacity increase when having a compressive normal force (F_H), this was iterative taken into account. The effect of the normal force slightly increased the moment capacity from 198 kNm to 211 kNm, according to the M-N-diagram in Appendix A.

Dragosavic et al. (1975) and Hao (2004) formulated each an expression to calculate the actual stress in the steel when the concrete inside of the loop crushed, and in that way estimated an ultimate loop moment capacity according to Equation 2.4 and 2.8. However, it should be mentioned that these equations do not account for a compressive normal force. Joergensen (2015) also developed an equation to estimate the maximum capacity when using loop connection, see Equation 2.10. Although this method assumes that the compression zone is within the top cover. As this was not the case in the performed analyses, due to the relatively high amount of reinforcement, Joergensen's estimation gave deviating results.

Table 4.6: *Summary of moment capacities [kNm]*

	M_{Rd}	$M_{l.Drago}$	$M_{l.Hao}$	$M_{l.Joerg}$	M_{Exp}	M_{FE}
RV5	211	176	205	61	178	215
RV6	211	176	205	61	180	215

4.2.5 Verification

The results obtained in the FE analysis were continuously verified along the modelling process. The influencing factors that was verified was:

- The symmetry
- The mesh geometry of the reinforcement
- The mesh of the concrete
- The viscosity parameter
- The steel strains
- The used bond strength
- The fracture energy
- The dilation angle

To verify the behaviour of the used symmetry a full-scale model was constructed and analysed. The results showed the same behaviour and peak stress as the reduced model when multiplied with a scale factor accordingly.

The effect on the result by different geometry meshes of the reinforcement have been studied, from the used 4-node quadratic mesh up to a 8-node hexagon mesh. In all cases, the size of the rebar was adjusted so the circumference corresponded to the one of a ϕ16 and thereafter the material properties was adjusted accordingly by the difference in area. The concrete mesh size was kept the same for all verification analyses, with a small variation to match the nodes on the reinforcement. When made properly the mesh geometry of the reinforcement turned out to have a minor difference on the overall results. The quadratic shape resulted in shortest computational time which was desirable for the upcoming analyses.

A mesh convergence study was performed to validate the use of a proper element size. The length of the concrete elements varied from 20 mm up to 80 mm, while the mesh of the reinforcement was kept with a quadratic geometry. The maximum force in ultimate state only differed with 1-4 %, which made the element length of 40 mm appropriate.

The influence on the structural behaviour implementing different values on the viscosity parameter (μ) in the CDP model was also studied. Having the value not equal to 0 gave less convergence problems as expected and decreased the computational time drastically. However, increasing it too much gave results far from the reality. So, the viscosity parameter was set to 0.00005 during this analysis, giving an advantage in computational time while still giving a minor difference in the obtained results.

The steel strain obtained in the numerical analysis only reached a maximum value of 0.66% meaning no strain hardening occurred. This implies that the ultimate strength of the steel had no effect in the numerical results on the moment capacity of the corner, as the stresses only reached the yield plateau. This corresponds well with the test results where the specimen failed with a maximum stress in the steel of 567 MPa (Johansson, 2000b).

The maximum bond strength is highly dependent on which type of reinforcement being used and the corresponding reinforcement ribs. In the pull-out tests the concrete samples were also casted with SCC concrete which could have an increasing effect on the bond. Therefore, the value of the maximum bond strength was reduced in one of the analyses. This however, did not change any results and a bond failure could be neglected.

The value of the fracture energy, G_f, in the performed tests was measured to 110-130 N/m by Johansson (2000a). Based on the recommendations in Modelcode (2010) presented in Section 3.1, the value was calculated to 140 N/m. The importance of this difference on the results of the structure was examined, since there will not be any experimental values available in the upcoming analyses. The numerical model was analysed with the different values on G_f giving a total difference in the results of only 0.5 %. Subsequently, the mean value of 120 N/m from the experimental data was used in the analyses.

The dilation angle (ψ), mentioned as one of the input plastic damage parameters in Section 3.4, has a recommended value in ABAQUS of 35° - 45° (Dassault-Systèmes, 2014). The impact of this parameter on the results were studied, and tested for the different values within the range, without any notable effect on the final results and kept as 35° further in the analyses.

4.2.6 Conclusions

The results from the finite element analyses corresponds well with the estimated moment capacity according to force equilibrium calculations on the cross section. However, the finite element model cannot capture the spalling of the concrete cover in the experiments performed by Johansson (2000b). The side spalling has shown to reduce the anchorage in the corresponding loops, where the force no longer can be transferred, and instead increases the stresses in the remaining loops (Grassl, 1999). Accordingly, side cover spalling results in a lower capacity for the cross section than estimated. The numerical model instead showed a capacity according to when a pure bending failure would occur.

Spalling of the concrete cover might be a major problem in a beam column joint as studied, for which this failure mode cannot be neglected. Side cover spalling will however not be a problem in three-dimensional tunnel or bridge structures being confined in the transverse direction. So, the issue of being able to properly reflect this specific failure mode in the FE-analyses was therefore not within the scope of this thesis.

The initial analyses performed in this section were simultaneously performed using both explicit and implicit solvers. However, the explicit solver were soon ruled out. The main reason for this were the small sized elements generated in the reinforcement resulting in extensive running times.

The presented results in Figure 4.13, implies a much stiffer behaviour of the finite element analyses in comparison to the experiments. Using elastic beam elements for the frame members outside of the corner area is most likely the reason behind this overall stiffer result, in combination with force application. This is because no cracking, and by that no stiffness reduction, can appear outside of the corner. However, the reduction in number of elements of the model was decisive and a decision was made to keep the model this way. In addition to this, the construction joint positioned below the corner, at the top of the column in the experiments (see Figure 4.10) was not included in the FE-analyses. These two parameters are in combination thought to be part of the reason behind the stiffer behaviour compared to the experiments seen in Figure 4.13.

The estimated moment capacities from the different proposed equations, presented in Table 4.6, all lies in the range between the experimental results and the capacity of the critical cross section, except for Joergensen & Hoang (Equation 2.10). This because it was not applicable, having a compression zone which was bigger than the top concrete cover.

It was of interest to evaluate the difference in results using the fracture energy (G_f) measured from the experiments, in comparison to the recommendations according to Modelcode (CEB-FIB, 2010), since there will not be any experimental values available in the upcoming analyses. Though the measured value was used in these analyses, as presented in Table 4.3, the difference was negligible small and the recommendations according to Modelcode were regarded as valid in the upcoming analyses further on in the report.

5

Case study

The numerical analyses performed in the case study treated a reinforced concrete frame corner with long dimensions out of the plane, hereon referred to as *SB*, previously analysed at ELU's office in Gothenburg. It is an underground structure utilized for car parking, planned to be built at Skeppsbron in Gothenburg. It was designed using loop reinforcement in the connections between roof and walls, according to available recommendations and guidelines, upon request from the contractor. However, since available recommendations are based on experiments performed on structures with low reinforcement ratios, further analyses on the structure were desirable. This structure was therefore analysed thoroughly in this thesis to get a better understanding regarding the possibility to use loop connections in structures with high reinforcement ratios, big dimensions and multiple layers of reinforcement bars.

The analyses were performed with two different reinforcement configurations. The first type, hereon referred to as *SB1*, with two layers of reinforcement according to the drawings produced by ELU, seen in Appendix E. The second type, referred to as *SB2*, were additionally reinforced to further distinguish the influence on the behaviour due to a higher reinforcement ratio (ω). *SB2* does not correspond to any existing project; it originated from *SB1* with equal concrete dimensions and material properties but was provided with extra layers of reinforcement to increase the reinforcement ratio.

5.1 Structure

The structures analysed in the case study have a wall-slab connection with large dimensions and reinforcement bars in multiple layers, in comparison to previously analysed and tested frame corners in this thesis. However, despite this size increment, the reinforcement ratio (ω) of *SB1* was of the same magnitude as in the frame corner studied in Section 4.2. Additionally, the structures of *SB1* and *SB2* were analysed as a thin strip in the middle of the structure which influenced the symmetry conditions as well as excluded the risk of failure due to side cover spalling.

In Figure 5.1a and Figure 5.1b, the difference in reinforcement configuration between *SB1* and *SB2* is presented. The concrete cover and the spacing between the layered reinforcement bars as well as the number of bars in depth were kept the same. In Figure 5.1c, *RV5/RV6* is presented for size comparison. This is for the reader to fully understand the large difference in size.

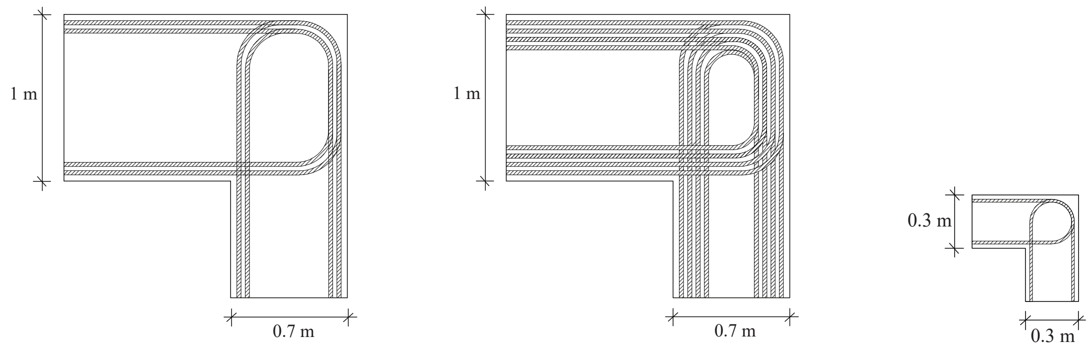

(a) *SB1* **(b)** *SB2* **(c)** *RV5/6*

Figure 5.1: *Schematic figure of SB1 and SB2 with two and four layers of reinforcement respectively compared to RV5/RV6 with its smaller dimensions and one layer reinforcement*

It can also be seen in Figure 5.1a and Figure 5.1b, that the dimensions between the beam member and the column member are not equal. The column width of 0.7 m being slightly smaller than the beam, with a width of 1.0 m. The depth was modelled with a thickness of 0.424 m, after decision by the authors to model two bars in each direction, given the defined distance of 0.106 m between the perpendicular loops. A detailed sketch over the critical cross-section and the reinforcement placement can be found in Appendix B-C.

In Table 5.1, the reinforcement and dimensional specifications for *SB1* and *SB2* are presented. As previously mentioned, the only part differentiating the two numerical models were the number of reinforcement bars in each layer. Thus, *SB2* had a reinforcement ratio (ω) of much higher magnitude.

Table 5.1: *Reinforcement amount and detailing in frame corner SB1 and SB2*

	Reinforcement	A_c **beam** [m^2]	A_c **column** [m^2]	ω [%]
SB1	2x2 layers ϕ25	1.0 x 0.242	0.7 x 0.242	0.74
SB2	2x4 layers ϕ25	1.0 x 0.242	0.7 x 0.242	1.51

5.2 Material

The material model used in ABAQUS was the same as described and verified in Chapter 4. The characteristic concrete material properties were chosen according to specifications from ELU and are presented in Table 5.2.

Table 5.2: *Summary of concrete input used in the FE-analysis of SB1/SB2*

	f_c [MPa]	f_{ct} [MPa]	G_f [N/m]	E_c [GPa]	υ_c [-]	ρ_c [kg/m^3]
Concrete	35.0	2.2	144	34	0.2	2500

The reinforcement properties was chosen as standard characteristic value of 500 MPa for the yield strength and a slightly higher ultimate strength of 550 MPa according to recommendations in Eurocode (CEN, 2005). The properties of the steel reinforcement is presented in Table 5.3.

Table 5.3: *Summary of reinforcement input used in the FE-analysis of SB1/SB2*

	f_y [MPa]	f_u [MPa]	E_s [GPa]	υ_s [-]	ρ_s [kg/m^3]
Reinforcement	500	550	200	0.3	7850

5.3 Numerical model

The finite element models were configured and tested in a similar manner as the frame corner in the verification (Section 4.2), according to the illustration in Figure 4.11. This was performed by using an implicit solution technique, as the explicit solver were ruled out in previous chapter. The corner part was modelled using 3D solid elements for both concrete and reinforcement bars while the extent of the beam and the column was modelled using elastic beam elements, connected with a kinematic coupling. The set up of the finite element models are illustrated in Figure 5.2.

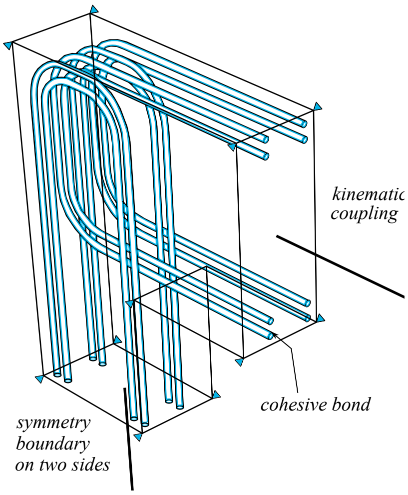

(a) *SB1*

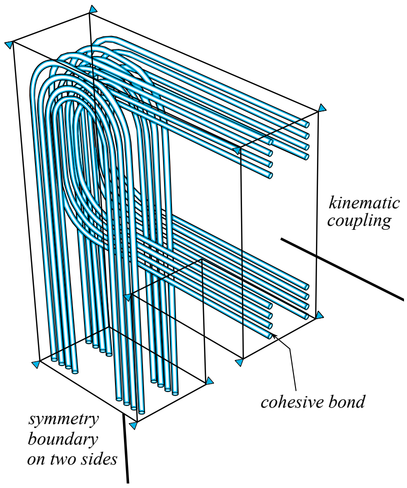

(b) *SB2*

Figure 5.2: *FE-model set up for corner part*

The mesh in the FE-models were chosen as presented in Figure 5.3a and 5.3b, with a quadratic mesh on the reinforcement shown in Figure 5.3c. Again, the elements used in the corner were linear tetrahedral elements due to the complicated curved shape of the reinforcement loops. Due to early convergence errors in *SB1*, the results with the finest mesh are presented, consequently resulting in a higher number of elements compared to what is needed in *SB2*.

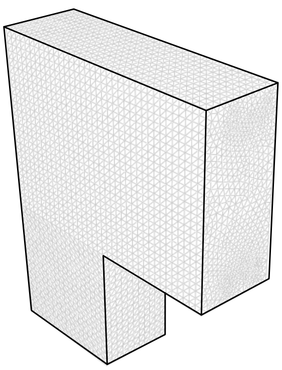

(a) *Mesh configuration on SB1*

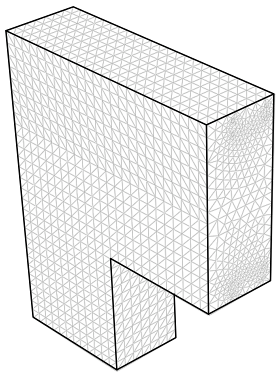

(b) *Mesh configuration on SB2*

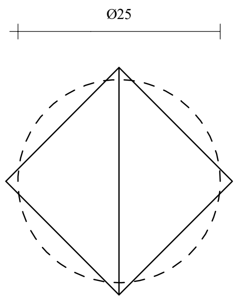

(c) *Simplified quadratic sectional steel area*

Figure 5.3: *Mesh specifications of numerical model SB1/SB2*

The size of the reinforcement in the model was adjusted to have the same circumference as the ϕ25 bar after being meshed, still resulting in a reduction of the area. This was compensated by increasing Young's modulus (E_s) and the strength (f_{yk}/f_{uk}) of the steel with a corresponding factor of 25%.

The number of elements were desired to be as few as possible, to decrease the size of the finite element model, while keeping the results unaffected. Sensitivity analyses of the mesh was performed parallel to ensure this, presented in the Section 5.4.4. The appropriate mesh size found and used in the presented results is found in Table 5.4.

Table 5.4: *Approximate mesh size used in the presented result of SB1/SB2*

	Mesh size [mm]	**No of elements**
Concrete corner	25/90	≈ 370 000/240 000
Extended concrete members	100/100	≈ 20/20
Reinforcement	22/22	≈ 30 000/60 000

5.4 Results

To validate the numerical model and ensure that extracted results simulates reality is as mentioned before one of the main issues with FE-modelling. This validation can be done in numerous ways, where comparison to experimental data is one example. This is however both expensive and not always an option; for instance when studying large structures.

So, in contrast to previous analyses, no experiments have been performed to compare and verify against. Therefore, experience and results gained from all previous analyses performed in this thesis were crucial for further verification. The results from previous studies could obviously not be applied directly to this analysis, but knowing that bond model, applied symmetry conditions etc. reflected reality properly was important.

5.4.1 SB1

The force-displacement response, gained from the finite element analyses of *SB1*, is presented in Figure 5.4 together with the estimated capacity of 377 kN obtained according to Appendix B. In the analyses, the structure had its peak at 340 kN, and thereby never reached the estimated capacity. The analyses ended due to problems with convergence, appearing after a major drop of the structure's stiffness. The structure could still take more load, after the sudden reduction in stiffness. However, it was not sure if it would be able to reach up to the estimated capacity.

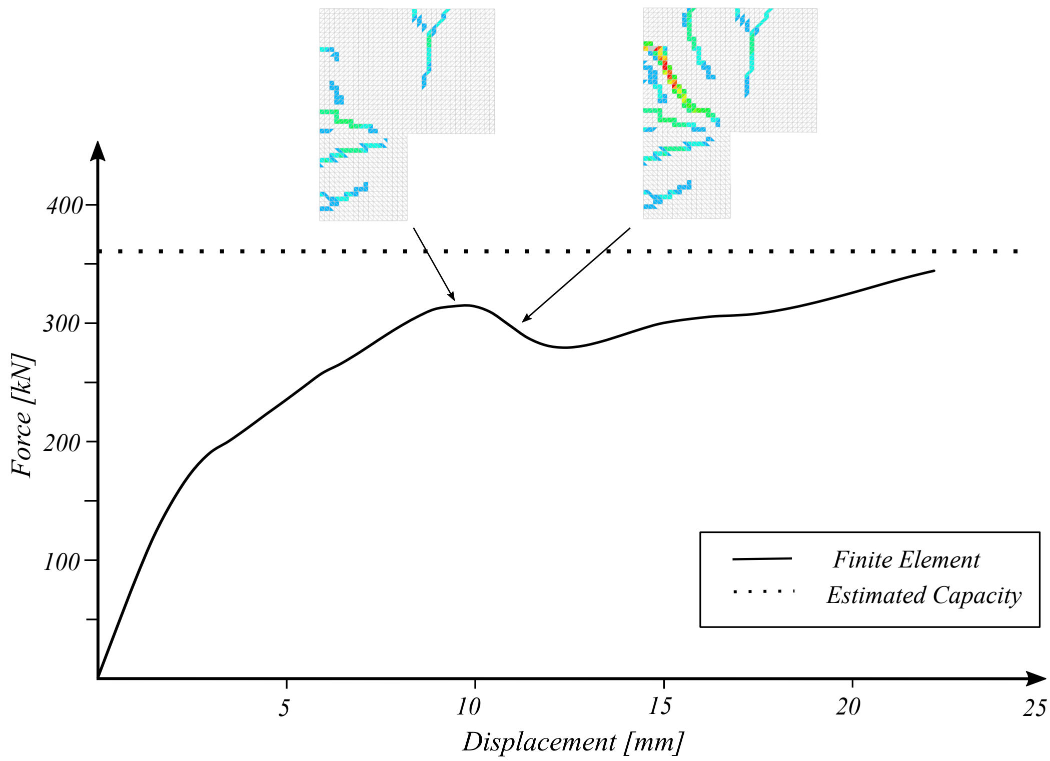

Figure 5.4: *Force-displacement response for SB1*

The sub figures, in Figure 5.4, representing the crack pattern before and after the load drop, indicates that the diagonal crack, that appeared straight through the corner, was the reason for the major load drop.

The observed crack pattern at the final step, in sections adjacent to the reinforcement, is presented in detail in Figure 5.5. These show bending cracks as well as the diagonal crack through the corner. This specific crack reached higher plastic strains than the other cracks. It has a maximum crack width of approximately 1.9 mm.

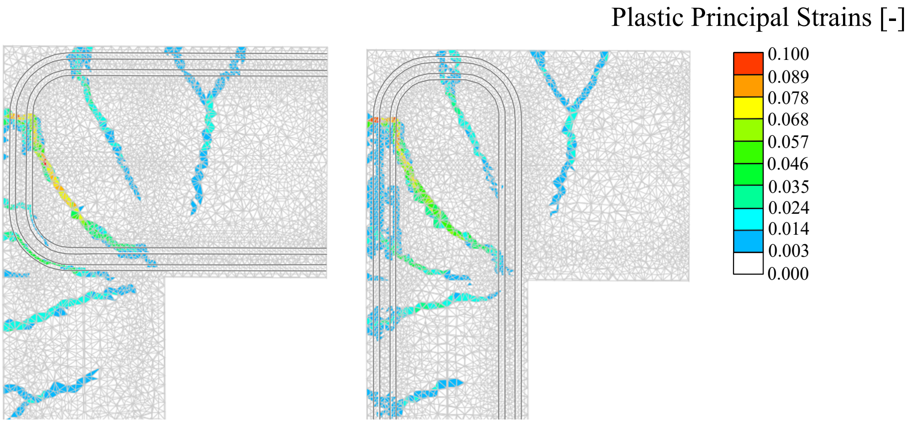

Figure 5.5: *Plastic strains in concrete displaying the crack pattern in the last step of the analyses of SB1. Taken in section cuts at position of vertical and horizontal loops*

However, the overall crack pattern was similar to the one obtained in the verified frame corner *RV5/6*, seen in Figure 4.15. But instead of bending around the semi-circular loop, the diagonal crack was formed propagating on the inside. The different fracture behaviour may depend on the different shapes of the loops as well as the big difference in sizes. Dragosavic et al. (1975) performed tests on both semi-circular and rectangular loops and concluded no observed difference in behaviour. However, their study included slab joints with low reinforcement ratios; thus the same conclusion can not be directly adapted to the analyses in this thesis.

The stresses in the reinforcement in the last step of the analysis, presented in Figure 5.6, verify that the convergence problems appeared before yielding was fully developed in the reinforcement. Instead, only a few elements reached the yield stress of 500 MPa in the numerical model, marked red. This indicates that the ultimate capacity probably was higher than what was presented in Figure 5.4.

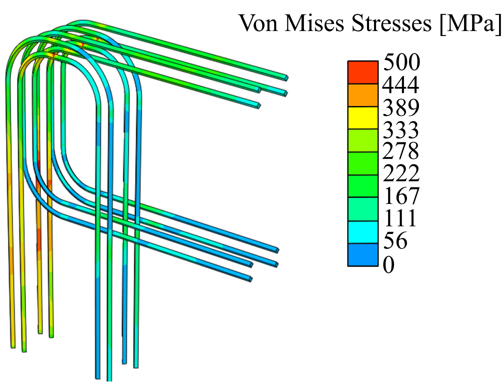

Figure 5.6: *Von Mises stresses in reinforcement at last step for SB1*

5.4.2 SB2

The analyses of *SB2*, a similar structure as the case study but with higher reinforcement ratio, resulted in a force-displacement relationship according to Figure 5.7. It is presented together with the estimated capacity of the cross section, according to calculations in Appendix C. The response was smooth until the maximum force of 736 kN, where the analysis did not converge any longer. However, the decreased slope towards the end may indicate that the maximum force has been reached. The measured maximum capacity was approximately 100 kN higher than the estimated.

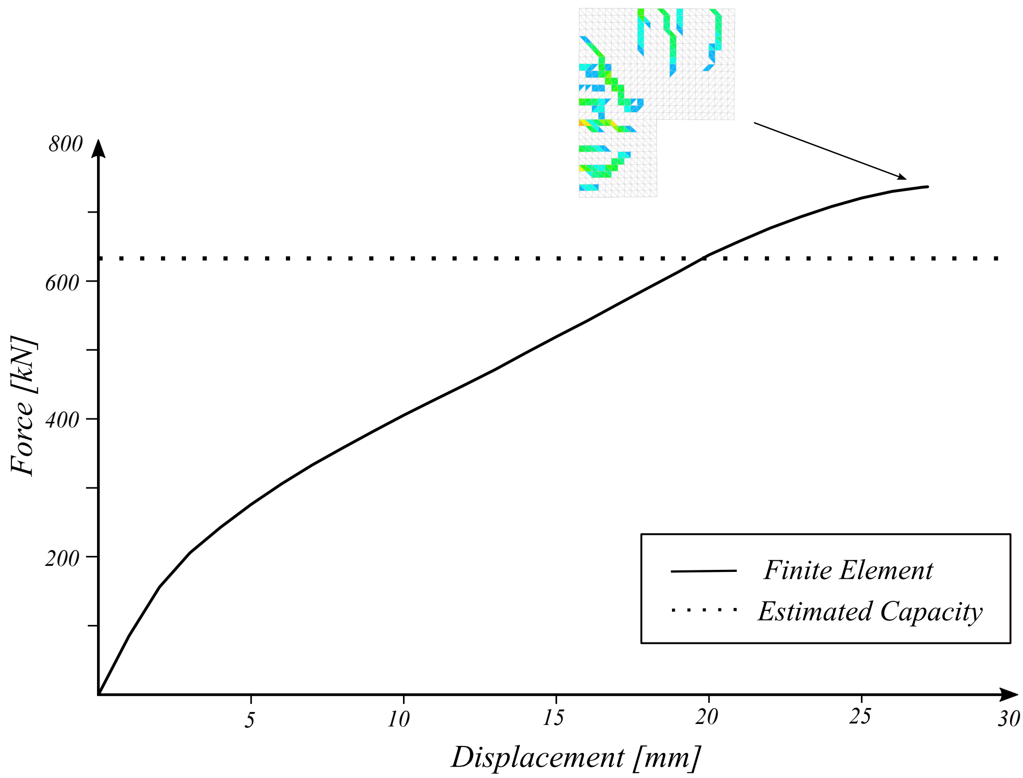

Figure 5.7: *Force-displacement response for SB2*

The constraints on both sides, due to the applied symmetry conditions, induced a triaxial stress-state. This, as described in Chapter 3, may according to Eurocode (2005) increase the compressive strength significantly, which could explain the much higher capacity recorded for *SB2* in comparison to the estimated. This also apply to the case of *SB1*, but was difficult to distinguish due to the large load drop and convergence problems observed. The stresses exceeding the input compressive strength of 35 MPa in the finite element analyses of *SB2* can be seen in Figure 5.8.

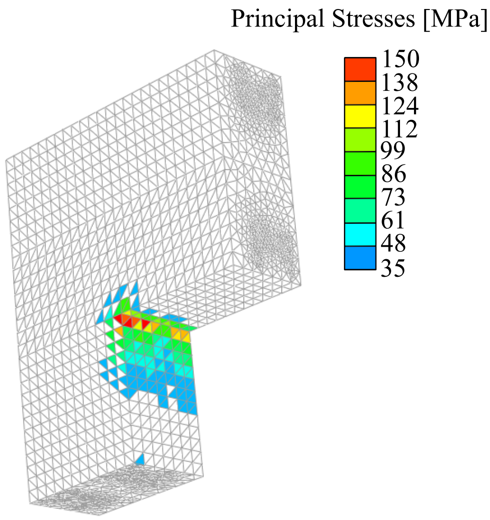

Figure 5.8: *Compressive stresses in concrete exceeding 35 MPa*

The crack pattern within the section in the final step, presented in Figure 5.9, is similar to the results in *SB1* but with smaller crack widths. Here, the maximum crack width was estimated to 1.1 mm. The pattern indicates pure bending cracks, but the increased amount of reinforcement redistributes the stresses and prevents one large crack to develop as in the previous analyses.

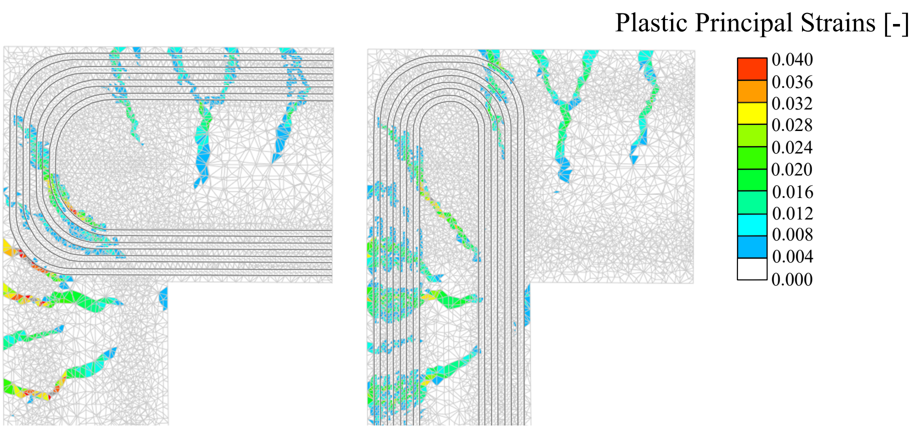

Figure 5.9: *Plastic strains in concrete displaying the crack pattern in the last step of the numerical model of SB2. Taken in section cuts at position of vertical and horizontal loops*

Before failure, extensive yielding of the reinforcement in the column part occured. This can be seen in Figure 5.10, where most of the outer rebars reached the yield stress of 500 MPa.

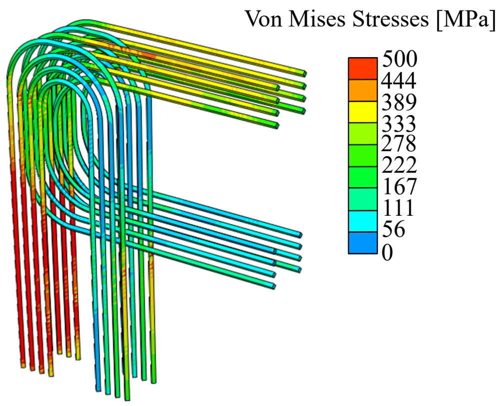

Figure 5.10: *Von Mises stresses in reinforcement at last step for SB2*

When having high reinforcement ratios, the risk of premature crushing of concrete in the inside of the corner is higher, as mentioned in Section 2.1.1. However, the results of the analyses show no indications of this and instead fails in a rather ductile manner.

5.4.3 Moment capacities

A summary of the ultimate moments obtained from the finite element analyses are presented and compared to the estimated moment capacities in Table 5.5. The partial safety factors were set to $\gamma = 1$, as presented in detail in Appendix B and C, and the influence of the normal force was taken into account. The capacities according to Dragosavic (Equation 2.4), Hao (Equation 2.8) and Joergensen (Equation 2.10) were also compared.

Table 5.5: *Summary of moment capacities [kNm]*

	$\boldsymbol{M_{Rd}}$	$\boldsymbol{M_{l.Drago}}$	$\boldsymbol{M_{l.Hao}}$	$\boldsymbol{M_{l.Joerg}}$	$\boldsymbol{M_{FE}}$
SB1	720	1295	613	184	570
SB2	1141	1808	1142	184	1331

The scatter in estimated moment capacities obtained from the equations above are obvious when studying Table 5.5. Dragosavic's equation predicted a much higher capacity than allowed for a structure of this size as no limit for the steel stress was included in the equations, stated in Section 2.2.7. The capacity estimated through the equations developed by Joergensen were way too low. This since the equations were not applicable for structures where the compressive zone is larger than the concrete cover, see Section 2.2.6, which was the case for the analysed structures. Hao's equation resulted in a bit lower capacity for *SB1*, than estimated by the cross-sectional analyses, and very similar for *SB2*. However, both slightly differed from the results of the finite element analyses.

5.4.4 Validation

A mesh convergence study was done to validate the chosen meshes. The run time for the numerical analyses was very much dependent on the number of elements and especially in the reinforcement bars, due to the small size in comparison to the rest of the concrete corner. The complexity of the model induced many parameters that could be varied, therefore the convergence study was limited to altering the number of elements in the concrete only, while keeping the number of elements in the reinforcement constant. However, the number of elements could not be chosen below 100 000 and above 350 000 dues to the limitations of the reinforcement mesh and tetrahedral shapes. The mesh was therefore kept within these numbers. The results are presented in Figure 5.11.

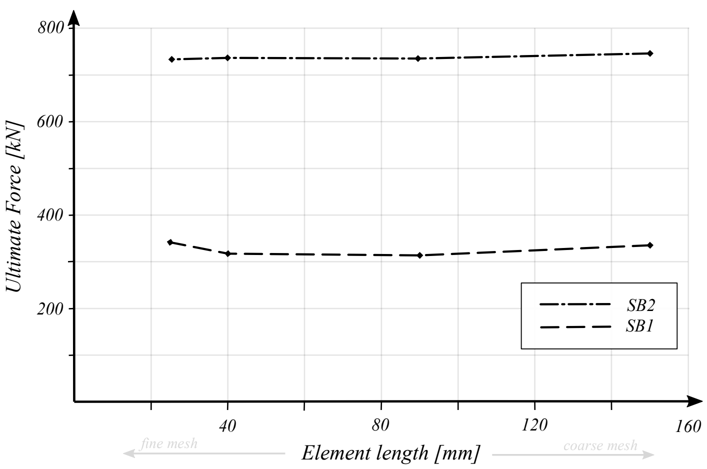

(a) *Ultimate force corresponding to varying mesh sizes*

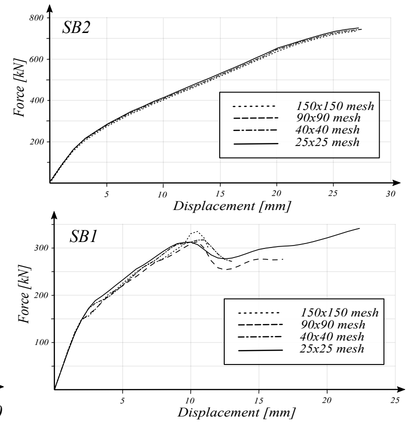

(b) *Variation in the structural response for SB2 & SB1 for different mesh sizes*

Figure 5.11: *Mesh convergence study for SB1/SB2*

It can be seen that the results were very stable, independently of the used mesh size of the concrete, but alternated slightly up and down for *SB1*. The sub-figures in Figure 5.11b, shows the structural response for the different meshes. It illustrates that *SB1* was more sensitive to the used mesh size, having different drops and displacement before convergence error occurred. The different scales on the axis in the sub-figures should be noted.

Again, different dilation angles (ψ) and viscosity parameters (μ) were used in the analyses to distinguish their influence on the results. The dilation angle were varied between 35° to 45°, with no difference noted. The viscosity parameter were varied between 0 and 0.0001, where only the last one gave results with 10% offset compared to the rest. The usage of 35° dilation angle and 0.00005 viscosity parameter in the presented analyses were by that verified.

6
Conclusions

The main aim of the thesis was to investigate to which extent it was possible to implement loop connections in large concrete frame corners, heavily reinforced with multiple layers of reinforcement. This was done through a thorough literature study, by looking into previous recommendations from researchers and by running a number of finite element analyses with different levels of detailing. These analyses were continuously verified against previously performed experiments and hand calculations.

6.1 General

The usage of finite element analyses in design, within the field of structural engineering, is a powerful tool and the validation of the behaviour of the analyses is one of the most important parts. To ensure that the method of modelling captures the interaction between the reinforcement and the concrete, it was verified against pull-out tests comparing crack pattern and bond stresses. The method with surface cohesion interaction gave satisfying results and was used throughout this work.

The finite element analyses, of a frame corner with loop connections in one layer, were verified against experimental test results. Even though good correlation was achieved, it was not possible to simulate the failure mode of side spalling observed in the experiments. This was because the multi-axial stress states appearing in reality is very complicated and difficult to capture. This was found to be the main reason behind the higher capacity obtained in the finite element analyses compared to the experiments. Instead the maximum capacity reached in the verifying analyses represented the capacity for a frame corner where side spalling was prevented. However, this discrepancy was acceptable because the following study was limited to plain-strain conditions.

In the case study analyses, of a frame corner with large dimensions and multiple layers of reinforcement, a diagonal crack in the corner was developed. This turned out to have a more serious effect when designed with two layers of reinforcement, compared to a higher reinforcement ratio with four layers. Due to the tri-axial stress condition, as a result from the constrains out of plane of the corner, the compressive strength could be increased; thus, increasing the ultimate moment capacity. This could be seen mainly in the analyses with four layer of reinforcement where the obtained moment capacity from the finite element analyses was approximately 16 % higher than estimated.

Frame corners with conventional detailing subjected to closing moments, if properly designed, fails by yielding of the reinforcement and crushing of the concrete at the inside of the corner simultaneously, as cracks propagates from the edges. Since the results from the finite element analyses does not show any other failure modes or deviating crack pattern, this thesis supports the usage of loop reinforcement within large corner regions under plain-strain conditions. Though to be noted, the usage of loop reinforcement leads to an increased total amount of reinforcement since all bars goes back in a U-turn.

In addition, it is worth noting that for certain conditions, the capacity of the corner may be lower than the ones of the adjoining sections. Splitting of the side concrete cover must be prevented with a sufficient thickness of the concrete cover when the corner has free edges. If so, or if the structure does not have free edges as in the studied case under plain-strain conditions, the capacity of the corner is commonly higher than the adjoining sections. Though, analyses indicated that a diagonal crack could still be induced resulting in an undesired drop of the stiffness before ultimate capacity is reached.

The guidelines for usage of loop connections in Modelcode (2010), and upcoming in Eurocode, are developed for structures loaded in pure tension. However, in pure tension the concrete within the loop is exposed to higher compressive stresses than in loops loaded in bending. Thus, the recommendations can be expected to be conservatively for bending. The available estimations of moment capacity according to Dragosavic et al. (1975), Hao (2004) and Joergensen & Hoang (2015) were compared to that of the finite element analyses. For a large structure with multiple layers of reinforcement, it was found that Dragosavic overestimated the capacity with ≈ 40-120 %, not being limited by yield stresses in the steel. Joergensen's equation underestimated with ≈ 70-85 %, since the compressive zone was bigger than the concrete cover which was one of the prerequisites stated. Hao's equation was found to be within reasonable limits to the obtained results from the analyses. However, extra caution must be taken to all case specific requirements when using all three equations.

6.2 Suggestions for further research

Initially, it was intended to evaluate both implicit and explicit modelling techniques. However, the explicit solver was soon ruled out since the tetrahedral mesh combined with the geometry of the loops complicated the ability to control the smallest elements size, which led to extensive computational time. This, in combination with a functioning implicit solver, led to the decision to put explicit solving techniques a side focusing on other issues.

Nevertheless, one of the main issues with implicit finite element modelling is convergence problems, causing uncertainties whether any results will be accessible on time during the design process. Add to this the large amount of time already required to run analyses of this size. So, if the possibility is given to focus on background and implementation of cohesive attributes in combination with explicit solver in ABAQUS, this might be a good approach to reduce computational uncertainties and be able to further study the post-peak behaviour of frame corners with loop connections.

In this thesis the post-peak response of concrete in compression was assumed to be constant, and convergence errors anyhow occurred before this phase started. However, if the analyses would have continued, this behaviour also becomes relevant to obtain a proper structural post-peak response. In that case, the mesh dependency of concrete in post-peak compression is important to consider.

For a model to fully reflect the influence of loop reinforcement on crack pattern and ultimate failure modes, it would be necessary to use a concrete material model that describes the multi-axial stress state arising within the corner. It is suggested to look further into different implementation of the material models in combination with analyses mimicking performed experiments. It would be of relevance to capture the transverse forces and gain the observed crack pattern in slabs corresponding to experiments performed by Dragosavic et al. (1975), as well as capture the side concrete spalling related to published experiments by Grassl (1999) & Johansson (2000b).

To be able to draw direct conclusions of the usage of loop reinforcement in these type of structures, it would be valuable to analyse a frame corner with conventional reinforcement detailing with the same modelling technique and the same large dimensions as the case studied.

Finally, many structures are subjected to both opening and closing moments during their lifetime, requiring a design that is able to withstand both loading situations. However, the scope of this thesis only covers the concept of closing frame corners, i.e. corners subjected to a negative moment. So, to be able to find general design recommendations for loops connections in frame corners, further analyses on structures subjected to opening moments, i.e. corners subjected to a positive moment, are required.

References

Alfarah, B., López-Almansa, F., & Oller, S. (2017). New methodology for calculating damage variables evolution in plastic damage model for rc structures. *Engineering Structures*, *132*, 70 - 86.

Al-Osta, M., Al-Sakkaf, H., Sharif, A., Ahmad, S., & Baluch, M. (2018). Finite element modeling of corroded rc beams using cohesive surface bonding approach. *Computers and concrete*, *22*(2), 167–182.

CEB-FIB. (2010). *Ceb-fib model code 2010.* Federation internationale du beton (fib).

CEB-FIB (2008). *Bulletin 43: Structural connections for precast concrete.* Federation internationale du beton (fib).

CEN. (2005). *Eurocode 1992-1-1:2005.* SIS Förlag AB.

Dassault-Systèmes. (2014). *Abaqus 6.14 analysis user's guide.* Dassault Systèmes.

Demir, A., Aztur, H., Edip, K., Stojmanovska, M., & Bogdanovic, A. (2018). Effect of viscosity parameter on the numerical simulation of reinforced concrete deep beam behavior. *The Online Journal of Science and Technology*, *8*(3), 50-56.

Dragosavic, M., van den Beukel, A., & Gijsbers, F. (1975). Loop connections between precast concrete components loaded in bending. *Heron*, *Volume 20*(Issue 3), 1-36.

Grassl, P. (1999). *Splicing of reinforcement loops in beams.* Chalmers Tekniska Högskola.

Hao, J. B. (2004). *Structural behaviour of precast component joints with loop connections.* National University of Singapore.

Henriques, J., Simões da Silva, L., & Valente, I. (2013). Numerical modeling of composite beam to reinforced concrete wall joints: Part i: Calibration of joint components. *Engineering Structures*, *52*, 747 - 761.

Hillerborg, A., & Gustafsson, P. (1985). Improvements in concrete design achieved through the application of fracture mechanics. *Application of Fracture Mechanics to Cementitious Composites*(S. P. Shah ed.), 667-680.

Hordijk, D. (1992). Tensile and tensile fatigue behaviour of concrete; experiments, modelling and analyses. *Heron*, *37*, 1-79.

Jansson, A., Lundgren, K., Gylltoft, K., & Lofgren, I. (2012). Bond of reinforcement in self-compacting steel-fibre-reinforced concrete. *Magazine of Concrete Research*, *64*(7), 617-630.

Joergensen, H., & Hoang, L. (2013). Test and limit analysis of loop connections between precast concrete elements loaded in tension. *Engineering Structures*, *52*(1), 558-569.

Joergensen, H., & Hoang, L. (2015). Strength of loop connections between precast bridge decks loaded in combined tension and bending. *Structural Engineering International*, *25*(1), 7180.

Johansson, M. (2000a). Nonlinear finite-element analyses of concrete frame corners. *Journal of Structural Engineering*, *126*(2), 190–199.

Johansson, M. (2000b). *Structural behaviour in concrete frame corners of civil defence shelters.* Chalmers Tekniska Högskola.

Kupfer, H., Hilsdorf, H., & Rusch, H. (1969). Behavior of concrete under biaxial stresses. *ACI Structural Journal*, *66*, 656-666.

Lundgren, K. (1999). *Three-dimensional modelling of bond in reinforced concrete.* Chalmers Tekniska Högskola.

Malm, R. (2006). *Shear cracks in concrete structures subjected to in-plane stresses* (Unpublished doctoral dissertation). Kungliga Tekniska Högskolan.

Malm, R. (2016). *Guideline for fe analyses of concrete dams.* Energiforsk Report 2016:270.

Nilsson, I. (1973). *Reinforced concrete corners and joints subjected to bending moment.* Chalmers Tekniska Högskola.

Plos, M. (1996). *Finite element analyses of reinforced concrete structures.* Chalmers Tekniska Högskola.

Zhu, M., Sonebi, M., & Bartos, P. (2004). Bond and interfacial properties of reinforcement in self-compacting concrete. *Materials and Structures*, *37*(7), 442-448.

A

Appendix A

Cross sectional capacity of "RV5/RV6".

Calculated with Response 2000 v.1.0.5, developed at the University of Toronto by Evan Bentz in a project supervised by Professor Michael P. Collins. Verified with hand calculations according to Eurocode.

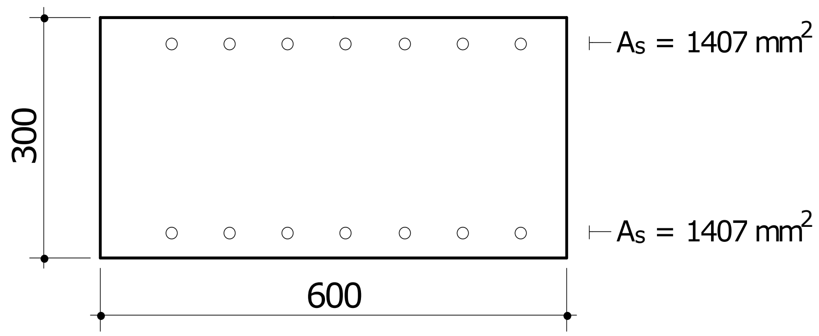

All dimensions in millimetres
Clear cover to reinforcement = 24 mm

Geometric Properties

	Gross Conc.	Trans (n=7.92)
Area (mm^2) x 10^3	180.0	199.5
Inertia (mm^4) x 10^6	1350.0	1621.0
y_t (mm)	150	150
y_b (mm)	150	150
S_t (mm^3) x 10^3	9000.0	10806.6
S_b (mm^3) x 10^3	9000.0	10806.6

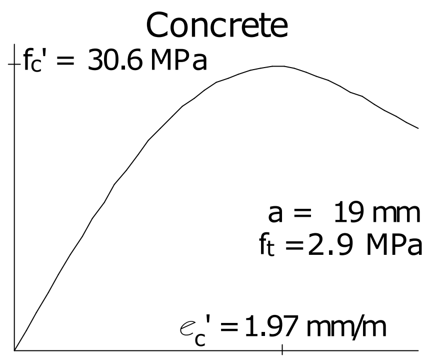

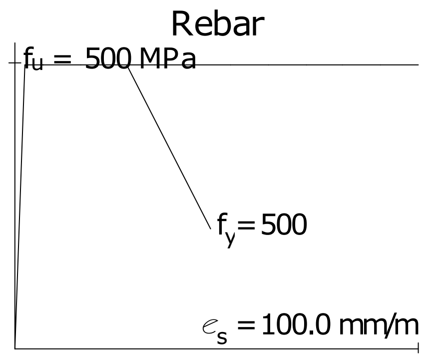

Cross Section

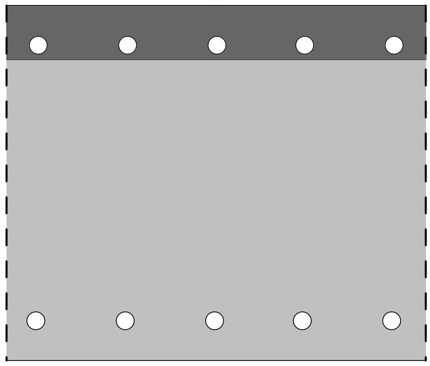

Internal Forces

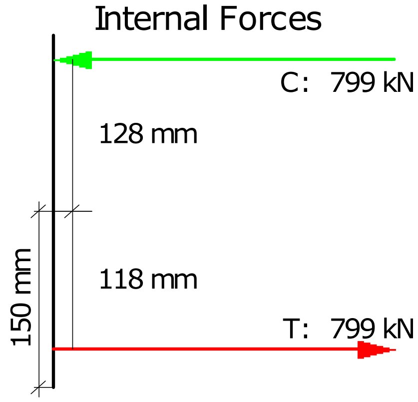

N+M

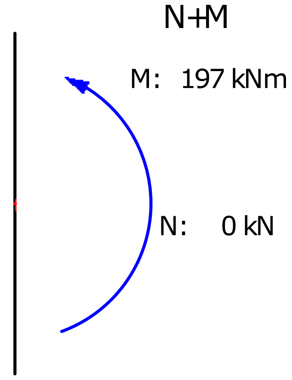

Longitudinal Concrete Stress

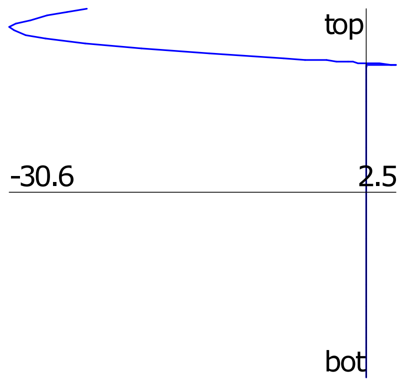

Long. Reinforcement Stress

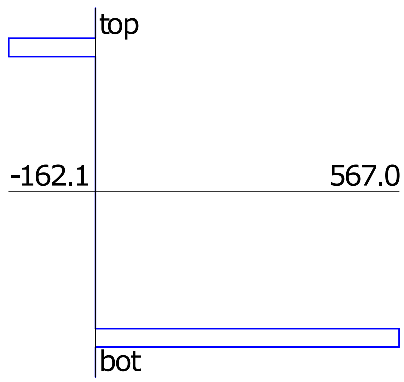

Longitudinal Strain

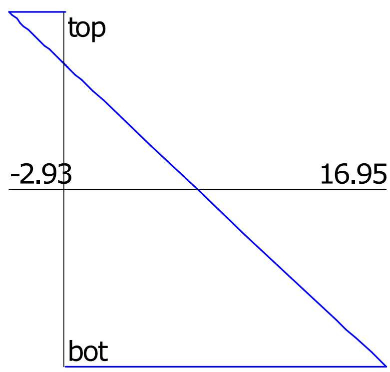

M-N-interaction

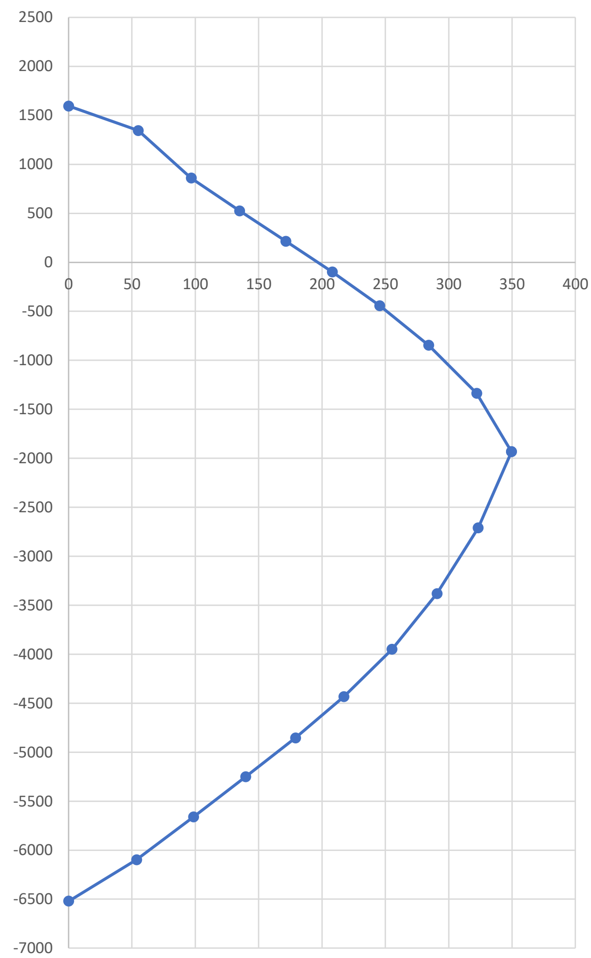

B

Appendix B

Cross sectional capacity of "SB1".

Calculated with Response 2000 v.1.0.5, developed at the University of Toronto by Evan Bentz in a project supervised by Professor Michael P. Collins. Verified with hand calculations according to Eurocode.

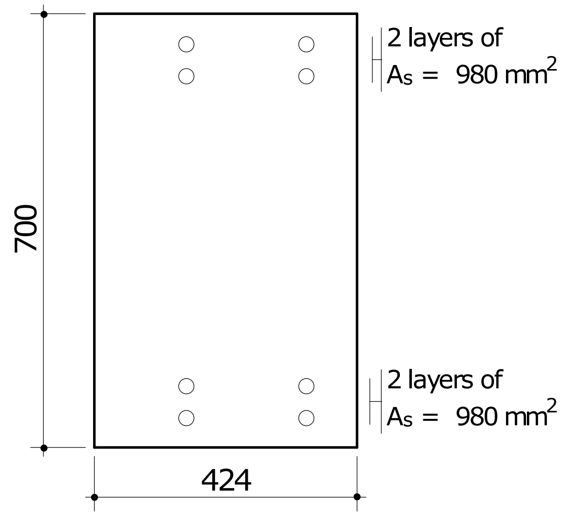

All dimensions in millimetres
Clear cover to reinforcement = 38 mm

Geometric Properties

	Gross Conc.	Trans (n=7.54)
Area (mm^2) x 10^3	296.8	322.4
Inertia (mm^4) x 10^6	12119.3	14072.8
y_t (mm)	350	350
y_b (mm)	350	350
S_t (mm^3) x 10^3	34626.7	40207.9
S_b (mm^3) x 10^3	34626.7	40207.9

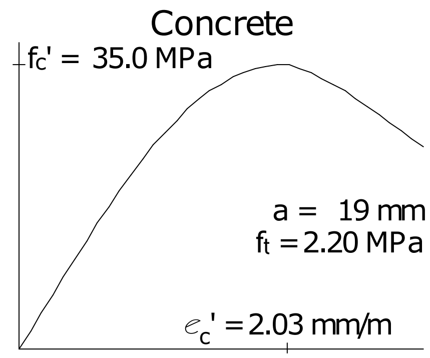

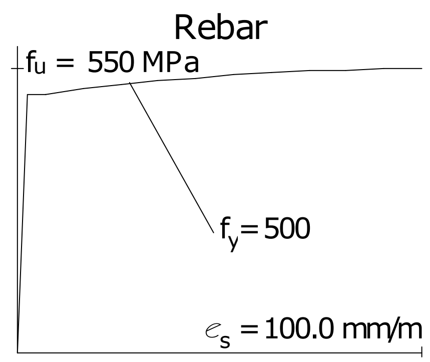

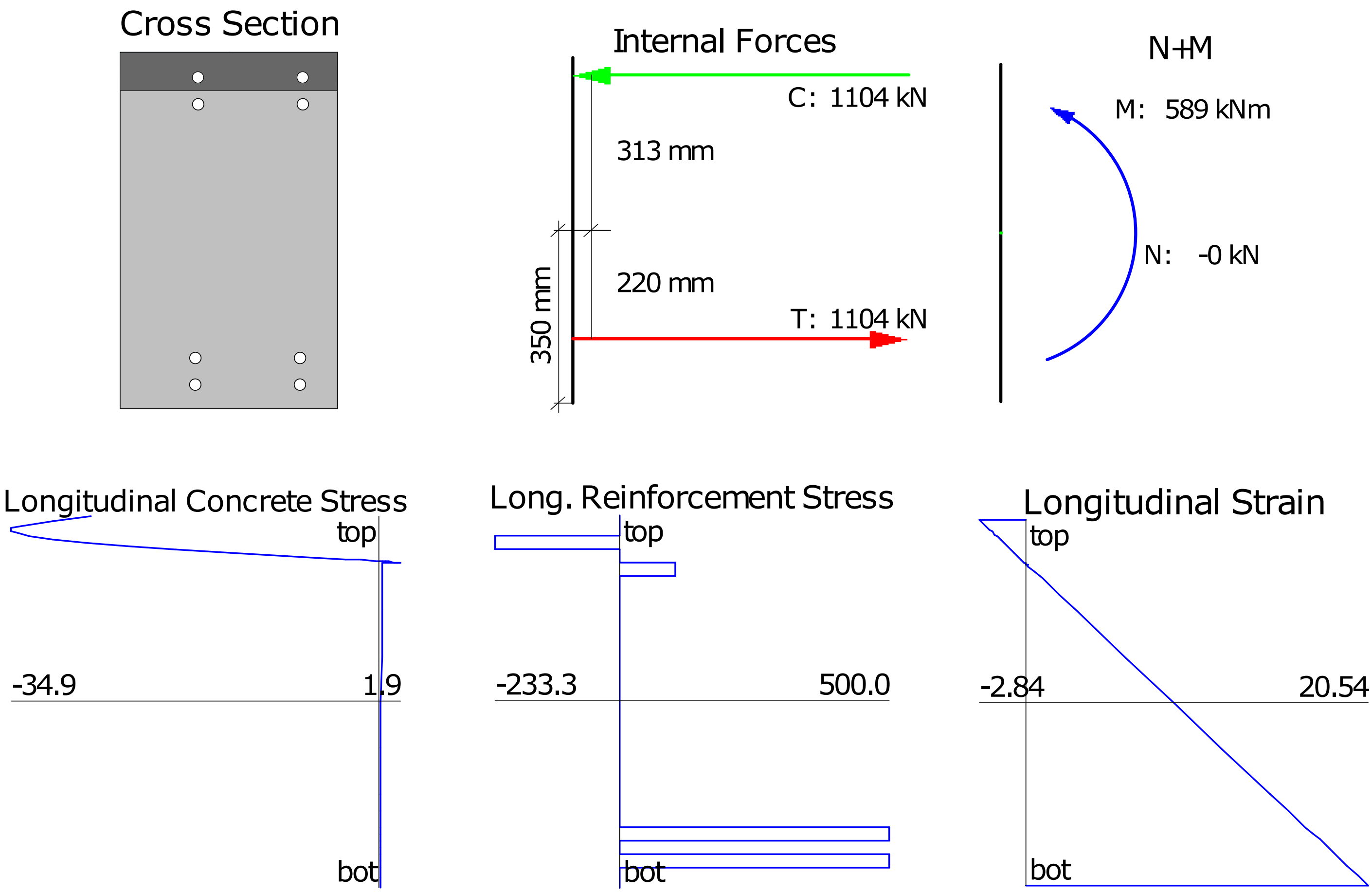
Cross Section
Internal Forces
C: 1104 kN
313 mm
350 mm
220 mm
T: 1104 kN
N+M
M: 589 kNm
N: -0 kN
Longitudinal Concrete Stress
top
-34.9
1.9
bot
Long. Reinforcement Stress
top
-233.3
500.0
bot
Longitudinal Strain
top
-2.84
20.54
bot

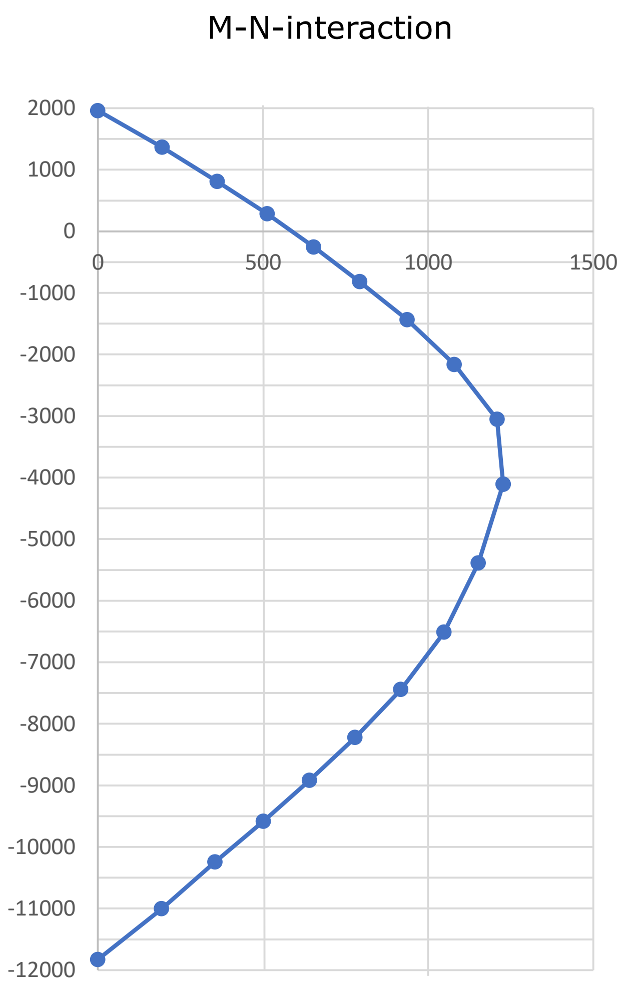
M-N-interaction
2000
1000
0
-1000
-2000
-3000
-4000
-5000
-6000
-7000
-8000
-9000
-10000
-11000
-12000
0
500
1000
1500

C

Appendix C

Cross sectional capacity of "SB2".

Calculated with Response 2000 v.1.0.5, developed at the University of Toronto by Evan Bentz in a project supervised by Professor Michael P. Collins. Verified with hand calculations according to Eurocode.

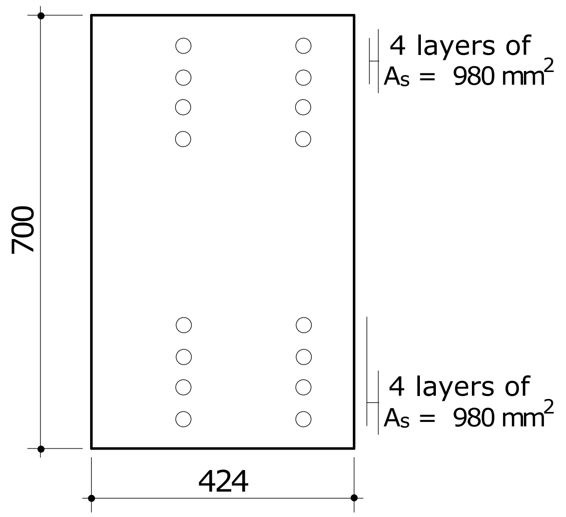

All dimensions in millimetres
Clear cover to reinforcement = 38 mm

Geometric Properties

	Gross Conc.	Trans (n=7.54)
Area (mm^2) x 10^3	296.8	348.0
Inertia (mm^4) x 10^6	12119.3	14873.4
y_t (mm)	350	350
y_b (mm)	350	350
S_t (mm^3) x 10^3	34626.7	42495.3
S_b (mm^3) x 10^3	34626.7	42495.3

Concrete

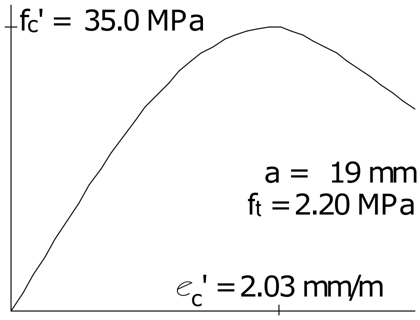

Rebar

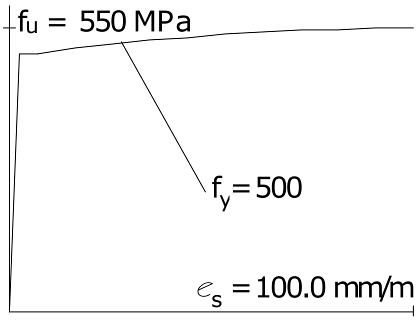

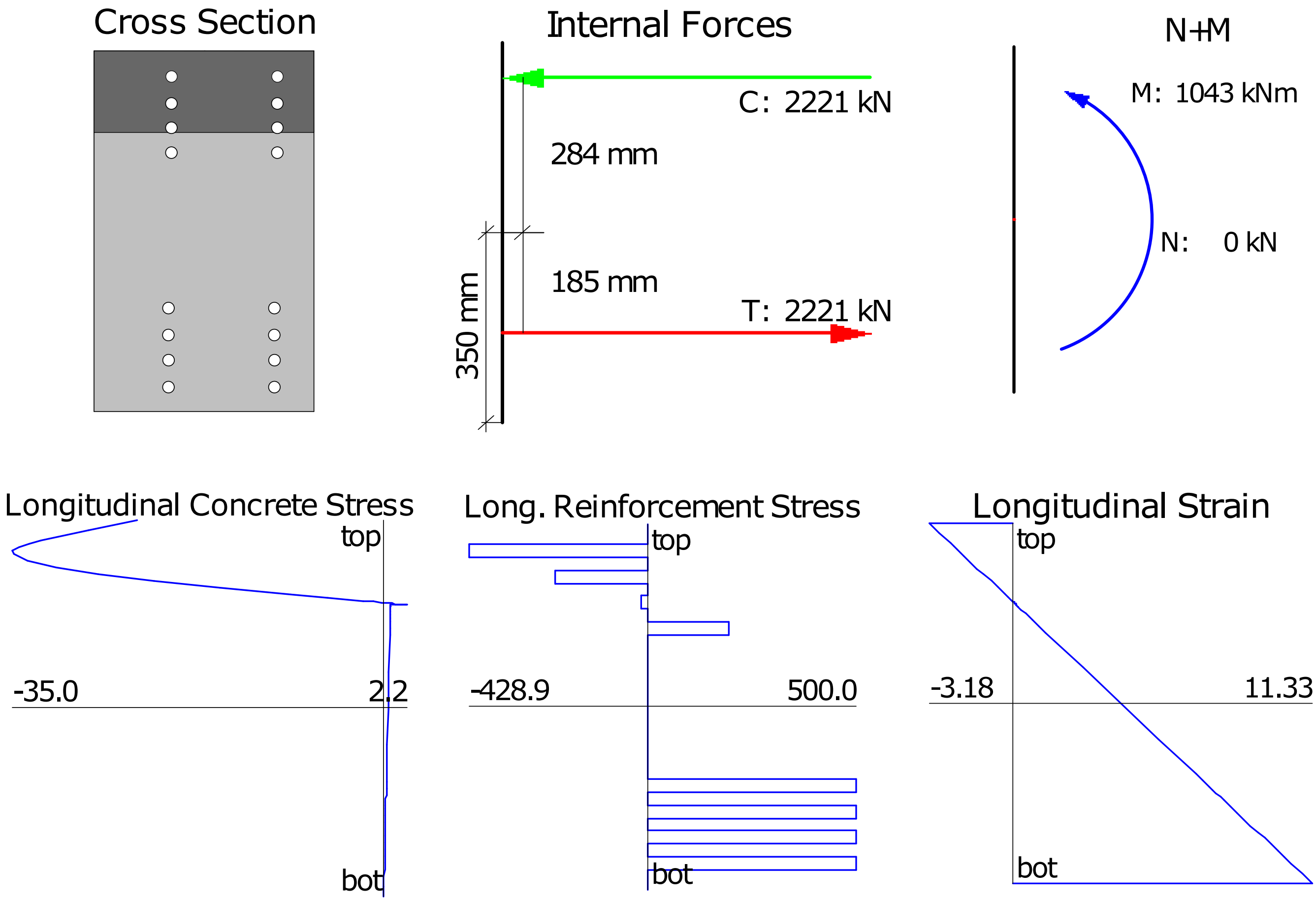
Cross Section
Internal Forces
C: 2221 kN
284 mm
185 mm
T: 2221 kN
350 mm
N+M
M: 1043 kNm
N: 0 kN
Longitudinal Concrete Stress
top
-35.0
2.2
bot
Long. Reinforcement Stress
top
-428.9
500.0
bot
Longitudinal Strain
top
-3.18
11.33
bot

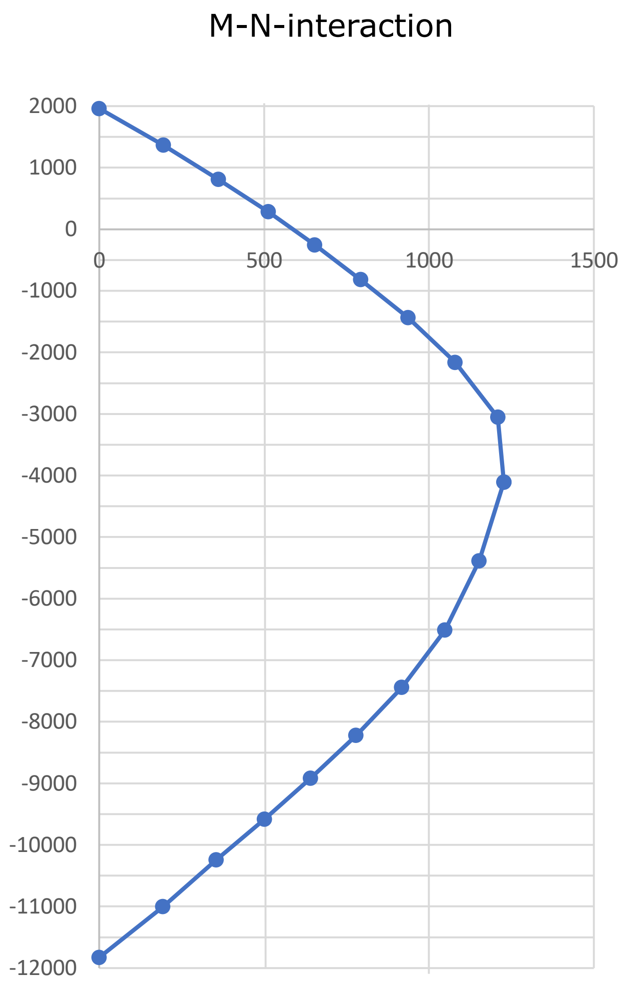
M-N-interaction
2000
1000
0
-1000
-2000
-3000
-4000
-5000
-6000
-7000
-8000
-9000
-10000
-11000
-12000
0
500
1000
1500

D

Appendix D

```
# LOOP CONNECTIONS IN HEAVILY REINFORCED CONCRETE FRAME CORNERS
# DEVELOPED BY: JENNY BERGLUND AND MALIN IVARSSON HOLMSTROM
# DATE: 2019-05-27

# NOTES: MOST PARTS ARE CONTROLLED BY THE VARIABLES IN THE FIRST SECTION AND
# WILL BE CHANGED ACCORDINGLY. THIS APPLIES FOR ALL SECTIONS APART FROM THE
# SECTIONS MARKED WITH (*), THESE WILL HAVE TO BE MANUALLY UPDATED IF THE
# NUMBER OF BARS IN EACH LAYER ARE CHANGED

from abaqus import *
from abaqusConstants import *
import __main__
import section
import regionToolset
import displayGroupMdbToolset as dgm
import part
import material
import assembly
import step
import interaction
import load
import mesh
import optimization
import job
import sketch
import visualization
import xyPlot
import displayGroupOdbToolset as dgo
import connectorBehavior

Mdb()

# ---------- variables ----------

# DIMENSIONS
b = 0.424                       # same for both column and beam
ltot=1.7                        # total length beam and column

# BEAM INPUT
d_beam = 1.0                    # thickness
```

```
l_beam = 0.7                    # height furthest out to where meeting column
zb1 = 0.053                     # z-coordinate for layers (1) i depth   (*)
zb2 = 0.265                     # z-coordinate for layers (2) i depth   (*)
zb=[zb1,zb2]

# COLUMN INPUT
d_col = 0.7                     # thickness
l_col = 0.7 + d_beam            # height corner (making it symmetrical)
zc1 = 0.159                     # z-coordinate for layers (1) i depth   (*)
zc2 = 0.371                     # z-coordinate for layers (2) i depth   (*)
zc=[zc1,zc2]

# REINFORCEMENT INPUT
phi = 0.028                     # bar diameter
cover = 1.5*phi                 # concrete cover

# MATERIAL PROPERTIES
E_c = 34000000000.0             # concrete E-modulus
v_c = 0.2                       # concrete poisson ratio
fc = 35000000.0                 # charac. compressive strength concrete [Pa]
E_s = 250000000000.0            # steel E-modulus
v_s = 0.3                       # steel poisson ratio
fy = 625000000.0                # steel yield strength
ft = 3200000.0                  # mean tensile strength concrete
Gf = 73.*((fc+8000000.)*0.000001)**0.18         # fracture energy (+8 to get
                                                  mean according to EC)

# APPLIED DISPLACEMENT
disp = 0.1

# PARAMETERS FOR REINFORCMENT CONFIGURATION
scol=d_col-2*cover              # distance between reinforcement up and down
Rcol=0.25                       # radius (seperated)
c_bar_col=2.0*phi               # distance between inner/outer loop

hcol=l_col-cover-Rcol
Rcol_full_1=(scol-4*c_bar_col)/2        # radius (full, no1 counted from out)
Rcol_in=(scol-6*c_bar_col)/2            # radius (full, inner)

sbeam=d_beam-2*cover                    # distance between reinforcement
Rbeam=0.25                              # radius (seperated)
c_bar_be=2.0*phi                        # distance between inner/outer loop
hbeam=l_beam+d_col-cover-Rbeam          # length of beam utside of corner area

# LENGTH OF EXTENDED BEAM AND COLUMN (symmetric)
lb=ltot-l_beam
lc=0.85

#---------- create concrete part ----------

# CREATE BEAM PART
s_b = mdb.models['Model-1'].ConstrainedSketch(name='__profile__',
sheetSize=200.0)
s_b.rectangle(point1=(0.0, 0.0), point2=(l_beam, -d_beam))
```

```
p_cb = mdb.models['Model-1'].Part(name='beam', dimensionality=THREE_D,
type=DEFORMABLE_BODY)
p_cb.BaseSolidExtrude(sketch=s_b, depth=b)

# CREATE COLUMN PART
s_c = mdb.models['Model-1'].ConstrainedSketch(name='__profile__',
sheetSize=200.0)
s_c.rectangle(point1=(0.0, 0.0), point2=(-d_col, -l_col))
p_cc = mdb.models['Model-1'].Part(name='column', dimensionality=THREE_D,
type=DEFORMABLE_BODY)
p_cc.BaseSolidExtrude(sketch=s_c, depth=b)

# -------- create reinforcement column -----------

# OUTER REINFORCEMENT BAR COLUMN
s_rco = mdb.models['Model-1'].ConstrainedSketch(name='__sweep__',
sheetSize=200.0)

s_rco.Line(point1=(0.0, 0.0), point2=(0.0, hcol))
s_rco.ArcByCenterEnds(center=(Rcol, hcol), point1=(0.0, hcol), point2=(Rcol,
hcol+Rcol), direction=CLOCKWISE)
s_rco.Line(point1=(Rcol, Rcol+hcol), point2=(scol-Rcol, Rcol+hcol))
s_rco.ArcByCenterEnds(center=(scol-Rcol, hcol), point1=(scol-Rcol, hcol+Rcol),
point2=(scol, hcol), direction=CLOCKWISE)
s_rco.Line(point1=(scol, hcol), point2=(scol, 0.0))

srco = mdb.models['Model-1'].ConstrainedSketch(name='__profile__',
sheetSize=200.0, transform=(1.0, 0.0, 0.0, 0.0, 0.0, 1.0, -0.0, -1.0, -0.0, 0.0,
0.0, 0.0))
srco.CircleByCenterPerimeter(center=(0.0, 0.0), point1=(phi/2, 0.0))

p_rco = mdb.models['Model-1'].Part(name='reinforcementc_out',
dimensionality=THREE_D, type=DEFORMABLE_BODY)
p_rco = mdb.models['Model-1'].parts['reinforcementc_out']
p_rco.BaseSolidSweep(sketch=srco, path=s_rco)

# MID_OUT REINFORCEMENT BAR COLUMN
s_rcmo = mdb.models['Model-1'].ConstrainedSketch(name='__sweep__',
sheetSize=200.0)

s_rcmo.Line(point1=(c_bar_col, 0.0), point2=(c_bar_col, (hcol-c_bar_col)))
s_rcmo.ArcByCenterEnds(center=((Rcol+c_bar_col), (hcol-c_bar_col)),
point1=(c_bar_col, (hcol-c_bar_col)), point2=((Rcol+c_bar_col),
(hcol+Rcol-c_bar_col)), direction=CLOCKWISE)
s_rcmo.Line(point1=((Rcol+c_bar_col), (hcol+Rcol-c_bar_col)),
point2=((scol-Rcol-c_bar_col), (hcol+Rcol-c_bar_col)))
s_rcmo.ArcByCenterEnds(center=((scol-Rcol-c_bar_col), (hcol-c_bar_col)),
point1=(scol-Rcol-c_bar_col, hcol+Rcol-c_bar_col), point2=(scol-c_bar_col,
hcol-c_bar_col), direction=CLOCKWISE)
s_rcmo.Line(point1=(scol-c_bar_col, hcol-c_bar_col), point2=(scol-c_bar_col,
0.0))

srcmo = mdb.models['Model-1'].ConstrainedSketch(name='__profile__',
sheetSize=200.0, transform=(1.0, 0.0, 0.0, 0.0, 0.0, 1.0, -0.0, -1.0, -0.0, 0.0,
```

```
0.0, 0.0))
srcmo.CircleByCenterPerimeter(center=(0.0, 0.0), point1=(phi/2, 0.0))

p_rcmo = mdb.models['Model-1'].Part(name='reinforcementc_mido',
dimensionality=THREE_D, type=DEFORMABLE_BODY)
p_rcmo = mdb.models['Model-1'].parts['reinforcementc_mido']
p_rcmo.BaseSolidSweep(sketch=srcmo, path=s_rcmo)

# MID_IN REINFORCEMENT BAR COLUMN
s_rcmi = mdb.models['Model-1'].ConstrainedSketch(name='__sweep__',
sheetSize=200.0)

s_rcmi.Line(point1=(2*c_bar_col, 0.0), point2=(2*c_bar_col,
hcol+Rcol-(2*c_bar_col)-Rcol_full_1))
s_rcmi.Arc3Points(point1=(2*c_bar_col, hcol+Rcol-(2*c_bar_col)-Rcol_full_1),
point2=(scol-(2*c_bar_col), hcol+Rcol-(2*c_bar_col)-Rcol_full_1),
point3=((2*c_bar_col)+Rcol_full_1, hcol+Rcol-(2*c_bar_col)))
s_rcmi.Line(point1=(scol-(2*c_bar_col), hcol+Rcol-(2*c_bar_col)-Rcol_full_1),
point2=(scol-(2*c_bar_col), 0.0))

srcmi = mdb.models['Model-1'].ConstrainedSketch(name='__profile__',
sheetSize=200.0, transform=(1.0, 0.0, 0.0, 0.0, 0.0, 1.0, -0.0, -1.0, -0.0, 0.0,
0.0, 0.0))
srcmi.CircleByCenterPerimeter(center=(0.0, 0.0), point1=(phi/2, 0.0))

p_rcmi = mdb.models['Model-1'].Part(name='reinforcementc_midi',
dimensionality=THREE_D, type=DEFORMABLE_BODY)
p_rcmi = mdb.models['Model-1'].parts['reinforcementc_midi']
p_rcmi.BaseSolidSweep(sketch=srcmi, path=s_rcmi)

# INNER REINFORCEMENT BAR COLUMN
s_rci = mdb.models['Model-1'].ConstrainedSketch(name='__sweep__',
sheetSize=200.0)

s_rci.Line(point1=(3*c_bar_col, 0.0), point2=(3*c_bar_col,
hcol+Rcol-(3*c_bar_col)-Rcol_in))
s_rci.Arc3Points(point1=(3*c_bar_col, hcol+Rcol-(3*c_bar_col)-Rcol_in),
point2=(scol-(3*c_bar_col), hcol+Rcol-(3*c_bar_col)-Rcol_in),
point3=((3*c_bar_col)+Rcol_in, hcol+Rcol-(3*c_bar_col)))
s_rci.Line(point1=(scol-3*c_bar_col, hcol+Rcol-(3*c_bar_col)-Rcol_in),
point2=(scol-3*c_bar_col, 0.0))

srci = mdb.models['Model-1'].ConstrainedSketch(name='__profile__',
sheetSize=200.0, transform=(1.0, 0.0, 0.0, 0.0, 0.0, 1.0, -0.0, -1.0, -0.0, 0.0,
0.0, 0.0))
srci.CircleByCenterPerimeter(center=(0.0, 0.0), point1=(phi/2, 0.0))

p_rci = mdb.models['Model-1'].Part(name='reinforcementc_in',
dimensionality=THREE_D, type=DEFORMABLE_BODY)
p_rci = mdb.models['Model-1'].parts['reinforcementc_in']
p_rci.BaseSolidSweep(sketch=srci, path=s_rci)

# ------------- create reinforcement beam ------------
```

```
# OUTER REINFORCEMENT BAR BEAM
s_rbo = mdb.models['Model-1'].ConstrainedSketch(name='__sweep__',
sheetSize=200.0)

s_rbo.Line(point1=(0.0, 0.0), point2=(0.0, hbeam))
s_rbo.ArcByCenterEnds(center=(Rbeam, hbeam), point1=(0.0, hbeam), point2=(Rbeam,
hbeam+Rbeam), direction=CLOCKWISE)
s_rbo.Line(point1=(Rbeam, Rbeam+hbeam), point2=(sbeam-Rbeam, Rbeam+hbeam))
s_rbo.ArcByCenterEnds(center=(sbeam-Rbeam, hbeam), point1=(sbeam-Rbeam,
hbeam+Rbeam), point2=(sbeam, hbeam), direction=CLOCKWISE)
s_rbo.Line(point1=(sbeam, hbeam), point2=(sbeam, 0.0))

srbo = mdb.models['Model-1'].ConstrainedSketch(name='__profile__',
sheetSize=200.0, transform=(1.0, 0.0, 0.0, 0.0, 0.0, 1.0, -0.0, -1.0, -0.0, 0.0,
0.0, 0.0))
srbo.CircleByCenterPerimeter(center=(0.0, 0.0), point1=(phi/2, 0.0))

p_rbo = mdb.models['Model-1'].Part(name='reinforcementb_out',
dimensionality=THREE_D, type=DEFORMABLE_BODY)
p_rbo = mdb.models['Model-1'].parts['reinforcementb_out']
p_rbo.BaseSolidSweep(sketch=srbo, path=s_rbo)

# MID_OUT REINFORCEMENT BAR BEAM
s_rbmo = mdb.models['Model-1'].ConstrainedSketch(name='__sweep__',
sheetSize=200.0)

s_rbmo.Line(point1=(c_bar_be, 0.0), point2=(c_bar_be, hbeam-c_bar_be))
s_rbmo.ArcByCenterEnds(center=(Rbeam+c_bar_be, hbeam-c_bar_be),
point1=(c_bar_be, hbeam-c_bar_be), point2=(Rbeam+c_bar_be,
hbeam+(Rbeam-c_bar_be)), direction=CLOCKWISE)
s_rbmo.Line(point1=(Rbeam+c_bar_be, hbeam+(Rbeam-c_bar_be)),
point2=(sbeam-Rbeam-c_bar_be, hbeam+(Rbeam-c_bar_be)))
s_rbmo.ArcByCenterEnds(center=(sbeam-Rbeam-c_bar_be, hbeam-c_bar_be),
point1=(sbeam-Rbeam-c_bar_be, hbeam+(Rbeam-c_bar_be)), point2=(sbeam-c_bar_be,
hbeam-c_bar_be), direction=CLOCKWISE)
s_rbmo.Line(point1=(sbeam-c_bar_be, hbeam-c_bar_be), point2=(sbeam-c_bar_be,
0.0))

srbmo = mdb.models['Model-1'].ConstrainedSketch(name='__profile__',
sheetSize=200.0, transform=(1.0, 0.0, 0.0, 0.0, 0.0, 1.0, -0.0, -1.0, -0.0, 0.0,
0.0, 0.0))
srbmo.CircleByCenterPerimeter(center=(0.0, 0.0), point1=(phi/2, 0.0))

p_rbmo = mdb.models['Model-1'].Part(name='reinforcementb_mido',
dimensionality=THREE_D, type=DEFORMABLE_BODY)
p_rbmo = mdb.models['Model-1'].parts['reinforcementb_mido']
p_rbmo.BaseSolidSweep(sketch=srbmo, path=s_rbmo)

# MID_IN REINFORCEMENT BAR BEAM
s_rbmi = mdb.models['Model-1'].ConstrainedSketch(name='__sweep__',
sheetSize=200.0)

s_rbmi.Line(point1=(2*c_bar_be, 0.0), point2=(2*c_bar_be, hbeam-2*c_bar_be))
s_rbmi.ArcByCenterEnds(center=(Rbeam+2*c_bar_be, hbeam-2*c_bar_be),
```

```
point1=(2*c_bar_be, hbeam-2*c_bar_be), point2=(Rbeam+2*c_bar_be,
hbeam+(Rbeam-2*c_bar_be)), direction=CLOCKWISE)
s_rbmi.Line(point1=(Rbeam+2*c_bar_be, hbeam+(Rbeam-2*c_bar_be)),
point2=(sbeam-Rbeam-2*c_bar_be, hbeam+(Rbeam-2*c_bar_be)))
s_rbmi.ArcByCenterEnds(center=(sbeam-Rbeam-2*c_bar_be, hbeam-2*c_bar_be),
point1=(sbeam-Rbeam-2*c_bar_be, hbeam+(Rbeam-2*c_bar_be)),
point2=(sbeam-2*c_bar_be, hbeam-2*c_bar_be), direction=CLOCKWISE)
s_rbmi.Line(point1=(sbeam-2*c_bar_be, hbeam-2*c_bar_be),
point2=(sbeam-2*c_bar_be, 0.0))

srbmi = mdb.models['Model-1'].ConstrainedSketch(name='__profile__',
sheetSize=200.0, transform=(1.0, 0.0, 0.0, 0.0, 0.0, 1.0, -0.0, -1.0, -0.0, 0.0,
0.0, 0.0))
srbmi.CircleByCenterPerimeter(center=(0.0, 0.0), point1=(phi/2, 0.0))

p_rbmi = mdb.models['Model-1'].Part(name='reinforcementb_midi',
dimensionality=THREE_D, type=DEFORMABLE_BODY)
p_rbmi = mdb.models['Model-1'].parts['reinforcementb_midi']
p_rbmi.BaseSolidSweep(sketch=srbmi, path=s_rbmi)

# INNER REINFORCEMENT BAR BEAM
s_rbi = mdb.models['Model-1'].ConstrainedSketch(name='__sweep__',
sheetSize=200.0)

s_rbi.Line(point1=(3*c_bar_be, 0.0), point2=(3*c_bar_be, hbeam-3*c_bar_be))
s_rbi.ArcByCenterEnds(center=(Rbeam+3*c_bar_be, hbeam-3*c_bar_be),
point1=(3*c_bar_be, hbeam-3*c_bar_be), point2=(Rbeam+3*c_bar_be,
hbeam+(Rbeam-3*c_bar_be)), direction=CLOCKWISE)
s_rbi.Line(point1=(Rbeam+3*c_bar_be, hbeam+(Rbeam-3*c_bar_be)),
point2=(sbeam-Rbeam-3*c_bar_be, hbeam+(Rbeam-3*c_bar_be)))
s_rbi.ArcByCenterEnds(center=(sbeam-Rbeam-3*c_bar_be, hbeam-3*c_bar_be),
point1=(sbeam-Rbeam-3*c_bar_be, hbeam+(Rbeam-3*c_bar_be)),
point2=(sbeam-3*c_bar_be, hbeam-3*c_bar_be), direction=CLOCKWISE)
s_rbi.Line(point1=(sbeam-3*c_bar_be, hbeam-3*c_bar_be),
point2=(sbeam-3*c_bar_be, 0.0))

srbi = mdb.models['Model-1'].ConstrainedSketch(name='__profile__',
sheetSize=200.0, transform=(1.0, 0.0, 0.0, 0.0, 0.0, 1.0, -0.0, -1.0, -0.0, 0.0,
0.0, 0.0))
srbi.CircleByCenterPerimeter(center=(0.0, 0.0), point1=(phi/2, 0.0))

p_rbi = mdb.models['Model-1'].Part(name='reinforcementb_in',
dimensionality=THREE_D, type=DEFORMABLE_BODY)
p_rbi = mdb.models['Model-1'].parts['reinforcementb_in']
p_rbi.BaseSolidSweep(sketch=srbi, path=s_rbi)

# CREATE EXTENDED BEAM + COLUMN
p_eb = mdb.models['Model-1'].parts['beam']
seb = mdb.models['Model-1'].ConstrainedSketch(name='__profile2__',
sheetSize=200.0)
seb.Line(point1=(0.0, 0.0), point2=(lb, 0.0))
p_eb = mdb.models['Model-1'].Part(name='ext_beam', dimensionality=THREE_D,
type=DEFORMABLE_BODY)
p_eb.BaseWire(sketch=seb)
```

```
p_ec = mdb.models['Model-1'].parts['beam']
sec = mdb.models['Model-1'].ConstrainedSketch(name='__profile3__',
sheetSize=200.0)
sec.Line(point1=(0.0, 0.0), point2=(lc, 0.0))
p_ec = mdb.models['Model-1'].Part(name='ext_col', dimensionality=THREE_D,
type=DEFORMABLE_BODY)
p_ec.BaseWire(sketch=sec)

# --------- material properties ---------

# CONCRETE ELASTIC MATERIAL
mdb.models['Model-1'].Material(name='Concrete elastic')
mdb.models['Model-1'].materials['Concrete elastic'].Elastic(table=((E_c, v_c),
))

# CONCRETE NON-LINEAR MATERIAL (tension is ft=fctm)
mdb.models['Model-1'].Material(name='Concrete')
mdb.models['Model-1'].materials['Concrete'].Elastic(table=((E_c, v_c), ))
mdb.models['Model-1'].materials['Concrete'].ConcreteDamagedPlasticity(table=((35
.0, 0.1, 1.16, 0.6667, 0.00005), ))
mdb.models['Model-1'].materials['Concrete'].concreteDamagedPlasticity.ConcreteCo
mpressionHardening(table=((1.24e7, 0.0), (fc, 0.00173), (fc, 0.00313)))
mdb.models['Model-1'].materials['Concrete'].concreteDamagedPlasticity.ConcreteTe
nsionStiffening(table=((ft, 0.0), (ft/3.0, 0.7*Gf/ft), (0, 4.0*Gf/ft)),
type=DISPLACEMENT)

# STEEL MATERIAL
mdb.models['Model-1'].Material(name='Steel')
mdb.models['Model-1'].materials['Steel'].Elastic(table=((E_s, v_s), ))
mdb.models['Model-1'].materials['Steel'].Plastic(table=((500000000.0, 0.0),
(500000000.0, 0.3)))

# --------- create section properties----------

# SECTION PROPERTIES
mdb.models['Model-1'].HomogeneousSolidSection(name='Concrete',
material='Concrete', thickness=None)
mdb.models['Model-1'].HomogeneousSolidSection(name='Reinforcement',
material='Steel', thickness=None)

# ASSIGN SECTIONS (*)
# (cb=concrete beam, cc=concrete column)
region = regionToolset.Region(cells=p_cb.cells.findAt(((l_beam/2, 0.0, 0.0), )))
p_cb.SectionAssignment(region=region, sectionName='Concrete', offset=0.0,
offsetType=MIDDLE_SURFACE, offsetField='', thicknessAssignment=FROM_SECTION)

region = regionToolset.Region(cells=p_cc.cells.findAt(((-d_col/2, 0.0, 0.0), )))
p_cc.SectionAssignment(region=region, sectionName='Concrete', offset=0.0,
offsetType=MIDDLE_SURFACE, offsetField='', thicknessAssignment=FROM_SECTION)

# (rbo=reinforcement beam outer, rbmo=reinforcement beam mid outer etc)
region = regionToolset.Region(cells=p_rbo.cells.findAt(((0.0, 0.0, 0.0), )))
p_rbo.SectionAssignment(region=region, sectionName='Reinforcement', offset=0.0,
```

```
offsetType=MIDDLE_SURFACE, offsetField='', thicknessAssignment=FROM_SECTION)

region = regionToolset.Region(cells=p_rbmo.cells.findAt(((c_bar_be, 0.0, 0.0),
)))
p_rbmo.SectionAssignment(region=region, sectionName='Reinforcement', offset=0.0,
offsetType=MIDDLE_SURFACE, offsetField='', thicknessAssignment=FROM_SECTION)

region = regionToolset.Region(cells=p_rbmi.cells.findAt(((2*c_bar_be, 0.0, 0.0),
)))
p_rbmi.SectionAssignment(region=region, sectionName='Reinforcement', offset=0.0,
offsetType=MIDDLE_SURFACE, offsetField='', thicknessAssignment=FROM_SECTION)

region = regionToolset.Region(cells=p_rbi.cells.findAt(((3*c_bar_be, 0.0, 0.0),
)))
p_rbi.SectionAssignment(region=region, sectionName='Reinforcement', offset=0.0,
offsetType=MIDDLE_SURFACE, offsetField='', thicknessAssignment=FROM_SECTION)


region = regionToolset.Region(cells=p_rco.cells.findAt(((0.0, 0.0, 0.0), )))
p_rco.SectionAssignment(region=region, sectionName='Reinforcement', offset=0.0,
offsetType=MIDDLE_SURFACE, offsetField='', thicknessAssignment=FROM_SECTION)

region = regionToolset.Region(cells=p_rcmo.cells.findAt(((c_bar_col, 0.0, 0.0),
)))
p_rcmo.SectionAssignment(region=region, sectionName='Reinforcement', offset=0.0,
offsetType=MIDDLE_SURFACE, offsetField='', thicknessAssignment=FROM_SECTION)

region = regionToolset.Region(cells=p_rcmi.cells.findAt(((2*c_bar_col, 0.0,
0.0), )))
p_rcmi.SectionAssignment(region=region, sectionName='Reinforcement', offset=0.0,
offsetType=MIDDLE_SURFACE, offsetField='', thicknessAssignment=FROM_SECTION)

region = regionToolset.Region(cells=p_rci.cells.findAt(((3*c_bar_col, 0.0, 0.0),
)))
p_rci.SectionAssignment(region=region, sectionName='Reinforcement', offset=0.0,
offsetType=MIDDLE_SURFACE, offsetField='', thicknessAssignment=FROM_SECTION)


mdb.models['Model-1'].RectangularProfile(name='CS-beam-1', a=b, b=d_beam)
mdb.models['Model-1'].BeamSection(name='Beam', integration=DURING_ANALYSIS,
poissonRatio=0.2, profile='CS-beam-1', material='Concrete elastic',
    temperatureVar=LINEAR, consistentMassMatrix=False)
region = regionToolset.Region(edges=p_eb.edges.findAt(((0.0, 0.0, 0.0), )))
p_eb.SectionAssignment(region=region, sectionName='Beam', offset=0.0,
offsetType=MIDDLE_SURFACE, offsetField='', thicknessAssignment=FROM_SECTION)
p_eb.assignBeamSectionOrientation(region=region, method=N1_COSINES, n1=(0.0,
0.0, -1.0))

mdb.models['Model-1'].RectangularProfile(name='CS-col-1', a=b, b=d_col)
mdb.models['Model-1'].BeamSection(name='Col', integration=DURING_ANALYSIS,
poissonRatio=0.2, profile='CS-col-1', material='Concrete elastic',
    temperatureVar=LINEAR, consistentMassMatrix=False)
region = regionToolset.Region(edges=p_eb.edges.findAt(((0.0, 0.0, 0.0), )))
p_ec.SectionAssignment(region=region, sectionName='Col', offset=0.0,
```

```
offsetType=MIDDLE_SURFACE, offsetField='', thicknessAssignment=FROM_SECTION)
p_ec.assignBeamSectionOrientation(region=region, method=N1_COSINES, n1=(0.0,
0.0, -1.0))

# ASSEMBLY AND MERGE PARTS
a = mdb.models['Model-1'].rootAssembly

# CONCRETE
a.DatumCsysByDefault(CARTESIAN)
a.Instance(name='beam-1', part=p_cb, dependent=OFF)
a.Instance(name='column-1', part=p_cc, dependent=OFF)
a.InstanceFromBooleanMerge(name='frame', instances=(a.instances['beam-1'],
a.instances['column-1'], ), originalInstances=SUPPRESS, domain=GEOMETRY)

a.makeIndependent(instances=(a.instances['frame-1'], ))                 # make
frame independent

# VERTICAL REINFORCEMENT (*)
ZC=int(len(zc))
for x in range(0,ZC):
    a.Instance(name='reinforcementc_out-%d' % (x+1), part=p_rco, dependent=OFF)
    a.translate(instanceList=('reinforcementc_out-%d' % (x+1), ),
vector=(-(d_col-cover), -(l_col), zc[x]))
    a.Instance(name='reinforcementc_mido-%d' % (x+1), part=p_rcmo,
dependent=OFF)
    a.translate(instanceList=('reinforcementc_mido-%d' % (x+1), ),
vector=(-(d_col-cover), -(l_col), zc[x]))
    a.Instance(name='reinforcementc_midi-%d' % (x+1), part=p_rcmi,
dependent=OFF)
    a.translate(instanceList=('reinforcementc_midi-%d' % (x+1), ),
vector=(-(d_col-cover), -(l_col), zc[x]))
    a.Instance(name='reinforcementc_in-%d' % (x+1), part=p_rci, dependent=OFF)
    a.translate(instanceList=('reinforcementc_in-%d' % (x+1), ),
vector=(-(d_col-cover), -(l_col), zc[x]))

# HORISONTAL REINFORCEMENT (*)
ZB=int(len(zb))
for x in range(0,ZB):
    a.Instance(name='reinforcementb_out-%d' % (x+1), part=p_rbo, dependent=OFF)
    a.rotate(instanceList=('reinforcementb_out-%d' % (x+1), ), axisPoint=(0.0,
0.0, 0.0), axisDirection=(0.0, 0.0, 1.0), angle=90.0)
    a.translate(instanceList=('reinforcementb_out-%d' % (x+1), ),
vector=(l_beam, -(d_beam-cover), zb[x]))
    a.Instance(name='reinforcementb_mido-%d' % (x+1), part=p_rbmo,
dependent=OFF)
    a.rotate(instanceList=('reinforcementb_mido-%d' % (x+1), ), axisPoint=(0.0,
0.0, 0.0), axisDirection=(0.0, 0.0, 1.0), angle=90.0)
    a.translate(instanceList=('reinforcementb_mido-%d' % (x+1), ),
vector=(l_beam, -(d_beam-cover), zb[x]))
    a.Instance(name='reinforcementb_midi-%d' % (x+1), part=p_rbmi,
dependent=OFF)
    a.rotate(instanceList=('reinforcementb_midi-%d' % (x+1), ), axisPoint=(0.0,
0.0, 0.0), axisDirection=(0.0, 0.0, 1.0), angle=90.0)
    a.translate(instanceList=('reinforcementb_midi-%d' % (x+1), ),
```

```
vector=(l_beam, -(d_beam-cover), zb[x]))
    a.Instance(name='reinforcementb_in-%d' % (x+1), part=p_rbi, dependent=OFF)
    a.rotate(instanceList=('reinforcementb_in-%d' % (x+1), ), axisPoint=(0.0,
0.0, 0.0), axisDirection=(0.0, 0.0, 1.0), angle=90.0)
    a.translate(instanceList=('reinforcementb_in-%d' % (x+1), ), vector=(l_beam,
-(d_beam-cover), zb[x]))

a.InstanceFromBooleanMerge(name='reinforcement',
instances=(a.instances['reinforcementc_out-1'],
a.instances['reinforcementc_out-2'], a.instances['reinforcementc_mido-1'],
a.instances['reinforcementc_mido-2'],
    a.instances['reinforcementc_midi-1'], a.instances['reinforcementc_midi-2'],
a.instances['reinforcementc_in-1'], a.instances['reinforcementc_in-2'],
a.instances['reinforcementb_out-1'],
    a.instances['reinforcementb_out-2'], a.instances['reinforcementb_mido-1'],
a.instances['reinforcementb_mido-2'], a.instances['reinforcementb_midi-1'],
    a.instances['reinforcementb_midi-2'], a.instances['reinforcementb_in-1'],
a.instances['reinforcementb_in-2'], ), originalInstances=SUPPRESS,
domain=GEOMETRY)

# COT HOLE IN CONCRETE WHERE REINFORCEMENT WILL BE PLACED
a.InstanceFromBooleanCut(name='concreteframe',
instanceToBeCut=mdb.models['Model-1'].rootAssembly.instances['frame-1'],
        cuttingInstances=(a.instances['reinforcement-1'], ),
originalInstances=SUPPRESS)
a.resumeFeatures(('reinforcement-1', )) #take back the reinforcement

a.makeIndependent(instances=(a.instances['reinforcement-1'], ))
a.makeIndependent(instances=(a.instances['concreteframe-1'], ))

# ASSEMBLY EXTENDED BEAM + COLUMN
a.Instance(name='ext_beam-1', part=p_eb, dependent=OFF)
a.instances['ext_beam-1'].translate(vector=(l_beam, -d_beam/2, b/2))

a.Instance(name='ext_col-1', part=p_ec, dependent=OFF)
a.rotate(instanceList=('ext_col-1', ), axisPoint=(0.0, 0.0, 0.0),
axisDirection=(0.0, 0.0, 1.0), angle=-90.0)
a.translate(instanceList=('ext_col-1', ), vector=(-d_col/2, -l_col, b/2))

# ---------- step -----------

# CREATE STEP
mdb.models['Model-1'].StaticStep(name='Step-1', previous='Initial',
maxNumInc=10000, stabilizationMagnitude=0.0002,
stabilizationMethod=DISSIPATED_ENERGY_FRACTION,
        continueDampingFactors=False, adaptiveDampingRatio=0.05,
initialInc=0.01, maxInc=0.01, nlgeom=ON)
# ALLOW FOR LOWER MIN VALUE
mdb.models['Model-1'].steps['Step-1'].setValues(minInc=1e-10)
# GIVES POSSIBILITY FOR 15 TRIES AT CONVERGENCE
mdb.models['Model-1'].steps['Step-1'].control.setValues(allowPropagation=OFF,
resetDefaultValues=OFF, timeIncrementation=(4.0, 8.0, 9.0, 16.0, 10.0, 4.0,
12.0, 10.0, 6.0, 3.0, 50.0))
```

```
# ---------- interaction model ----------

# CONTACT SURFACES CONCRETE (*)
side1Faces1 = a.instances['concreteframe-1'].faces.findAt(
        ((l_beam/2, -(d_beam-cover-phi/2), zb1), ), ((l_beam/2,
-(d_beam-cover-phi/2)+sbeam, zb1), ), ((-(d_col-cover-phi/2), -(Rbeam + cover),
zb1 ), ),
    ((l_beam/2, -(d_beam-cover-phi/2-c_bar_be), zb1), ), ((l_beam/2,
-(cover+phi/2+c_bar_be), zb1), ), ((-(d_col-cover-phi/2-c_bar_col), -(d_beam/2),
zb1 ), ),
    ((l_beam/2, -(d_beam-cover-phi/2-2*c_bar_be), zb1), ), ((l_beam/2,
-(cover+phi/2+2*c_bar_be), zb1), ), ((-(d_col-cover-phi/2-2*c_bar_col),
-(d_beam/2), zb1 ), ),
    ((l_beam/2, -(d_beam-cover-phi/2-3*c_bar_be), zb1), ), ((l_beam/2,
-(cover+phi/2+3*c_bar_be), zb1), ), ((-(d_col-cover-phi/2-3*c_bar_col),
-(d_beam/2), zb1 ), ),
        ((l_beam/2, -(d_beam-cover-phi/2), zb2), ), ((l_beam/2,
-(d_beam-cover-phi/2)+sbeam, zb2), ), ((-(d_col-cover-phi/2), -(Rbeam + cover),
zb2 ), ),
    ((l_beam/2, -(d_beam-cover-phi/2-c_bar_be), zb2), ), ((l_beam/2,
-(cover+phi/2+c_bar_be), zb2), ), ((-(d_col-cover-phi/2-c_bar_col), -(d_beam/2),
zb2 ), ),
    ((l_beam/2, -(d_beam-cover-phi/2-2*c_bar_be), zb2), ), ((l_beam/2,
-(cover+phi/2+2*c_bar_be), zb2), ), ((-(d_col-cover-phi/2-2*c_bar_col),
-(d_beam/2), zb2 ), ),
    ((l_beam/2, -(d_beam-cover-phi/2-3*c_bar_be), zb2), ), ((l_beam/2,
-(cover+phi/2+3*c_bar_be), zb2), ), ((-(d_col-cover-phi/2-3*c_bar_col),
-(d_beam/2), zb2 ), ),
    ((-(d_col-cover-Rcol+phi/1000), -(cover-phi/2), zb1), ),
((-(d_col-cover-Rcol-c_bar_be+phi/1000), -(c_bar_be+cover-phi/2), zb1), ),
((-(d_col-cover-Rcol-2*c_bar_be+phi/1000), -(2*c_bar_be+cover-phi/2), zb1), ),
    ((-(d_col-cover-Rcol-3*c_bar_be+phi/1000), -(3*c_bar_be+cover-phi/2), zb1),
),
    ((-(d_col-cover-Rcol+phi/1000), -(cover-phi/2), zb2), ),
((-(d_col-cover-Rcol-c_bar_be+phi/1000), -(c_bar_be+cover-phi/2), zb2), ),
((-(d_col-cover-Rcol-2*c_bar_be+phi/1000), -(2*c_bar_be+cover-phi/2), zb2), ),
    ((-(d_col-cover-Rcol-3*c_bar_be+phi/1000), -(3*c_bar_be+cover-phi/2), zb2),
),
    ((-(d_col-Rcol-cover+phi/1000), -(d_beam-cover-phi/2), zb1), ),
((-(d_col-Rcol-cover-c_bar_be+phi/1000), -(d_beam-cover-c_bar_be-phi/2), zb1),
), ((-(d_col-Rcol-cover-2*c_bar_be+phi/1000), -(d_beam-cover-2*c_bar_be-phi/2),
zb1), ),
    ((-(d_col-Rcol-cover-3*c_bar_be+phi/1000), -(d_beam-cover-3*c_bar_be-phi/2),
zb1), ),
    ((-(d_col-Rcol-cover+phi/1000), -(d_beam-cover-phi/2), zb2), ),
((-(d_col-Rcol-cover-c_bar_be+phi/1000), -(d_beam-cover-c_bar_be-phi/2), zb2),
), ((-(d_col-Rcol-cover-2*c_bar_be+phi/1000), -(d_beam-cover-2*c_bar_be-phi/2),
zb2), ),
    ((-(d_col-Rcol-cover-3*c_bar_be+phi/1000), -(d_beam-cover-3*c_bar_be-phi/2),
zb2), ),
        ((-(cover-phi/2), -(l_col/2), zc1), ), ((-(d_col-cover-phi/2),
-(l_col/2), zc1), ), ((-(d_col-Rcol-cover), -(cover-phi/2), zc1 ), ),
    ((-(d_col/2), -(cover-phi/2+2*c_bar_col), zc1 ), ), ((-(d_col/2),
-(cover-phi/2+3*c_bar_col), zc1 ), ),
```

```
    ((-(cover-phi/2+c_bar_col), -(l_col/2), zc1), ),
((-(cover-phi/2+2*c_bar_col), -(l_col/2), zc1), ), ((-(cover-phi/2+3*c_bar_col),
-(l_col/2), zc1), ),
    ((-(d_col-cover-phi/2-c_bar_col), -(l_col/2), zc1), ),
((-(d_col-cover-phi/2-2*c_bar_col), -(l_col/2), zc1), ),
((-(d_col-cover-phi/2-3*c_bar_col), -(l_col/2), zc1), ),
    ((-(cover-phi/2), -(l_col/2), zc2), ), ((-(d_col-cover-phi/2), -(l_col/2),
zc2), ), ((-(d_col-Rcol-cover), -(cover-phi/2), zc2 ), ),
    ((-(d_col/2), -(cover-phi/2+2*c_bar_col), zc2 ), ), ((-(d_col/2),
-(cover-phi/2+3*c_bar_col), zc2 ), ),
    ((-(cover-phi/2+c_bar_col), -(l_col/2), zc2), ),
((-(cover-phi/2+2*c_bar_col), -(l_col/2), zc2), ), ((-(cover-phi/2+3*c_bar_col),
-(l_col/2), zc2), ),
    ((-(d_col-cover-phi/2-c_bar_col), -(l_col/2), zc2), ),
((-(d_col-cover-phi/2-2*c_bar_col), -(l_col/2), zc2), ),
((-(d_col-cover-phi/2-3*c_bar_col), -(l_col/2), zc2), ), #---
    ((-(d_col-cover-Rcol-c_bar_col+phi/1000), -(cover-phi/2+c_bar_be), zc1), ),
((-(cover+Rcol+c_bar_col-phi/1000), -(cover-phi/2+c_bar_be), zc1), ),
    ((-(d_col-cover+phi/2)+scol, -(cover+Rcol-phi/1000), zc1), ),
((-(cover+Rcol-phi/1000), -(cover-phi/2), zc2), ),
    ((-(d_col-cover-Rcol-c_bar_col+phi/1000), -(cover-phi/2+c_bar_be), zc2), ),
((-(cover+Rcol+c_bar_col-phi/1000), -(cover-phi/2+c_bar_be), zc2), ),
    ((-(d_col/2), -(cover-phi/2+c_bar_be), zc1), ), ((-(d_col/2),
-(cover-phi/2), zc1), ), ((-(d_col/2), -(cover-phi/2+c_bar_be), zc2), ),
((-(d_col/2), -(cover-phi/2), zc2), ))

# CONTACT PROPERTIES
mdb.models['Model-1'].ContactProperty('Interaction property')
mdb.models['Model-1'].interactionProperties['Interaction
property'].CohesiveBehavior(defaultPenalties=OFF, table=((3300000000000.0,
33000000000.0, 33000000000.0), ))
mdb.models['Model-1'].interactionProperties['Interaction
property'].Damage(initTable=((50000000.0, 23000000.0, 23000000.0), ),
useEvolution=ON, evolTable=((0.003, ), ))

a.Surface(side1Faces=side1Faces1, name='conc_internal')
region1=a.surfaces['conc_internal']

side1Faces1 = a.instances['reinforcement-1'].faces.getByBoundingBox()
a.Surface(side1Faces=side1Faces1, name='reinforcement_external')
region2=a.surfaces['reinforcement_external']

mdb.models['Model-1'].SurfaceToSurfaceContactStd(name='Bond interaction',
createStepName='Initial', master=region1, slave=region2, sliding=SMALL,
    thickness=ON, interactionProperty='Interaction property',
adjustMethod=OVERCLOSED, initialClearance=OMIT, datumAxis=None,
clearanceRegion=None, tied=OFF)

# ---------- datum coordinate system ----------

# CREATE CSYS COORD IN BEAM END TO APPLY DISPLACMENT IN 45 DEGEREE ANGLE
x=a.DatumCsysByThreePoints(origin=a.instances['ext_beam-1'].vertices[1],
name='Beamend', coordSysType=CARTESIAN,
    point1=((2*ltot+d_col/2), -(d_beam+l_beam+lc), b/2), point2=(2*ltot, b/2,
```

```
b/2))
id=x.id

# ---------- create symmetry ----------

faces1 = a.instances['concreteframe-1'].faces.findAt(((0.0, 0.0, 0.0), ), ((0.0, 
0.0, b), ))
region = regionToolset.Region(faces=faces1)
mdb.models['Model-1'].DisplacementBC(name='Symmetry', createStepName='Initial', 
region=region, u1=UNSET, u2=UNSET, u3=0.0, ur1=UNSET, ur2=UNSET, 
    ur3=UNSET, amplitude=UNSET, fixed=OFF, distributionType=UNIFORM, 
fieldName='', localCsys=None)

# ---------- create coupling extended beams/columns to frame corner ----------

# ELASTIC BEAM END
verts1 = a.instances['ext_beam-1'].vertices.findAt(((l_beam, -d_beam/2, b/2), ))
region1=regionToolset.Region(vertices=verts1)

# EDGES FOR CONCRETE AND REINFORCEMENT (*)
side1Faces1 = a.instances['concreteframe-1'].faces.findAt(((l_beam, -d_beam/2, 
b/2), ))
side1Faces2 = a.instances['reinforcement-1'].faces.findAt(
        ((l_beam, -(cover-phi/2+sbeam), zb1), ), ((l_beam, -(cover-phi/2), zb1), 
),
    ((l_beam, -(cover-phi/2-c_bar_be+sbeam), zb1), ), ((l_beam, 
-(cover-phi/2+c_bar_be), zb1), ),
    ((l_beam, -(cover-phi/2-2*c_bar_be+sbeam), zb1), ), ((l_beam, 
-(cover-phi/2+2*c_bar_be), zb1), ),
    ((l_beam, -(cover-phi/2-3*c_bar_be+sbeam), zb1), ), ((l_beam, 
-(cover-phi/2+3*c_bar_be), zb1), ),
        ((l_beam, -(cover-phi/2+sbeam), zb2), ), ((l_beam, -(cover-phi/2), zb2), 
),
    ((l_beam, -(cover-phi/2-c_bar_be+sbeam), zb2), ), ((l_beam, 
-(cover-phi/2+c_bar_be), zb2), ),
    ((l_beam, -(cover-phi/2-2*c_bar_be+sbeam), zb2), ), ((l_beam, 
-(cover-phi/2+2*c_bar_be), zb2), ),
    ((l_beam, -(cover-phi/2-3*c_bar_be+sbeam), zb2), ), ((l_beam, 
-(cover-phi/2+3*c_bar_be), zb2), ))
region2=regionToolset.Region(side1Faces=side1Faces1+side1Faces2)
mdb.models['Model-1'].Coupling(name='Beam-frame', controlPoint=region1, 
surface=region2, influenceRadius=WHOLE_SURFACE, couplingType=KINEMATIC, 
    localCsys=None, u1=ON, u2=ON, u3=ON, ur1=ON, ur2=ON, ur3=ON)

# ELASTIC COLUMN END
verts1 = a.instances['ext_col-1'].vertices.findAt(((-d_col/2, -l_col, b/2), ))
region1=regionToolset.Region(vertices=verts1)

# EDGES FOR CONCRETE AND REINFORCEMENT (*)
side1Faces1 = a.instances['concreteframe-1'].faces.findAt(((-d_col/2, -l_col, 
b/2), ))
side1Faces2 = a.instances['reinforcement-1'].faces.findAt(
        ((-(cover-phi/2), -l_col, zc1), ), ((-(cover-phi/2+scol), -l_col, zc1), 
),
```

```
    ((-(cover-phi/2+c_bar_col), -l_col, zc1), ),
((-(cover-phi/2+scol-c_bar_col), -l_col, zc1), ),
    ((-(cover-phi/2+2*c_bar_col), -l_col, zc1), ),
((-(cover-phi/2+scol-2*c_bar_col), -l_col, zc1), ),
    ((-(cover-phi/2+3*c_bar_col), -l_col, zc1), ),
((-(cover-phi/2+scol-3*c_bar_col), -l_col, zc1), ),
        ((-(cover-phi/2), -l_col, zc2), ), ((-(cover-phi/2+scol), -l_col, zc2),
),
    ((-(cover-phi/2+c_bar_col), -l_col, zc2), ),
((-(cover-phi/2+scol-c_bar_col), -l_col, zc2), ),
    ((-(cover-phi/2+2*c_bar_col), -l_col, zc2), ),
((-(cover-phi/2+scol-2*c_bar_col), -l_col, zc2), ),
    ((-(cover-phi/2+3*c_bar_col), -l_col, zc2), ),
((-(cover-phi/2+scol-3*c_bar_col), -l_col, zc2), ))
region2=regionToolset.Region(side1Faces=side1Faces1+side1Faces2)
mdb.models['Model-1'].Coupling(name='Col-frame', controlPoint=region1,
surface=region2, influenceRadius=WHOLE_SURFACE, couplingType=KINEMATIC,
    localCsys=None, u1=ON, u2=ON, u3=ON, ur1=ON, ur2=ON, ur3=ON)

# ---------- applied displacement and bc ----------

# BC LOWER COLUMN END
verts1 = a.instances['ext_col-1'].vertices.findAt(((-d_col/2,
-(d_beam+l_beam+lc), b/2), ))
region = regionToolset.Region(vertices=verts1)
mdb.models['Model-1'].DisplacementBC(name='BC_bot', createStepName='Step-1',
region=region, u1=0.0, u2=0.0, u3=0.0,
    ur1=UNSET, ur2=UNSET, ur3=UNSET, amplitude=UNSET, fixed=OFF,
distributionType=UNIFORM, fieldName='', localCsys=None)

# BC UPPER BEAM END
verts1 = a.instances['ext_beam-1'].vertices.findAt(((ltot, -d_beam/2, b/2), ))
region = regionToolset.Region(vertices=verts1)
mdb.models['Model-1'].DisplacementBC(name='Displacement',
createStepName='Step-1', region=region, u1=0.0, u2=-disp, u3=0.0,
    ur1=UNSET, ur2=UNSET, ur3=UNSET, amplitude=UNSET, fixed=OFF,
distributionType=UNIFORM, fieldName='', localCsys=a.datums[id])

# ----------- create datum planes through structure to be able to make smaller
mesh ----------

y1=a.DatumPlaneByPrincipalPlane(principalPlane=XZPLANE, offset=-d_beam/2)
id1=y1.id

y2=a.DatumPlaneByPrincipalPlane(principalPlane=YZPLANE, offset=-d_col/2)
id2=y2.id

pickedCells = a.instances['concreteframe-1'].cells.findAt(((0, 0, 0), ))
a.PartitionCellByDatumPlane(datumPlane=a.datums[id1], cells=pickedCells)
a.PartitionCellByDatumPlane(datumPlane=a.datums[id2], cells=pickedCells)

session.viewports['Viewport:
1'].assemblyDisplay.geometryOptions.setValues(datumPlanes=OFF) # hide
datumplanes
```

```
# ----------- define field outputs ----------

mdb.models['Model-1'].fieldOutputRequests['F-Output-1'].setValues(variables=('S'
, 'PE', 'PEEQ', 'LE', 'U', 'RF', 'SF', 'CSTRESS', 'CDISP', 'MVF'),
timeInterval=0.01)

# ---------- create mesh ----------

partInstances =(a.instances['reinforcement-1'], a.instances['concreteframe-1'],
a.instances['ext_beam-1'], a.instances['ext_col-1'] )
a.seedPartInstance(regions=partInstances, size=0.12, deviationFactor=0.11,
minSizeFactor=0.1)      #mesh size

cells1 =
a.instances['reinforcement-1'].cells.getByBoundingBox(-100.,-100,-100,100,100,10
0)
cells2 =
a.instances['concreteframe-1'].cells.getByBoundingBox(-100.,-100,-100,100,100,10
0)
pickedRegions = cells1+cells2

a.setMeshControls(regions=pickedRegions, elemShape=TET, technique=FREE)
elemType1 = mesh.ElemType(elemCode=C3D20R)
elemType2 = mesh.ElemType(elemCode=C3D15)
elemType3 = mesh.ElemType(elemCode=C3D10)

a.generateMesh(regions=partInstances)
```

E

Appendix E

Provided in this section are the drawings used as reference, with dimensions and reinforcement configuration, for the underground structure studied and analysed in Chapter 5, provided by ELU Konsult AB. The first figure shows the full structure without dimensions and details for the reader to understand the structure. Marked in a square in the upper left corner and then presented on the following page, is the corner structure studied in detail.

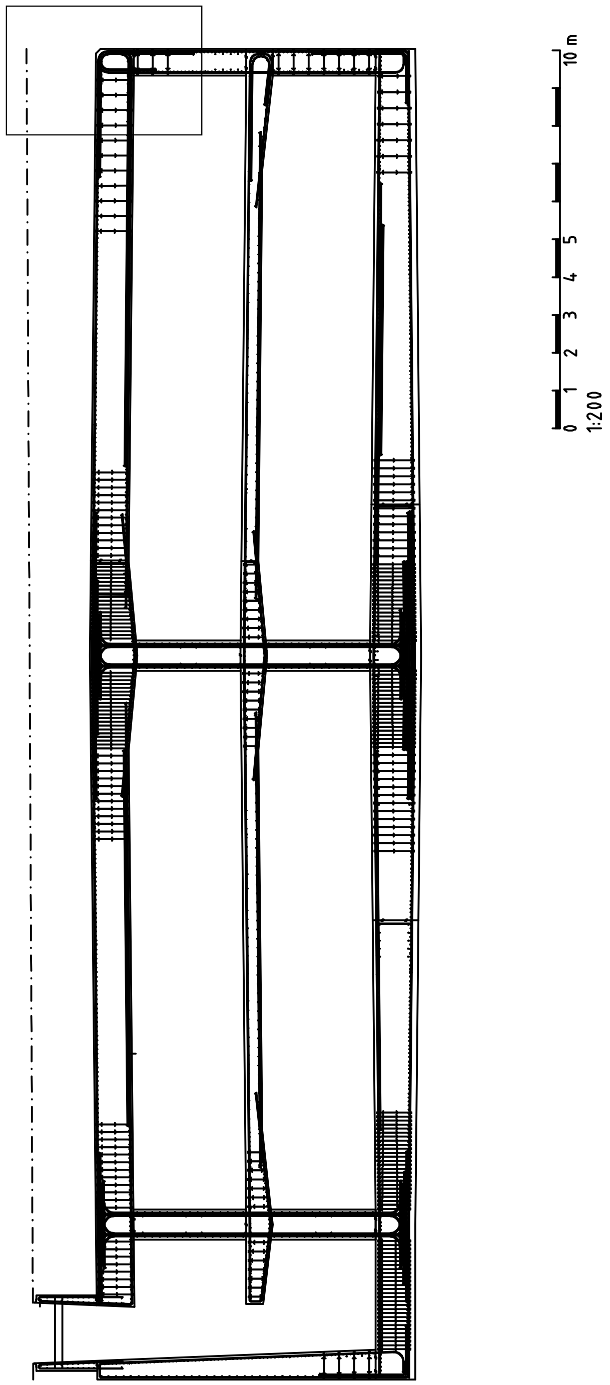

	REINF. DETAILING			ORT GÖTEBORG / DATUM 2019-06-07
	UNDERGROUND STRUCTURE FOR CAR PARKING AT SKEPPSBRON, GÖTEBORG			ANSVARIG
				SKALA 1:200 (A4) / REV
	UPPDRAG NR	KONSTR	HANDLÄGGARE	NUMMER

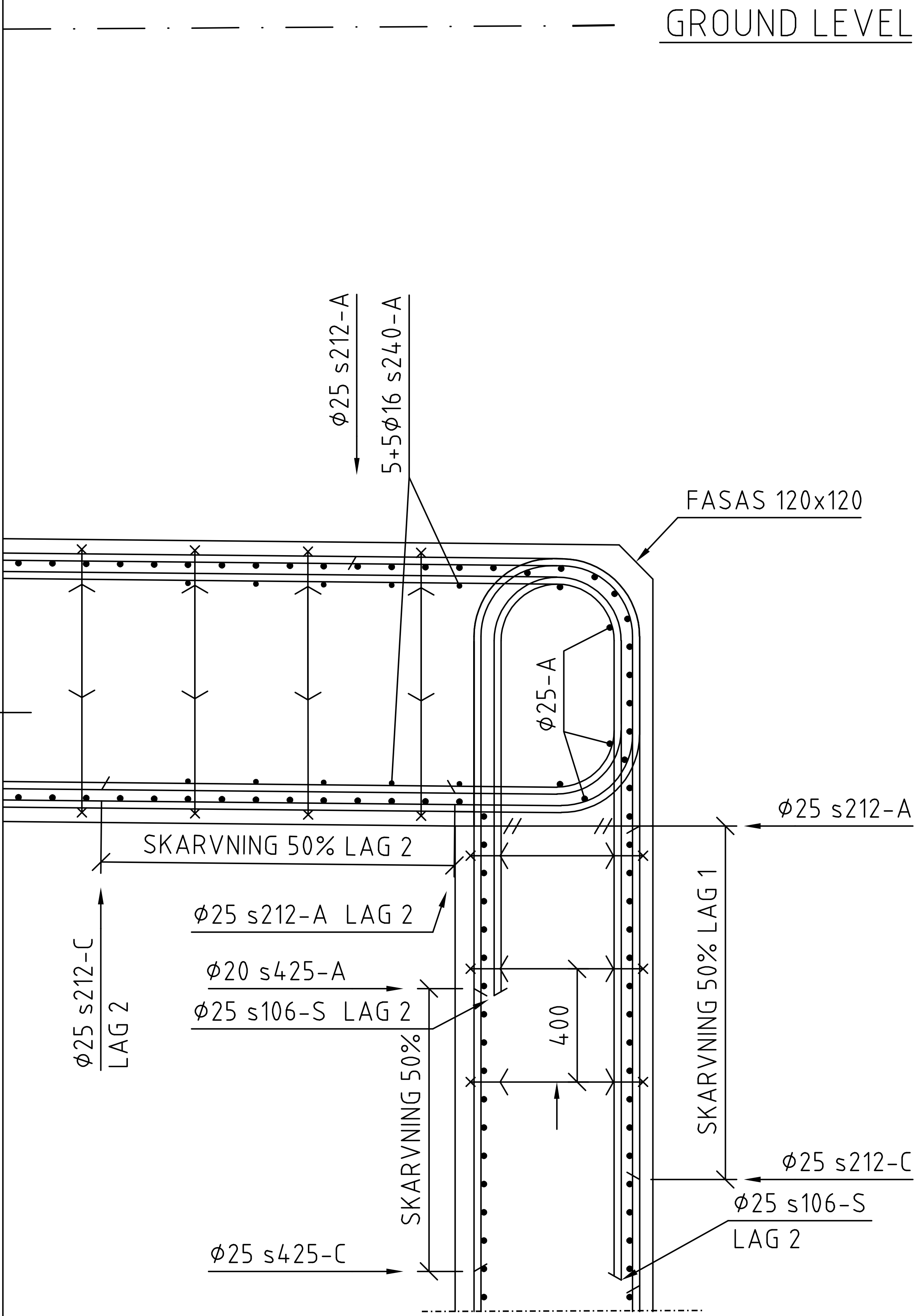

	CORNER DETAILING			ORT GÖTEBORG / DATUM 2019-06-07
				ANSVARIG
	UNDERGROUND STRUCTURE FOR CAR PARKING AT SKEPPSBRON, GÖTEBORG			SKALA 1:20 (A4) / REV
	UPPDRAG NR	KONSTR	HANDLÄGGARE	NUMMER